A BIFURCATION STUDY OF WRINKLING IN DEEP DRAWING

By

MEDHAT MOHAMED NASSOUH KARIMA, M.Eng.

A Thesis

Submitted to the School of Graduate Studies

in Partial Fulfilment of the Requirements

for the Degree

Doctor of Philosophy

McMaster University

July 1980

A BIFURCATION STUDY OF WRINKLING IN DEEP DRAWING

DOCTOR OF PHILOSOPHY (1980)
(Mechanical Engineering)

McMASTER UNIVERSITY
Hamilton, Ontario

TITLE: A Bifurcation Study of Wrinkling in Deep Drawing

AUTHOR: Medhat Mohamed Nassouh Karima B.Sc. (Alexandria University)
M.Eng. (McGill University)

SUPERVISOR: Professor R. Sowerby

NUMBER OF PAGES: XViii, 235

ABSTRACT

This work is concerned with the wrinkling behaviour when deep drawing cylindrical cups from circular blanks. Wrinkling is a uniqueness problem, and the present work uses a bifurcation approach to predict its occurrence. The results are presented in terms of a critical ratio of blank diameter to thickness above which wrinkling commences, along with the number of waves into which the flange of the cup buckles.

It is demonstrated that when the classical Prandtl-Reuss equations are incorporated into the bifurcation analysis, the theoretical predictions are at variance with the published experimental data.

A number of ad-hoc modifications are made to the classical elastic-plastic model to make the predictions conform with the experimental results.

A critical re-examination of both the flow and deformation theories of plasticity was carried out, leading to the proposal of a modified incremental theory. The modified constitutive equations is shown to reduce to an appropriate model for both elastic and rigid-plastic solids, as limiting cases. The consequence of the modified equations is non-coaxiality of the principal axes of stress and plastic strain increment, and this is supported by published experimental data. The proposed constitutive equations lead to a better prediction of the

wrinkling behaviour vis a vis the other models discussed here-in.

An experimental investigation of the wrinkling behaviour of a number of materials, drawn through a conical and a modified tractrix die, was undertaken. The study has resulted in proposals for certain material parameters as being beneficial for inhibiting wrinkling.

A theoretical study of wrinkling when drawing through a conical die is also presented.

ACKNOWLEDGEMENTS

The author would like to record his deep gratitude to his supervisor, Professor R. Sowerby, for his guidance, encouragement and for providing an enjoyable working atmosphere.

He would also like to thank Professors J.L. Duncan and G.AE. Oravas for their inspiring teaching and the numerous helpful comments, his colleague M.S. Gadala for many interesting discussions and his colleague F. Ismail for coordinating the finished typing and reproduction of the manuscripts.

Financial support for this work was provided by the National Research Council of Canada, whose help is gratefully acknowledged.

Thanks also go to the staff of the Faculty of Engineering Word Processing Centre for the typing of this work.

Last, but far from the least, he would like to thank his wife Abla for her continued encouragement and assistance in the proofreading.

TO MY PARENTS AND WIFE

TABLE OF CONTENTS

Table of Contents (continued)

Table of Contents (continued).

LIST OF FIGURES

List of Figures (continued)

LIST OF TABLES

LIST OF SYMBOLS

$\overline{\overline{\overline{\overline{K}}}}$	Tensor of elastic moduli	$\overline{\overline{\overline{\overline{I}}}}$	Identity tensor
$(\frac{\delta \bar{\bar{\sigma}}}{\delta t})^{J}$	Jaumann derivative	$(\frac{\delta \bar{\bar{\sigma}}}{\delta t})^{C}$	Convected derivative
$\bar{\bar{\sigma}}$	Cauchy stress tensor	$\bar{\bar{S}}$	Nominal stress tensor
$\bar{\bar{\sigma}}'$	Deviatoric Cauchy stress tensor	$\bar{\bar{\sigma}}^{\cdot}$	Cauchy stress rate tensor
$\bar{\bar{\tau}}$	Kirchhoff stress tensor	$\bar{\bar{\epsilon}}$	Eulerian strain rate tensor
$\bar{\bar{D}}$	Rate of deformation tensor	$\bar{\bar{\epsilon}}_o$	Middle surface strain rate
$\bar{\bar{k}}$	Change of curvature tensor	$\bar{\bar{L}}$	Velocity gradient
$\bar{\bar{m}}$	Unit normal to deviatoric yield surface (initial configuration)	$\bar{\bar{m}}^{*}$	Unit normal to deviatoric yield surface (final configuration)
$\bar{\bar{W}}$	Spin tensor	$\bar{\bar{1}}$	Identity tensor
$\bar{F}$	Surface traction vector	$\bar{g}$	Body force vector
$\bar{n}$	Unit normal to surface	$\bar{u}$	Displacement vector
$\bar{v}$	Velocity vector	$\bar{\sigma}$	Representative stress
α_{ij}	Elastic-Plastic moduli	$\bar{e}$	Representative strain
λ	Lame's constant	ϕ	Semi cone angle
d_p	Punch diameter	D_b	Blank diameter

List of Symbols (continued)

E_T	Tangent modulus	E_s	Secant modulus
E	Young's modulus	$f(\bar{\bar{\sigma}}')$	Yield function
$2G$	Elastic shear modulus	h	Hardening parameter
h^*	Relative hardening	$2J_2'$	Second invariant of the deviatoric stress tensor
n	Number of waves	r	Radius
$\bar{F}$	Normal anisotropy parameter	R_o	Outer radius
R_1	Inner radius	R	Drawing ratio
S_F	Part of surface where traction forces are prescribed	S_u	Part of surface where displacements are prescribed
t	Thickness	t^*	Critical thickness ratio

BASIC OPERATIONS

Some basic operations carried out in the work are shown below using dyadic and indicial notation.

$$\overline{\overline{T}}:\overline{\overline{D}} = T_{ij}\,\bar{e}_i\bar{e}_j : D_{k\ell}\,\bar{e}_k\bar{e}_\ell$$

$$= T_{ij}D_{k\ell}(\bar{e}_i.\bar{e}_k)(\bar{e}_j.\bar{e}_\ell)$$

$$= T_{ij}D_{ij}$$

$$\overline{\overline{T}}.\overline{\overline{1}} = T_{ij}\,\bar{e}_i\bar{e}_j.\bar{e}_\ell\bar{e}_\ell$$

$$= T_{ij}\,\bar{e}_i\,\bar{e}_\ell\,\delta_j^{\ell}$$

$$= T_{i\ell}\,\bar{e}_i\,\bar{e}_\ell = \overline{\overline{T}}$$

$$\overline{\overline{\overline{\overline{K}}}}:\overline{\overline{D}} = K_{ijk\ell}\,\bar{e}_i\,\bar{e}_j\,\bar{e}_k\,\bar{e}_\ell : D_{uv}\,\bar{e}_u\,\bar{e}_v$$

$$= K_{ijk\ell}\,D_{uv}\,\bar{e}_i\,\bar{e}_j(\bar{e}_k.\,\bar{e}_u)\,(\bar{e}_\ell.\,\bar{e}_v)$$

$$= K_{ijk\ell}\,D_{k\ell}\,\bar{e}_i\,\bar{e}_j$$

$$\overline{\overline{T}}.\overline{\overline{T}}^{-1} = \overline{\overline{1}}$$

$$\overline{\overline{\overline{\overline{K}}}}:\overline{\overline{\overline{\overline{K}}}}^{-1} = \overline{\overline{\overline{\overline{1}}}}$$

$$d\overline{\overline{\overline{F}}}^{n} = d\bar{r}.\frac{\partial\overline{\overline{\overline{F}}}^{n}}{\partial\bar{r}}$$

where $\overline{\overline{\overline{F}}}^{n}$ is a tensor of nth order.

INTRODUCTION

0.1 Preliminary Remarks

In many metal forming applications involving thin sections subjected to predominantly compressive stresses, failure often occurs by buckling. There is, however, a limited amount of data available on the buckling phenomena in metal forming operations.

To predict the onset of wrinkling it is necessary to understand the nature of the stresses and strains in the material undergoing plastic deformation and to investigate the conditions under which the state of stress is non-unique. In this dissertation an attempt is made to predict the onset of wrinkling by making use of different buckling theories. In a series of articles, Hill [46, 49, 50 and 51] placed the bifurcation criterion for rigid-plastic and elastic-plastic solids on a firm mathematical base, allowing for bifurcation under compressive and also tensile loading e.g. necking. His work has formed the basis of many subsequent bifurcation studies.

A great deal of the published literature on the subject up to 1972 has been cited in the comprehensive survey by Sewell [128]. The extensive article by Hutchison [65] also provides much theoretical background, while emphasizing the post-bifurcation and imperfection sensitivity aspects of plastic buckling.

0.2 Object and Scope

The basic theory of Hill is described in chapter 1 along

with its specialization to plates and shells. Because of the complexity of the equations involved, a variational formulation is presented so that an approximate upper bound solution can be obtained.

At first sight the basic formulation appears appropriate. However, it transpires that the prediction of buckling loads (or stresses), when based on the classical Prandtl-Reuss constitutive equations, is invariably much in excess of the experimentally determined values - the so-called "buckling paradox". Hence one of the difficulties is the identification of an adequate plasticity theory which can be incorporated into the bifurcation analyses.

The two most widely applied plasticity theories, the J_2 flow and J_2 deformation theories, are examined in chapter 2 along with certain contemporary trends in bifurcation analyses. The chapter concludes with a proposal for a modified incremental theory to be used in bifurcation analyses.

Chapter 3 deals with the analysis of the wrinkling behaviour when producing cylindrical cups from circular blanks in the Swift cupping test [12]. This is usually regarded as the conventional deep drawing operation and is shown schematically in Figure 3.1.

The theoretical fundamentals developed in chapter 2 are applied to predict a critical ratio of blank diameter to thickness, above which wrinkling occurs. A number of different

models are presented and it is demonstrated that the results are strongly dependent upon the selected constitutive equation. Predictions based on the proposed constitutive equations, introduced at the end of chapter 2, compare quite favourably with published experimental data.

Cylindrical cups can also be produced by alternative means as shown in Figures 4.1 and 5.14. A more detailed discussion on this drawing technique is given later in the text. These methods have found favour in the production of cylinder liners, gas bottles and beverage cans.

In chapter 4, an attempt is made to analyse the wrinkling behaviour when drawing through conical dies using the techniques described in chapters 2 and 3.

Chapter 5 presents the findings of an experimental program undertaken to assess the wrinkling behaviour of blanks produced from a number of different materials, when drawn through a conical and a modified tractrix shaped die. The results indicate that the wrinkling behaviour is influenced both by the material properties and the shape of the die. The materials investigated possessed a wide range of mechanical properties; and while data from other materials would always be useful, certain material parameters were identified from the selected materials as being beneficial to inhibiting wrinkling. Only two die profiles were inspected and further work, to determine an optimum drawing die shape, could prove fruitful.

CHAPTER 1

FORMULATION OF THE RATE PROBLEM

1.1 Basic Theory

In what follows we are concerned with the isothermal quasi-static incremental behaviour of a solid. The response of the material is governed by the following constitutive rate equations, which are assumed not to involve natural time

$$\overset{=}{S}^{\bullet} = \frac{\partial \overset{=}{U}(\overset{=}{L})}{\partial \overset{=}{L}^{T}} \quad \text{or} \quad S_{ij}^{\bullet} = \frac{\partial U}{\partial(\partial v_j/\partial x_i)} \tag{1.1}$$

$$\overset{=}{\tau}^{\bullet} = \frac{\partial W(\overset{=}{\varepsilon})}{\partial \overset{=}{\varepsilon}} \quad \text{or} \quad \tau_{ij}^{\bullet} = \frac{\partial W}{\partial \varepsilon_{ij}} \tag{1.2}$$

The above rate equations will usually be "linear" relations between stress rate and strain rate with coefficients which are either independent of the variables for a linear solid or at most step functions of them for an elastic-plastic (E-P) solid. These rate equations obey the Euler Legendre canonical transformation. The current mechanical state of the body is supposed to be known, the current distributions of velocity $\bar{v}$ and surface tractions rates $\bar{F}^{\bullet}$ are prescribed functions of position on complementary parts S_V and S_F of the surface, and body forces rates per unit volume, $\bar{g}^{\bullet}$, are given within the volume, see Figure 1.1.

Essentially, the problem here is to investigate the quasi-static behaviour which can ensue, see Figure 1.2. If changes in geometry are taken into account, the boundary value

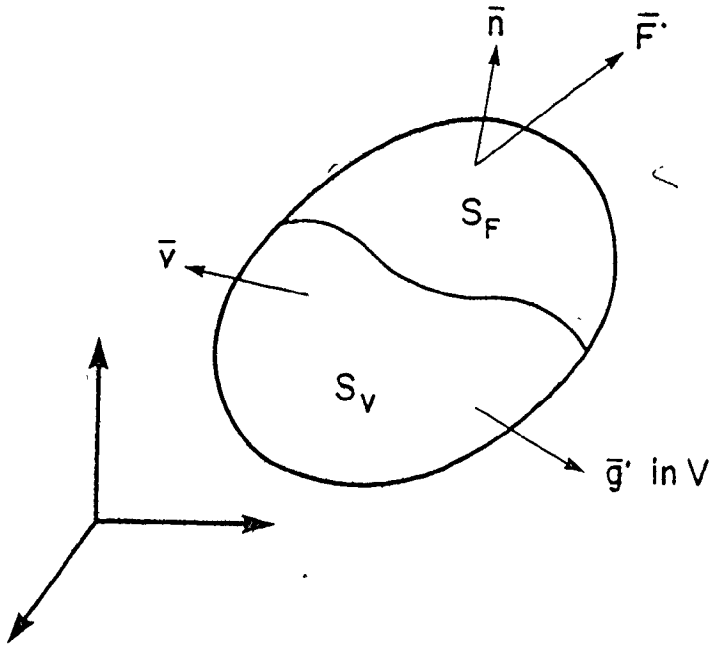

Figure 1.1 Boundary value problem

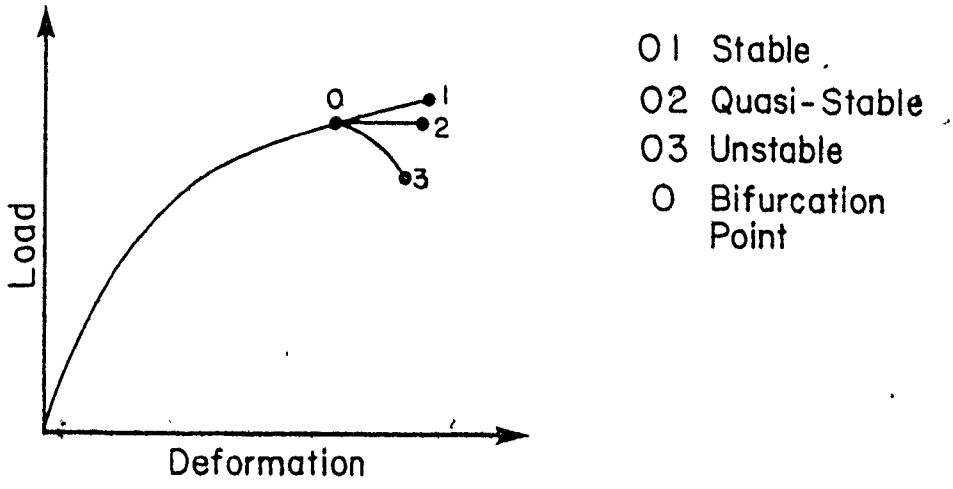

Figure 1.2 Bifurcation and stability

problem does not necessarily possess a unique solution and a bifurcation therefore results at a certain stage of the deformation. It is, however, possible to have a stable bifurcation with the load increasing with continuing deformation. This was first indicated by Shanley [132] in relation to the failure of inelastic columns.

The present chapter is concerned with the uniqueness and stability of elastic-plastic (E-P) and rigid-plastic (R-P) solids under continuing finite deformation. The effect of changes in geometry and rotation of material elements is included by expressing the traction rate in terms of the material derivative of the nominal stress tensor, whereas the material properties are given in terms of the frame indifferent Jaumann derivative.

1.1.1 Uniqueness

For uniqueness the difference between two solutions has to be tested. The difference has to satisfy the following field equations;

$$\frac{\partial}{\partial \bar{x}} \cdot \Delta \dot{\bar{\bar{S}}} = \bar{0} \quad \text{in } V \tag{1.3}$$

$$\bar{n} \cdot \Delta \dot{\bar{\bar{S}}} = \bar{0} \quad \text{on } S_F \tag{1.4}$$

$$\Delta \bar{v} = \bar{0} \quad \text{on } S_v, \tag{1.5}$$

where Δ signifies the difference in the two solutions.

The identification of bifurcation states involves demonstrating solutions to (1.3)-(1.5), see Hill [50] and Chakrabarty [14,16] (uniqueness in the small).

An alternative formulation for the uniqueness of the velocity solution is to apply the principle of the virtual work to the difference i.e.,

$$0 = \int \Delta\bar{F}^{\cdot} \cdot \Delta\bar{v}\, dS = \int \Delta\overset{=}{S}^{\cdot} : \Delta\overset{=}{L}^{T}\, dV .$$

Hence, a sufficient criterion of uniqueness (in the large) is that

$$I = \int \Delta\overset{=}{S}^{\cdot} : \Delta\overset{=}{L}^{T}\, dV > 0 , \tag{1.6}$$

where $\Delta\overset{=}{S}^{\cdot} = \overset{=}{S}_1^{\cdot} - \overset{=}{S}_2^{\cdot}$, are calculated from the rate equations (1.1). Combining (1.1) and (1.6) results in

$$\int \Delta \left(\frac{\partial U}{\partial \overset{=}{L}^{T}}\right) : \Delta\overset{=}{L}^{T}\, dV > 0, \tag{1.7}$$

which is also the condition of convexity of U, for a linear solid.

For application to elastic-plastic (E-P) solids, it is convenient to write (1.6) in terms of the Jaumann derivative. Since

$$\overset{=}{S}^{\cdot} = \left(\frac{\delta \overset{=}{\tau}}{\delta t}\right)^{J} + \overset{=}{\sigma} \cdot \overset{=}{L}^{T} - (\overset{=}{\sigma} \cdot \overset{=}{\varepsilon} + \overset{=}{\varepsilon} \cdot \overset{=}{\sigma}), \tag{1.8}$$

then (1.6) can be expressed in the form

$$H(\bar{w}) - \Sigma(\bar{w}) > 0. \tag{1.9}$$

Where $\bar{w} = \Delta \bar{v}$,

$$H(\bar{w}) = \int \Delta\left(\frac{\delta \underline{\underline{\tau}}}{\delta t}\right)^{J} : \Delta \underline{\underline{\varepsilon}} \, dV \qquad (1.10)$$

and $$\Sigma(\bar{w}) = \int \underline{\underline{\sigma}} : (2\Delta \underline{\underline{\varepsilon}} \cdot \Delta \underline{\underline{\varepsilon}} - \Delta \underline{\underline{L}}^{T} \cdot \Delta \underline{\underline{L}}) \, dV. \qquad (1.11)$$

In suffix notation (1.11) can be written

$$\Sigma(\bar{w}) = \int \sigma_{ik} \left(2\Delta\varepsilon_{ij}\Delta\varepsilon_{jk} - w_{j,i}\, w_{j,k}\right)$$

For the special case where $\bar{v}=\bar{o}$ on S_v, equation (1-7) can be expressed as

$$\int \frac{\partial U}{\partial \underline{\underline{L}}^{T}} : \underline{\underline{L}}^{T} \, dV > 0 \qquad (1.12)$$

or

$$\int U(\underline{\underline{L}}) \, dV > 0 , \qquad (1.13)$$

for all fields vanishing on S_v, but not identically zero. Equation (1.13) does not involve the actual boundary conditions on S_v and S_F, since these cannot affect the question of uniqueness in a LINEAR SOLID; for whatever are the inhomogeneous boundary conditions, the difference of two modes is always an eigenfield, Hill [50]. Hence the solution to every INHOMOGENEOUS problem is indeterminate to the extent of an arbitrary additive multiple of the eigenfield. When the current and the original configuration coincide then,

$$\underline{\underline{\sigma}} = \underline{\underline{\tau}} = \underline{\underline{S}} ,$$

$$\overset{=}{S} = \left(\frac{\delta \overset{=}{\tau}}{\delta t}\right)^{c} + \overset{=}{\sigma} \cdot \overset{=}{L}^{T} = \left(\frac{\delta \overset{=}{\tau}}{\delta t}\right)^{c} + \overset{=}{\tau} \cdot \overset{=}{L}^{T} \quad ,$$

and

$$U(\overset{=}{L}) = W(\overset{=}{\varepsilon}) + \frac{1}{2} \overset{=}{\tau} : \overset{=}{L}^{T} \cdot \overset{=}{L}$$

Equation (1.13) can then be expressed as,

$$\int \left[W(\overset{=}{\varepsilon}) + \frac{1}{2} \overset{=}{L} \cdot \overset{=}{\tau} : \overset{=}{L}\right] dV > 0 \qquad (1.14)$$

where the contributions of rotations now appear separately in the second term.

The set of equations (1.3)-(1.5) show that in a linear solid, the question of UNIQUENESS is entirely equivalent to the existence of EIGENSTATES (or more loosely to adjacent equilibrium configurations). The situation is otherwise when the solid is non-linear, in this case (1.12) is a sufficient condition for the nonexistence of eigenfields. It should be noted that (1.13) need by no means be a necessary condition for uniqueness.

1.1.2 Stability

Hill [48], used the term "STABILITY" in its classical dynamic context. A loaded body, initially at rest, is imagined to be set in motion. In this setting a state of equilibrium is said to be stable if the amplitude of the additional displacement is always vanishingly small when the disturbance itself is.

A sufficient condition for stability can be expressed as,

Internal Work > External Work.

Accordingly a sufficient condition for stability in a displacement $\delta\bar{u}$ is,

$$\int [\bar{\bar{S}} + \delta\bar{\bar{S}}]: \frac{\partial}{\partial \bar{x}} (\delta\bar{u}) dV - \int \bar{F} \cdot \delta\bar{u}\, dS > 0.$$

To a second order it is given by

$$\frac{1}{2} (\delta t)^2 \int \dot{\bar{\bar{S}}}: \bar{\bar{L}}^T dV > 0$$

$$\text{or } \int \dot{\bar{\bar{S}}} : \bar{\bar{L}}^T dV > 0. \qquad (1.15)$$

Combining (1.1) and (1.15) yields,

$$\int U (\bar{\bar{L}})\, dV > 0, \qquad (1.16)$$

$$\text{or} \qquad H(\bar{v}) - \Sigma(\bar{v}) > 0, \qquad (1.17)$$

where H ( ) and Σ ( ) are given by (1.10) and (1.11). Note that the occurrence of instability was taken as synonymous with the existence of infinitesimally near positions of equilibrium, this may be quite unjustified when the system is non-linear or non-conservative, Hill [49].

1.1.3 Uniqueness versus Stability

Comparing (1.6) and (1.15), we notice that the functionals in the stability and uniqueness criteria are identical, however, the class of admissible velocity fields are different. Every kinematically admissible field is tested for stability whereas for uniqueness the difference between two fields is checked. The

class of velocity fields involved in the uniqueness criterion therefore contains the class in the stability criterion and hence the lack of uniqueness may preceed the loss of stability, Shanley [131,132].

For a linear solid,

$$\overset{=}{S}^{\cdot} = \overset{4}{\overline{C}} : \overset{=}{L}^{T} , \tag{1.18}$$

and the condition of uniqueness may be written as

$$\int \overset{=}{\Delta L} : \overset{4}{\overline{C}} : \overset{=}{\Delta L}^{T} \, dV > 0 \tag{1.19a}$$

whereas for stability the corresponding expression is

$$\int \overset{=}{L} : \overset{4}{\overline{C}} : \overset{=}{L}^{T} \, dV > 0. \tag{1.19b}$$

When the boundary conditions are such that $\bar{v}=\bar{0}$ on S_V we can see that the questions of stability and uniqueness are intimately related; the incremental boundary value problem for a linear solid has a unique solution when the system is stable. It was shown by (1.16) that for a linear solid, the question of uniqueness is entirely equivalent to the existence of eigenstates. In this case

$$\int \bar{F}^{\cdot} \cdot \bar{v} \, dS = 2 \int U(\overset{=}{L}) \, dV = 0, \tag{1.20}$$

for which deformation can proceed under temporarily CONSTANT LOADING and hence stability is characterized by a dead loading, Hill [48]. It is worth mentioning that in the case of a linear solid (1.7) is the strict condition of convexity of the strain energy density. Furthermore, for a stable bifurcation, the

loading must change in such a way that, according to Hill [49],

$$\int \bar{F}^{\bullet}.\bar{v}\, dS = 2 \int U\,(\underline{\underline{L}})\, dV > 0. \qquad (1.21)$$

Suppose for a non-linear solid that (1.6) is satisfied for $\bar{v}=\bar{0}$ on S_V. Since $\bar{v}=\bar{0}$ is admissible in (1.6), the value of the functional (1.15) with any other field is also assumed in (1.6) when this and the zero field are taken together as a pair. However, when (1.15) is satisfied, nothing can be concluded directly about the functional (1.6) since it is multi-valued. That is the boundary value problem need not have a unique solution in a stable state. Such a stable bifurcation could not occur under DEAD LOAD since (1.15) vanishes in this case for the actual state, Hill [49,50].

1.2 Comparison Theorems

When the solid is non-linear there are difficulties in applying (1.7) because the integral of U is multi-valued. To counteract the problem, Hill [50,51] suggested choosing a hypothetical "LINEAR" comparison solid U_L, so that (1.7) is rewritten as

$$\int \Delta\,(\frac{\partial U_L}{\partial \underline{\underline{L}}^T}) :\, \Delta\, \underline{\underline{L}}^T\, dV + \int \Delta\, \frac{\partial (U-U_L)}{\partial \underline{\underline{L}}^T} :\, \Delta\, \underline{\underline{L}}^T\, dV > 0 \qquad (1.22)$$

where

$$U - U_L = W - W_L = V - V_L = \phi\,(\underline{\underline{\varepsilon}}) \qquad (1.23)$$

and $\phi(\bar{\bar{\varepsilon}})$ is a strictly convex function of the strain rate. There-

fore $\phi(\bar{\bar{\varepsilon}}) \geq 0$, and it is a homogeneous function of second degree. It is clear that not only the first integral of (1.22) is single valued, but the second is never negative.

Hill [50,51] demonstrated that if it were possible to show that (1.7) was satisfied for U_L, then it would be satisfied for the solid U. The problem then becomes one of finding those mechanical states for L for which

$$\int \Delta\bar{\bar{S}} \cdot L : \Delta\bar{\bar{L}}^T \, dV \geq 0 \tag{1.24}$$

For the best results the second volume integral in (1.22) is taken to be as small as possible. Hence, the best choice of the linear solid is such that, Hill [49];

$$\Delta\left(\frac{\delta\bar{\bar{\tau}}}{\delta t}\right)^J : \Delta\varepsilon \geq \Delta\varepsilon : \bar{\bar{\bar{\bar{K}}}} : \Delta\varepsilon - \frac{(m : \bar{\bar{\bar{\bar{K}}}} : \Delta\varepsilon)^2}{h + m : \bar{\bar{\bar{\bar{K}}}} : m}, \tag{1.25}$$

which is a restatement of the convexity of $(V-V_L)$. If every non-zero difference field producing the equality in (1.24) is an eigensolution for the corresponding homogeneous problem for L, then an arbitrary additive multiple of it represents the extent of non-uniqueness now possible in the original non-homogeneous problem of L, and we can speak of the first bifurcation state for L as

$$\int U_L \left(\Delta\bar{\bar{L}}\right) dV \geq 0 \tag{1.26}$$

This amounts to a generalized "RAYLEIGH PRINCIPLE" with equality provided by eigensolutions.

The particular values of $\bar{F}^{\cdot}$ and $\bar{v}$ prescribed have no influence on the bifurcation states in a linear solid. They have a marked influence, however, in a non-linear solid. The multi-valued property of (1.6) means that in the same state, uniqueness may hold for some boundary values but not for others. In particular, suppose we are in a bifurcation state for L and the eigensolution have been found from (1.24) and (1.26). Then in the same state, the non-homogeneous problem in the non-linear solid may be non-unique to the extent of a certain "NOT ARBITRARY" range of multiples of these eigensolutions corresponding to some range of boundary values. The extent of this range will be determined by the necessary and sufficient requirement that the second integral of (1.22) shall vanish for the differences for all modes so constructed, Hill and Sewell [60], and bifurcation occurs only for those values which corresponds to no unloading of the current plastic region. When $\bar{v}=\bar{o}$ on S_V,

$$\int \overset{=}{U}_L (L)\, dV \geq 0 \qquad (1.27)$$

which represent eigenmodes possible under dead loads on S_F for the solid L. The eigenvalues calculated this way are relevant to any non-linear solid having a MORE CONVEX potential than W, and it can be asserted that the bifurcation load is certainly NOT LOWER than the one calculated for L, Hill and Sewell [60].

1.3 Application to Elastic-Plastic Solids

When the boundary conditions are such that $\bar{v}=\bar{o}$ on S_V, and for linear solids which are defined by

$$(\frac{\delta \overset{=}{\tau}}{\delta t}) = \overset{=}{\overset{4}{T}} : \overset{=}{\epsilon} \tag{1.28a}$$

where

$$\overset{=}{\overset{4}{T}} = \overset{=}{\overset{4}{K}} - \frac{\overset{=}{\overset{4}{K}} : \overset{=}{m} \; \overset{=}{m} : \overset{=}{\overset{4}{K}}}{h+m : \overset{=}{\overset{4}{K}} : m} \tag{1.28b}$$

then (1.27) becomes

$$\int \overset{=}{\epsilon} : \overset{=}{\overset{4}{T}} : \overset{=}{\epsilon} \, dV + \int \overset{=}{\sigma} : (2\overset{=}{\epsilon} \cdot \overset{=}{\epsilon} - \overset{=}{L}^T \cdot \overset{=}{L}) \, dV \geq 0 \tag{1.29}$$

for all continuous differentiable fields $\bar{v}$ which vanish on S_V and which satisfy any internal constraints which may be imposed. Therefore the first stage in the bifurcation analysis of an elastic-plastic solid under rigid constraints is the application of (1.29) with (1.28b)

where

$$\Delta(\frac{\delta \overset{=}{\tau}}{\delta t}) : \Delta\overset{=}{\epsilon} \geq \Delta(\frac{\delta \overset{=}{\tau}}{\delta t}) : \Delta\overset{=}{\epsilon} \tag{1.30}$$

The second stage is the determination of the boundary values of $\bar{F}$ for the non-linear solid for which all the associated boundary modes of (1.28) provide equality in (1.30). The stress $\bar{\sigma}$ and the instantaneous moduli of $\overset{4}{T}$ in (1.29) may be regarded as having assigned values, and the equation can then be used to determine within what limits these values must lie in order to ensure uniqueness, Sewell [129].

The material properties expressed by (1.2) are in terms of

the "frame indifferent" convected derivative formed by the contravariant components of the Kirchhoff stress. Various stress rates could also be used to express the material properties and satisfy the frame indifferent principle, see Masur [83], Malvern [80], Bazant [6], Nemat-Nasser [109] and Dubey [26]. Hill [53,57] has also discussed a whole family of such stress rates. There are however some reasons that favour the use of the Jaumann derivative, Prager [119], Dubey [24], for both R-P and E-P solids.

It should be noted that the laws of plasticity are expressed in terms of the Cauchy stress $\overline{\overline{\sigma}}$, and since

$$\left(\frac{\delta \overline{\overline{\tau}}}{\delta t}\right)^{J} = \left(\frac{\delta \overline{\overline{\sigma}}}{\delta t}\right)^{J} + \overline{\overline{\sigma}}\,(\overline{\overline{\varepsilon}}:\overline{\overline{1}}),$$

Then implicit in (1.28a) is the assumption of material incompressibility

$$\overline{\overline{\sigma}}\,(\overline{\overline{\varepsilon}}:\overline{\overline{1}}) = 0 \quad \text{or} \quad (\overline{\overline{\varepsilon}}:\overline{\overline{1}}) = 0.$$

1.4 Variational Principle

In order to apply the uniqueness and stability criteria, approximate methods are used. Hill [46] unified the concept of load bounding techniques by introducing the notions of convex functions.

By applying the conditions of strict convexity to the convex functions $E(\overline{\overline{\varepsilon}})$ and $E_c(\overline{\overline{\sigma}})$, it can be shown that

$$\int E(\overline{\overline{\varepsilon}}^{*})dV - \int \overline{F}\cdot\overline{u}^{*}\, dS_F \geq \int E(\overline{\overline{\varepsilon}})\, dV - \int \overline{F}\cdot\overline{u}\, dS_F \,, \qquad (1.31)$$

and $\int \bar{F}^{*}\cdot\bar{u}\, dS_u - \int E_c(\bar{\bar{\sigma}}^{*})\, dV \leq \int \bar{F}\cdot\bar{u}\, dS_u - \int E_c(\bar{\bar{\sigma}})\, dV$ (1.32)

and the solution is unique. Moreover, since $E(\bar{\bar{\varepsilon}})$ and $E_c(\bar{\bar{\sigma}})$ follow the Legendre dual transformation, the right hand sides of (1.31) and (1.32) are identical and hence the left hand side furnish bounds from above and below. It is also evident that the first variation of these functionals vanish in the actual state. The extrema in (1.31) and (1.32) are therefore analytic, and so close bounds can be obtained from relatively crude assumptions of $\bar{\bar{\sigma}}^{*}$ and $\bar{u}^{*}$.

Hill [50, 51, 53 and 54] generalized the above concept to embrace non-linear solids which admit constitutive rate equations of the type (1.1) and (1.2). The nominal and Kirchhoff stress rates are selected so that the influence of the rate of deformation of the boundaries of the body, does not complicate the variational principle commonly used to replace the equilibrium equations. The variational principle then involves an integral over the undeformed body, which is fixed. To ensure that the boundary value problem can be always given a variational formulation, the existence of a potential U or W was required, along with the condition of self adjoint-loading, see Hill [53].

Any solution of the boundary value problem, unique or not is characterized by a variational principle

$$\delta[\int(U^{\cdot} - \bar{g}^{\cdot}\cdot\bar{v})\, dV - \int \bar{F}^{\cdot}\cdot\bar{v}\, dS_F] = 0, \qquad (1.33)$$

which is stationary in the class of continuous velocity fields $\bar{v}$

satisfying the velocity boundary conditions, since it furnishes the equilibrium equations as the Euler equations, the traction rate boundary conditions and the natural boundary conditions. In particular for dead loading, with the rigid constraints on S_V, then,

$$\delta \int U \, dV = 0. \tag{1.34}$$

Conversely if there is a field for which (1.34) is satisfied, it must be an eigenfield.

The complementary principle is that

$$\delta[\int \dot{\bar{F}} \cdot \dot{\bar{v}} \, dS_V - \int (U_C(\dot{\bar{\bar{S}}}) + \dot{\bar{g}} \cdot \dot{\bar{v}}) \, dV] = 0 \tag{1.35}$$

in the class of $\dot{\bar{\bar{S}}}$ satisfying the equilibrium equations and traction rate boundary conditions. For an actual mode (1.33) and (1.35) have the same value. Combining (1.7) and (1.33), Hill [50] has shown that

$$\delta[\int (U - \dot{\bar{g}} \cdot \dot{\bar{v}}) \, dV - \int \dot{\bar{F}} \cdot \dot{\bar{v}} \, dS_F] > 0 \tag{1.36}$$

Hence the integrand is not only stationary but an absolute minimum. The variational principle (1.33) provides the theoretical foundation for a variety of possible numerical solutions, Hutchison [63], Needleman [106], and Hibbitt et al [43]. Generalization to mixed variational statements has been given by Neale [102].

1.5 Specialization to Plates and Shells

Bifurcation of an E-P solid becomes possible at a given deformation stage when there exists a non-zero velocity field $\bar{v}$ such that

$$H(\bar{v}) - \Sigma(\bar{v}) > 0, \tag{1.9}$$

where $H(\bar{v})$ and $\Sigma(\bar{v})$ are given by (1.10) and (1.11) respectively. For a thin shell, Love's first approximation applies

$$\bar{\bar{\varepsilon}} = \bar{\bar{\varepsilon}}_o + z\bar{\bar{k}} \tag{1.37}$$

where $\bar{\bar{\varepsilon}}_o$ is the middle surface strain rate, and $\bar{\bar{k}}$ is the change in curvature due to deformation. The first term in (1.9) becomes

$$\int_V \left(\frac{\delta \bar{\bar{\tau}}}{\delta t}^J\right) : \bar{\bar{\varepsilon}}\, dV = \int \dot{\bar{\bar{N}}} : \bar{\bar{\varepsilon}}_o\, dS + \int \dot{\bar{\bar{M}}} : \bar{\bar{k}}\, dS \tag{1.38}$$

where

$$\dot{\bar{\bar{N}}} = \int_{-t/2}^{t/2} \left(\frac{\delta \bar{\bar{\tau}}}{\delta t}^J\right) dz$$

$$\dot{\bar{\bar{M}}} = \int_{-t/2}^{t/2} z \left(\frac{\delta \bar{\bar{\tau}}}{\delta t}^J\right) dz \tag{1.39}$$

The first term in (1.38) expresses the stretching work, whereas the second gives the bending work.

For a linear solid an alternative form for the first term in (1.9) is usually employed namely,

$$\int \left(\frac{\delta \bar{\bar{\tau}}}{\delta t}^J\right) : \dot{\varepsilon}\, dV = \int \bar{\bar{\varepsilon}} : \overset{4}{\bar{T}} : \dot{\bar{\bar{\varepsilon}}}\, dV$$

$$= \int \bar{\bar{\varepsilon}}_o : \overset{4}{\bar{T}} : \bar{\bar{\varepsilon}}_o \, dV + \int z^2 \bar{\bar{k}} : \overset{4}{\bar{T}} : \bar{\bar{k}} \, dV, \qquad (1.40)$$

where $\overset{4}{\bar{T}}$ is given by (1.28). Again, the contribution to stretching and bending are quite apparent in (1.40).

When the usual assumptions of plates and shells are invoked we have,

(i) ε_{13} and $\varepsilon_{23} << \varepsilon_{11}$, ε_{22} and ε_{12},

(ii) $\sigma_{3i} = 0$

and (iii) $\tau^{33} \varepsilon_{33} = 0$.

Upon using (1.28a) it follows that

$$\varepsilon_{33} = - (T^{\alpha\beta 33}/T^{3333}) \, \varepsilon_{\alpha\beta} \qquad (1.42)$$

Therefore the plane stress moduli $\overset{4}{\bar{M}}$ relating in-plane stress rates and strain rates become

$$\left(\frac{\delta \bar{\bar{\tau}}}{\delta t}\right)^{\nabla J} = \overset{4}{\bar{M}} : \bar{\bar{\varepsilon}} \qquad (1.43)$$

where

$$\overset{4}{\bar{M}} = \overset{4}{\bar{T}} - T^{\alpha\beta 33} T^{33k\delta}/T^{3333} \qquad (1.44)$$

The above equations constitute a full complement of equations for first order plate and shell theories including finite strain effects.

CHAPTER 2

CONSTITUTIVE EQUATIONS

2.1 Introduction

In problems involving the finite deformation of elastic-plastic solids there is a need for an adequate formulation which embraces both geometric and material non-linearities. The latter is embodied in the choice of an appropriate constitutive equation, and the present chapter takes as its theme the role of the constitutive equations in bifurcation analyses. Only these constitutive equations which have been most widely applied to model the behaviour of a rigid-plastic (R-P) or elastic-plastic (E-P) solid are examined. No attempt is made to generalize their form, following the more recent trends in the continuum theory of constitutive equations. This latter treatment begins with very general functional constitutive equations, and aims to define the restrictions imposed on the form of the equations through having to satisfy certain general principles. The works of Leigh [78] and Malvern [80] serve as a useful introduction to the topic.

The constitutive equation would appear to be crucial in bifurcation studies of a variety of structural and metalforming problems, and the root cause behind the so-called bifurcation paradox. Two of the most widely applied plasticity theories in bifurcation analyses are the incremental (J_2' flow) theory and the

J_2' deformation theory. The latter theory can be regarded as totally unacceptable under a general loading history, i.e. where both repeated loading and unloading is permitted. Nevertheless proponents of the theory have pointed to its utility in predicting bifurcation loads etc., more in keeping with experimental observations, assuming the material to be loading everywhere up to this point. Note, in the post-bifurcation regime where unloading becomes possible, the deformation theory must be suspect. The deformation theory permits a reduced value of the effective shear modulus vis à vis the elastic value in the incremental theory, and it is recognized that this leads to lower predicted values of bifurcation loads etc.. While this point is well documented, the purpose of the present chapter is to display the strengths and weaknesses of the respective theories in simple terms.

There is nothing to choose between the incremental and deformation theories for the case of radial loading. The differences arise under curved loading paths or when a sudden departure from radial loading arises (material still loading everywhere), and the resulting strain increment is required. As already mentioned, and discussed elsewhere by Sewell [130] and Hutchinson and Budiansky as quoted in [25], the elastic shear modulus is retained in the incremental theory while the secant modulus appears in the deformation theory. The latter, depending upon the level of plastic strain, can be considerably less than the former. As discussed herein weaknesses are present with both

theories. They both rely on the deviatoric stress state existing before the stress increment (change in path) is made. This leads to predictions such that if a torsional load increment was superimposed on a previous tensile loading history no plastic shear strain would accrue with the incremental theory, and it would be scaled according to the secant modulus in the deformation theory. Conversely, an axial load increment following axial and torsional loading gives rise to torsional strains with either theory.

The results of experimental investigations aimed at verifying one or another theory have not been unequivocal, and can prove to be at variance with either theory, Feigen [37]. Considerable difficulties might be anticipated with the experimentation when small loads (stresses) are superimposed on existing yield stress states, and the resulting strain response has to be recorded. Justification for the use of the deformation theory has been made on the basis of the development of a vertex on the yield surface. The experimental evidence for this fact is by no means conclusive, regions of high curvature have been reported but here again the experimental procedures are fraught with difficulty.

In modelling material behaviour great reliance is placed on data gathered from uniaxial tensile tests coupled with the oft-made assumption of a unique representative stress-strain behaviour, even though it is recognized that in many instances different deformation modes cannot be made equivalent by some

simple processing of the data. There is a paucity of published data dealing with the immediate material response once the loading path is changed, in particular the subsequent hardening rate may be very different from our expectations.

In the next sections an outline of both the flow and deformation theories is presented. Some other contemporary trends in bifurcation analyses are then reviewed briefly and the chapter concludes by discussing certain modifications to the classical incremental theory and the implication of the modifications.

2.2 General Considerations for Elastic-Plastic Constitutive Equations

Consider the isothermal deformation of a solid (in our case a metallic solid) whose mechanical properties do not depend on time. For an element of such a material, it is proposed that there exists a single-valued tensor relation of the form

$$\text{stress-rate component} = f(\text{strain-rate components}) \tag{2.1}$$

It is assumed that the strain increment be so small such that it can be decomposed into elastic and plastic part, in the following way

$$\dot{\underline{\underline{\varepsilon}}} = \dot{\underline{\underline{\varepsilon}}}^{e} + \dot{\underline{\underline{\varepsilon}}}^{p} \tag{2.2}$$

Lee [76] and Nemat-Nasser [110] have discussed alternative ways of decomposing the elastic and plastic terms, more suited for larger strain measures.

For elastic solids (2.1) can be expressed as

$$\overset{=}{\sigma}^{\cdot} = \overset{4}{\overline{K}} : \overset{=}{\epsilon} \tag{2.3}$$

where $\overset{4}{\overline{K}}$ is expressible in terms of Lamé's constants, G and λ, as

$$\overset{4}{\overline{K}} = 2G \overset{4}{\overline{1}} + \lambda \overset{==}{11} \tag{2.4}$$

It is to be understood that the elastic region is bounded by a hypersurface in the stress space, as shown diagrammatically in two dimensions in Figure 2.1.

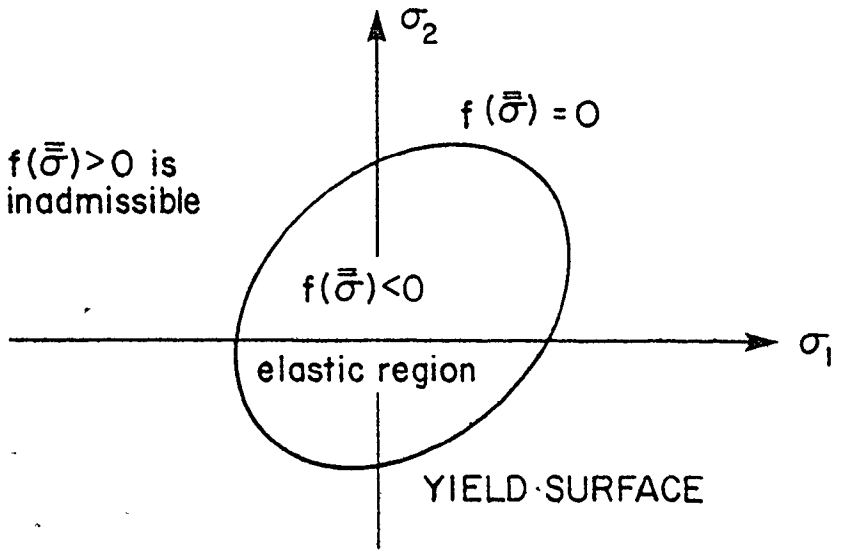

Figure 2.1 Yield surface in stress space

The different theories of plasticity relate the way the plastic strain increment changes for a given increment of stress, and hence specify equations (2.1). As already mentioned in section (1.3), frame indifferent stress rates should be used in

the constitutive relations for large deformations, and for E-P solids Jaumann's stress rate is the appropriate one.

2.2.1 J_2 Flow Theory

It is assumed that a plastic potential function exists which is identical to the von Mises yield function. In this case the rate equations (2.1) are linear and the plastic component of the strain rate can be expressed, according to Hill [50], as

$$\overset{=}{\dot{\varepsilon}}^{p} = \frac{\overset{=}{m}}{h}\, \overset{=}{m}:\left(\frac{\delta \overset{=}{\sigma}}{\delta t}\right)^{J} \quad , \quad \overset{=}{m}:\left(\frac{\delta \overset{=}{\sigma}}{\delta t}\right)^{J} > 0 \ . \tag{2.5}$$

Combining (2.2), (2.3) and (2.5) results in

$$\overset{=}{\dot{\varepsilon}} = \begin{bmatrix} \left[\overset{4}{K}^{-1} + \dfrac{\overset{=}{m}\,\overset{=}{m}}{h}\right]:\left(\dfrac{\delta \overset{=}{\sigma}}{\delta t}\right)^{J} & , \quad \overset{=}{m}:\left(\dfrac{\delta \overset{=}{\sigma}}{\delta t}\right)^{J} > 0 \\ \overset{4}{K}^{-1}:\left(\dfrac{\delta \overset{=}{\sigma}}{\delta t}\right)^{J} & , \quad \overset{=}{m}:\left(\dfrac{\delta \overset{=}{\sigma}}{\delta t}\right)^{J} \leq 0 \end{bmatrix} \tag{2.6}$$

The inverse is given by

$$\left(\frac{\delta \overset{=}{\sigma}}{\delta t}\right)^{J} = \begin{bmatrix} \left[\overset{4}{K} - \dfrac{\overset{4}{K}:\overset{=}{m}\;\overset{=}{m}^{T}:\overset{4}{K}}{h + \overset{=}{m}^{T}:\overset{4}{K}:\overset{=}{m}}\right]:\overset{=}{\dot{\varepsilon}} & , \quad \overset{=}{m}:\left(\dfrac{\delta \overset{=}{\sigma}}{\delta t}\right)^{J} > 0 \\ \overset{4}{K}:\overset{=}{\dot{\varepsilon}} & , \quad \overset{=}{m}:\left(\dfrac{\delta \overset{=}{\sigma}}{\delta t}\right)^{J} \leq 0 \end{bmatrix} \tag{2.7}$$

where

$$\overset{=}{m} = \overset{=}{m}^{T} = \frac{\overset{=}{\sigma}'}{||\overset{=}{\sigma}'||} \ ,$$

is the unit normal to the deviatoric yield surface. Upon expanding the $\frac{4}{K}$ term, the first of equations (2.7) can be rewritten as

$$\left(\frac{\delta \overset{=}{\sigma}^J}{\delta t}\right) = 2G \left[\overset{=}{I} + A \overset{=}{1}\overset{=}{1} - \mu \overset{=}{m}\overset{=}{m}\right] : \overset{=}{\epsilon} , \tag{2.8}$$

where

$$A = \frac{\nu}{1-2\nu} , \tag{2.9a}$$

and

$$\mu = \frac{2G}{h+2G} . \tag{2.9b}$$

Note that equations (2.5) can also be expressed as

$$\overset{=}{\epsilon}^p = \sqrt{\frac{2}{3}}\, \overset{=}{m}\, \frac{df(d\overset{=}{\sigma})}{h} \tag{2.10}$$

where

$$df(d\overset{=}{\sigma}) = d\overset{=}{\sigma} : \frac{\partial f}{\partial \overset{=}{\sigma}} = \sqrt{\frac{3}{2}}\, (d\overset{=}{\sigma} : \overset{=}{m}) , \tag{2.11}$$

and is to be interpreted as an increase in the size of the yield surface. Accordingly (2.10) states that any two stress increments $\Delta\overset{=}{\sigma}_1$ and $\Delta\overset{=}{\sigma}_2$ resulting in the same increase of the current yield surface would produce exactly the same plastic strain increment, see Figure 2.2.

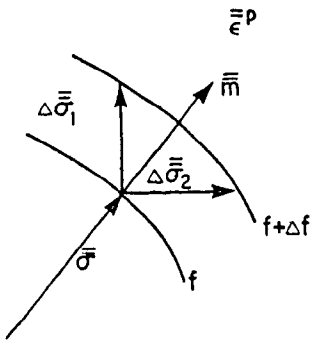

Figure 2.2 Stress rate and plastic strain rate vectors

The immediate outcome is that equations (2.5) and (2.10) cannot be inverted, as discussed by Hill [49, 53, 55], and the matrix of the plastic moduli in (2.5) is singular. We therefore cannot expect to obtain from (2.7) the result for a R-P solid as a limiting case when Young's modulus approaches infinity. This explains the reasoning behind the uniqueness of the deformation mode for R-P solids but not for the stress rates, where only the combination of stress rate components and not the components individually, is necessarily unique in the zone of deformation. Sewell [126] gave an inverse relation for the R-P solid, in which the stress rate is expressed in terms of the strain rate and an arbitrary tensor. He also pointed out that the inverse did not provide a unique dependence of stress-rate on strain-rate, even in the deforming region. On the other hand, for the E-P solid, the matrix of (2.6) can be inverted to yield (2.7). The inversion being possible because of the well behaved elastic matrix in (2.4). However, as shown in Appendix A, the matrix of (2.6) becomes more ill conditioned with plastic straining, especially for solids with negligible hardening.

A further drawback of the Prandtl-Reuss equations is that if a specimen had been previously deformed in uniaxial tension, the Prandtl-Reuss equations would imply that even if the next increment of stress were one of shear (e.g. torsional loading), the plastic shear strain increment would be zero. This is the result of the assumption that the directions of the plastic strain

increment and stress must coincide in spite of the fact that the two variables do not belong to the same configuration; see Figure 2.3.

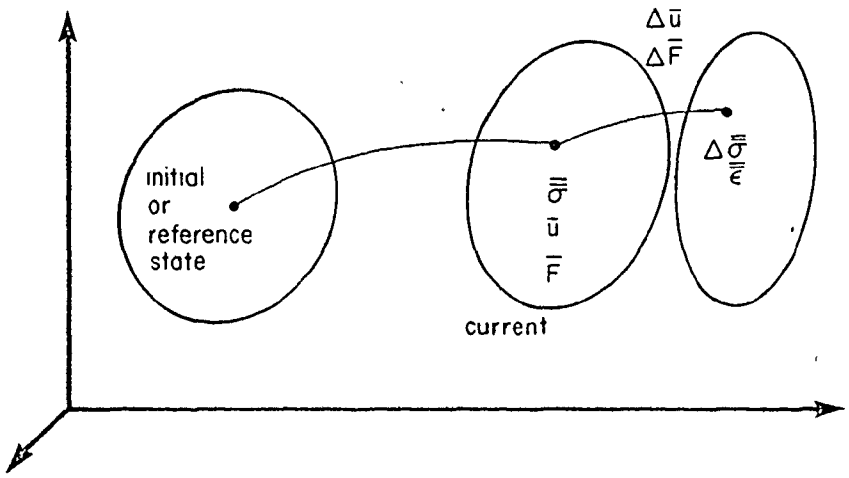

Figure 2.3 Variables in relation to different configurations

It is clear from (2.10) and Figure 2.2 that the plastic component of the strain rate is always lagging one step. Extreme care may therefore have to be exercised in any numerical technique when large increments are used and this becomes crucial in bifurcation analyses where all the calculations are based on one step.

To further examplify some of the difficulties that can be encountered with the Prandtl-Reuss equations, a typical rate problem, defined in Section 1.5 is considered and Kulkarni [73] has demonstrated that for plates and shells equations (1.42) reduce to

$$\begin{bmatrix} \frac{\delta\tau_{11}}{\delta t} \\ \frac{\delta\tau_{22}}{\delta t} \\ \frac{\delta\tau_{12}}{\delta t} \end{bmatrix}^{J} = \begin{bmatrix} \alpha_{11} & \alpha_{12} & \alpha_{13} \\ \alpha_{21} & \alpha_{22} & \alpha_{23} \\ \alpha_{31} & \alpha_{32} & \alpha_{33} \end{bmatrix} \begin{bmatrix} \epsilon_{11} \\ \epsilon_{22} \\ \epsilon_{12} \end{bmatrix} , \tag{2.12}$$

where

$$\alpha_{11} = 2G \frac{\{1-\mu[(m_{11}^2 + m_{33}^2) - \nu(m_{11}+m_{33})^2]\}}{(1-\nu) - \mu(1-2\nu)m_{33}^2} , \quad (a)$$

$$\alpha_{22} = 2G \frac{\{1-\mu[(m_{22}^2 + m_{33}^2) - \nu(m_{22}+m_{33})^2]\}}{(1-\nu) - \mu(1-2\nu)m_{33}^2} , \quad (b)$$

$$\alpha_{21} = \alpha_{12} = 2G \frac{\{\nu-\mu[2\nu\, m_{33}^2 + (1-\nu)\, m_{11}m_{22}]\}}{(1-\nu) - \mu(1-2\nu)\, m_{33}^2} , \quad (c) \tag{2.13}$$

$$\alpha_{33} = 2G , \quad (d)$$

and $$\alpha_{31} = \alpha_{32} = \alpha_{13} = \alpha_{23} = 0 . \quad (e)$$

Note that $\alpha_{33} = 2G$ irrespective of the stress increment, and moreover all the individual moduli in (2.13) are of the order of the elastic moduli.

When equations (2.12) are used in the bifurcation criterion (1.9), it is shown in chapter 3 that the resulting critical stresses are of the order of the elastic moduli. It is also demonstrated in chapter 3, section 3.4, that by invoking the condition of E-P incompressibility, it is possible to combine

certain terms in (2.13) such that the stress-rate components in (2.12) are in the order of the hardening parameter h. However, this approach cannot remove the α_{33} contribution dominating the bifurcation expression, which if it holds would imply that the buckling phenomenon is shear predominant. Such an assumption is untrue for elastic solids and therefore seems unrealistic for E-P solids. Another outcome of (2.12) and (2.13) is that the shear component of Jaumann stress rate is more than one order of magnitude higher than the two normal components depending on the ratio 2G/h, irrespective of the level of plastic straining. In other words, the above equations imply that the material response to different types of loading could be quite substantial (three orders of magnitude). Such a behaviour seems physically incorrect even for highly anisotropic materials.

2.2.2 J_2' Deformation Theory

In contrast to the incremental (flow) theories of plasticity, the deformation theory gives the total strain as a function of the current stress. In a scalar form this is given, for a R-P solid, as

$$\bar{\sigma} = E_s \bar{e}^p \tag{2.14}$$

where E_s is the secant modulus. The quantities $\bar{\sigma}$ and $\bar{e}^p$ are some scalar measures of the stress and total plastic strains respectively and defined in terms of the second invariant of the deviatoric components of these tensors as shown below;

$$\bar{\sigma} = \sqrt{3\, J_2'} = \sqrt{\frac{3}{2}\,(\overset{=}{\sigma}' : \overset{=}{\sigma}')} \; ; \tag{2.15}$$

$$\bar{e}^p = \sqrt{\frac{4}{3}\, J_{e^p}} = \sqrt{\frac{2}{3}\,(\overset{=}{e}^p : \overset{=}{e}^p)} \; . \tag{2.16}$$

Substituting from (2.15) and (2.16) into (2.14), the constitutive equations takes the form

$$\overset{=}{e}^p = \mu\, \overset{=}{\sigma}' \; , \; dJ_2' > 0 \tag{2.17}$$

The above equations represent a loading condition with

$$\overset{=}{\sigma}' : \overset{=}{\sigma}' = 2J_2'$$

and

$$\mu^2 = \frac{3}{2E_s} \tag{2.18}$$

The incremental form of (2.17) can be rewritten [65, 139] as

$$\dot{\overset{=}{\varepsilon}}^p = \frac{3}{2}\left[\frac{\overset{4.}{1}}{E_s} + \frac{1}{2J_2'}\left(\frac{1}{E_T} - \frac{1}{E_s}\right) \overset{=}{\sigma}' \overset{=}{\sigma}'\right] : \left(\frac{\delta \overset{=}{\sigma}}{\delta t}\right)^J \; , \; dJ_2' > 0 \; , \tag{2.19}$$

whose inverse is given by

$$\left(\frac{\delta \overset{=}{\sigma}}{\delta t}\right)^J = \frac{2}{3}\left[E_s \frac{4}{1} - \left(\frac{E_s - E_T}{2J_2'}\right) \overset{=}{\sigma}' \overset{=}{\sigma}'\right] : \dot{\overset{=}{\varepsilon}}^p . \tag{2.20}$$

Equations (2.19) and (2.20) show a linear relation between stress rate and strain rate. Equations (2.19) can also be expressed as

$$\overset{=}{\varepsilon}^{p} = \frac{3}{2E_s}\left(\frac{\delta \overset{=}{\sigma}}{\delta t}\right)^{J} + \sqrt{\frac{3}{2}}\left(\frac{1}{E_T} - \frac{1}{E_s}\right) df\ (d\overset{=}{\sigma}).\overset{=}{m} \qquad (2.19a)$$

where df is defined by (2.11). For unloading or a neutral change of stress ($df \leq 0$), such that $dJ_2' \leq 0$, it follows from (2.19a) that

$$\overset{=}{\varepsilon}^{p} = \frac{3}{2\,E_s}\left(\frac{\delta \overset{=}{\sigma}}{\delta t}\right)^{J}, \quad dJ_2' \leq 0 \qquad (2.21)$$

Objections to the deformation theory have been raised many times due to the prediction of a change in the plastic strain following unloading or a neutral loading as indicated above.

On the other hand Budiansky [9] has argued that the J_2' deformation theory cannot be labelled physically unacceptable for total loading histories. Batdorf [4] has pointed out that the bifurcation loads predicted by the deformation theory could be justified rigorously in nearly all cases by establishing the connection between the deformation and the incremental theory which develops a sharp corner on its yield surface provided we follow total loading histories, in which no activated loading function unloads. To be more specific suppose the fundamental solution satisfies proportional loading everywhere; the bifurcation solution is a linear combination of the fundamental solution increment and the eigenmode. We can always include a sufficiently large amount of the fundamental solution increment relative to the eigenmode (proper mode) such that the bifurcation mode satisfies the total loading restriction, see Hutchison [65].

The confusion in bifurcation applications apparently stems from the misconception that when bifurcation occurs total loading will be violated. As long as the fundamental solution satisfies total loading there are no grounds that we have yet mentioned which favour the bifurcation load predictions based on J_2' flow theory over those based on J_2' deformation theory or vice versa.

It is to be noted that when an increment of torsion is applied following uniaxial tension, (2.19) would indicate that

$$\dot{\bar{\bar{\varepsilon}}}^p = \frac{3}{2\,E_s}\left(\frac{\delta\bar{\bar{\sigma}}}{\delta t}\right)^{J_2'} , \quad dJ_2' > 0 \ ;$$

and the secant modulus may still be of the order of the elastic modulus for moderate strains. Similar to the J_2' flow theory, it is difficult to accept that a deviation, however small, from proportional loading could affect the material response in such a way that it could be more than one order of magnitude stiffer in one direction compared to the other directions, depending on the ratio (2G/h). It is also worth mentioning that the second contribution to the plastic moduli in equations (2.19) is singular (i.e. those in the direction of $\bar{\bar{\sigma}}'$ or $\bar{\bar{m}}$).

2.2.3 Contemporary Trends in Bifurcation Analyses

The bifurcation theory for compressive loading is reasonably well understood, but the difficulty in the application arises in identifying an adequate plasticity theory, Hutchison [65]. In the preceding sections, the advantages and limitations

of the J_2' deformation and flow theories were discussed, and in this section certain contemporary trends aimed at resolving the bifurcation paradox are summarised.

In general, the attempts to modify the incremental approaches have followed three main routes by allowing for:-

i) the concept of imperfections, Hutchison [64] and Neale [104],

ii) the introduction of a vertex at the current stress point on the yield surface, Sewell [130], and

iii) consideration of the rotations of the principal directions, Dubey [27].

Sewell [129] and Dubey [23] have shown that the critical stress is sensitive to the variations in the shape of the yield surface. Furthermore, if the yield surface has a corner, primary bifurcations involving no unloading from the yield surface within the body can occur; and the bifurcation loads could be markedly less than those associated with a smooth yield surface, Sewell [129, 130].

By using a flow rule at a yield vertex, Sewell [130] fitted the incipient moduli predicted by the constructed flow theory to the values which are given by J_2' deformation theory. However, it should be noted that the actual criteria of plastic loading in the two theories are different.

Dubey [28] and Dubey and Lind [33] have pointed out some inconsistencies in the Prandtl-Reuss equations and subsequently

Dubey [27] modified the constitutive relations to take into account the effect of rotation of the principal axes and thus to allow for a lower value of the effective shear modulus than the elastic shear modulus, see also Dubey and Pindera [34] and Elkholy [36]. Dubey [27] proposed an equation of the form,

$$\overset{=}{\sigma}' + \Delta\overset{=}{\sigma}' = 2\bar{G}\,(\overset{=}{e}'^{e} + \overset{=}{de}') \tag{2.22}$$

In the above equations $\overset{=}{e}'^{e}$ is the total deviatoric elastic strain, $\overset{=}{de}'$ is the total deviatoric strain increment, and $2\bar{G}$ a reduced shear modulus given by

$$2\bar{G} = \frac{2Gh}{h+2G\Delta f} \cdot \frac{2f+\Delta f}{2f+\Delta f} \tag{2.23}$$

However, Dubey, op. cit., does not point out that

$$\Delta f = \Delta f\,(\overset{=}{\Delta\sigma}) \tag{2.24}$$

Accordingly (2.22) is not a full inverse of the constitutive relations and therefore it is not legitimate to specify $\Delta\overset{=}{\sigma}$ and Δf separately. Hence, the conclusion reached by Dubey [30] and Elkholy [36], that the bifurcation stress depends on the increment of traction, in the manner specified above, has to be reviewed.

The generalizations of the constitutive relations which account for a singular yield surface with a pyramidal corner have been given by Koiter [72] and Sanders [123]. These theories are pertinent to the discussion of the use of the deformation theories in bifurcation analyses since for total loading histories they

coincide with the incremental theories of plasticity.

Hill [54] has shown that vertex formation is a general feature of a polycrystalline aggregate when localized slip in each grain is governed by the Schmid law. For a particular model of polycrystals, Hutchison [62], has demonstrated that a vertex does indeed develop on subsequent yield surfaces. He also observes that the plastic moduli predicted by the model in the case of increments of shear stress in a predominantly tensile loading program, are much closer to the predictions of deformation theory of plasticity than to those of a flow theory with a smooth yield surface. Stören and Rice [139] used a simplified constitutive model of a pointed vertex on subsequent yield loci, such that the equations of deformation theory for rigid-plastic solids apply. The derived equations are as follows; see Figure 2.4.

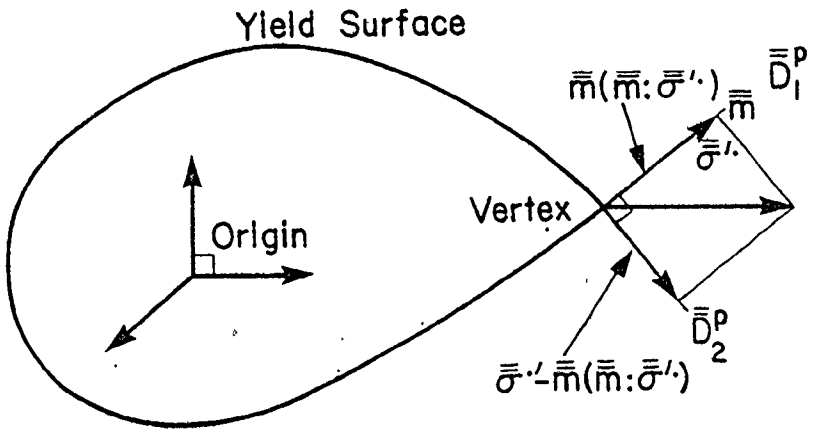

Figure 2.4 Constitutive model of a pointed vertex

$$\overset{=}{D}{}_1^p = \frac{1}{2E_T} \overset{=}{m}\ (\overset{=}{m}:\overset{=}{\sigma}{}^{\cdot\prime}), \tag{2.25}$$

and

$$\overset{=}{D}{}_2^p = \frac{1}{2E_s} [\overset{=}{\sigma}{}^{\cdot\prime} - \overset{=}{m}\ (\overset{=}{m}:\overset{=}{\sigma}{}^{\cdot\prime})] \tag{2.26}$$

With $\overset{=}{m}:\overset{=}{\sigma}{}^{\cdot\prime} = \overset{=}{m}:\overset{=}{\sigma}{}^{\cdot}$, the above equations reduce to

$$2\overset{=}{D}{}^p = \frac{1}{E_s} \overset{=}{\sigma}{}^{\cdot\prime} + (\frac{1}{E_T} - \frac{1}{E_s}) \overset{=}{m}\ (\overset{=}{m}:\overset{=}{\sigma}{}^{\cdot}) , \tag{2.27}$$

which are exactly the rate form equations of the deformation theory. The inverse is given by

$$\overset{=}{\sigma}{}^{\cdot\prime} = E_s\{2\ \overset{=}{D}{}^p - 2(\frac{E_s - E_t}{E_s})\ \overset{=}{\sigma}{}' \ \frac{\overset{=}{\sigma}{}' : \overset{=}{D}{}^p}{\overset{=}{\sigma}{}' : \overset{=}{\sigma}{}'}\ \} \tag{2.28}$$

It should be noted that eqns. (2.25) and (2.26) imply that the material properties in the increment correspond to an anisotropic solid, since a completely different relation is obtained if the moduli E_s and E_T were interchanged. If the moduli in the normal and tangential directions to the yield surface were given the same value, i.e.

$$\overset{=}{D}{}_1^p = \frac{1}{2E_T} \overset{=}{m}(\overset{=}{m}:\overset{=}{\sigma}{}^{\cdot})$$

and

$$\overset{=}{D}{}_2^p = \frac{1}{2E_T} [\overset{=}{\sigma}{}^{\cdot\prime} - \overset{=}{m}(\overset{=}{m}:\overset{=}{\sigma}{}^{\cdot})] , \tag{2.29}$$

it follows that $\overset{=}{D}{}^p = \frac{1}{2E_T} \overset{=}{\sigma}{}^{\cdot}$,

where $\overset{=}{D}^p$ and $\overset{=}{\sigma}^{\cdot}$ are deviatoric. Hutchison and Neale [66] applied a finite strain version of J_2' deformation theory, somewhat different to that proposed by Storen and Rice [139]. In this case the instantaneous shear modulus is given by Hill's formula [58] for the finite deformation of isotropic elastic solids.

Other attempts at modifying the Prandtl-Reuss equations are to be found in the work of Dubey and Ariaratnam [31] and Dubey and Mróz [32]. The applicability of these methods to practical problems has still to be demonstrated, although Bruhns and Thermann [7] have queried the order of approximation in some of the expressions in the work of Dubey and Ariaratnam, op. cit.

2.3 Alternative Approaches to Bifurcation Analyses

2.3.1 A Possible Approach for the Bifurcation of a Rigid-Plastic Solid

For rigid-plastic solids obeying the von Mises yield criterion, the deviatoric stresses and strain rates have the same directions. In this case $\Sigma(\bar{v})$ in (1.11) takes a simpler form. Since

$$\overset{=}{L} = \overset{=}{D} + \overset{=}{W} \quad , \tag{2.30a}$$

$$\overset{=}{L}^T = \overset{=}{D}^T + \overset{=}{W}^T = \overset{=}{D} - \overset{=}{W} \quad . \tag{2.30b}$$

Therefore

$$\overset{=}{\sigma}: \overset{=}{L}^T \cdot \overset{=}{L} = \overset{=}{\sigma}:[(\overset{=}{D}\cdot\overset{=}{D} - \overset{=}{W}\cdot\overset{=}{W}) + (\overset{=}{D}\cdot\overset{=}{W} - \overset{=}{W}\cdot\overset{=}{D})] \tag{2.31}$$

Furthermore since

$$\underline{\underline{\sigma}} = \underline{\underline{\sigma}}^T \ , \ \underline{\underline{D}} = \underline{\underline{D}}^T \text{ and } \underline{\underline{W}} = -\underline{\underline{W}}^T \ ,$$

it follows that

$$\underline{\underline{\sigma}} : \underline{\underline{D}} \cdot \underline{\underline{W}} = \underline{\underline{\sigma}} : \underline{\underline{W}} \cdot \underline{\underline{D}} = 0 \ , \tag{2.32}$$

and (2.31) reduces to

$$\underline{\underline{\sigma}} : \underline{\underline{L}}^T \cdot \underline{\underline{L}} = \underline{\underline{\sigma}} : [\underline{\underline{D}} \cdot \underline{\underline{D}} - \underline{\underline{W}} \cdot \underline{\underline{W}}] \ . \tag{2.33}$$

By substituting in (1.11), $\Sigma(\bar{v})$ can be rewritten as

$$\Sigma(\bar{v}) = \int \underline{\underline{\sigma}} : \underline{\underline{L}}^T \cdot \underline{\underline{L}}^T \, dV \ . \tag{2.34}$$

Similarly $H(\bar{v})$ of (1.10) can be expressed as,

$$H(\bar{v}) = \int (\frac{\delta \underline{\underline{\tau}}}{\delta t})^J : \underline{\underline{\varepsilon}} \, dV$$

$$= \int [\underline{\underline{\sigma}}^{\cdot} + \underline{\underline{\sigma}} \cdot \underline{\underline{W}} - \underline{\underline{W}} \cdot \underline{\underline{\sigma}}] : \underline{\underline{\varepsilon}} \, dV \ . \tag{2.35}$$

Substituting from (2.30) and (2.32) into (2.35) and considering that the strain rate is deviatoric, $H(\bar{v})$ takes the form

$$H(\bar{v}) = \int \underline{\underline{\sigma}}^{\cdot} : \underline{\underline{\varepsilon}} \, dV \ , \tag{2.36}$$

where the operator of the material derivative in (2.35) and (2.36) is defined as

$$(\ )^{\cdot} = \frac{\partial (\ )}{\partial t} + \bar{v} \cdot [\frac{\partial (\ )}{\partial \bar{x}}] \tag{2.37}$$

and the rate of deformation tensor $\underline{\underline{D}}$ is defined as the Eulerian

strain rate tensor $\dot{\bar{\bar{\varepsilon}}}$.

Instead of using (2.34) and (2.36), Kulkarni [73] adopted an approach identical to the one by Dubey and Ariaratnam [31] in which the incremental elastic work term in the uniqueness criterion is neglected. This can be achieved by first writing

$$(\frac{\delta\bar{\bar{\tau}}}{\delta t})^J : \dot{\bar{\bar{\varepsilon}}} = (\frac{\delta\bar{\bar{\tau}}}{\delta t})^J : (\dot{\bar{\bar{\varepsilon}}} - \dot{\bar{\bar{\varepsilon}}}^p) + (\frac{\delta\bar{\bar{\tau}}}{\delta t})^J : \dot{\bar{\bar{\varepsilon}}}^p \qquad (2.38)$$

Substituting into the above the expression for $(\delta\bar{\bar{\tau}}/\delta t)^J$, from (2.3) then (2.38) becomes

$$(\frac{\delta\bar{\bar{\tau}}}{\delta t})^J : \dot{\bar{\bar{\varepsilon}}} = (\dot{\bar{\bar{\varepsilon}}} - \dot{\bar{\bar{\varepsilon}}}^p) : \bar{\bar{\bar{\bar{K}}}} : (\dot{\bar{\bar{\varepsilon}}} - \dot{\bar{\bar{\varepsilon}}}^p) + (\dot{\bar{\bar{\varepsilon}}} - \dot{\bar{\bar{\varepsilon}}}^p) : \bar{\bar{\bar{\bar{K}}}} : \dot{\bar{\bar{\varepsilon}}}^p. \qquad (2.39)$$

The first term in (2.39) corresponds to the elastic contribution to the incremental energy and this is assumed negligible at large plastic strains. The expression for plastic strains is given by

$$\dot{\bar{\bar{\varepsilon}}}^p = \frac{\bar{\bar{m}}}{h} \bar{\bar{m}} : (\frac{\delta\bar{\bar{\tau}}}{\delta t})^J$$

$$= \frac{\bar{\bar{m}}}{h} \bar{\bar{m}} : [\bar{\bar{\bar{\bar{K}}}} - \frac{\bar{\bar{\bar{\bar{K}}}} : \bar{\bar{m}} \; \bar{\bar{m}} : \bar{\bar{\bar{\bar{K}}}}}{h + \bar{\bar{m}} : \bar{\bar{\bar{\bar{K}}}} : \bar{\bar{m}}}] : \dot{\bar{\bar{\varepsilon}}}$$

$$= \bar{\bar{m}} \frac{\bar{\bar{m}} : \bar{\bar{\bar{\bar{K}}}} : \dot{\bar{\bar{\varepsilon}}}}{h + \bar{\bar{m}} : \bar{\bar{\bar{\bar{K}}}} : \bar{\bar{m}}} \qquad (2.40)$$

Upon substituting (2.40) and the reduced form of (2.39) into (1.9) the resulting expression is

$$\delta \int \{h \left[\frac{\overline{\overline{\overline{\overline{m}}}}:\overline{\overline{\overline{\overline{K}}}}:\overline{\overline{\overline{\overline{\varepsilon}}}}}{h+\overline{\overline{\overline{\overline{m}}}}:\overline{\overline{\overline{\overline{K}}}}:\overline{\overline{\overline{\overline{m}}}}}\right]^2 - 2\,\overline{\overline{\overline{\sigma}}}:\overline{\overline{\overline{\varepsilon}}}^{\bullet}\overline{\overline{\overline{\varepsilon}}} + \overline{\overline{\overline{\sigma}}}:\overline{\overline{\overline{L}}}^{T}\cdot\overline{\overline{\overline{L}}}\} \, dV = 0 \qquad (2.41)$$

The first term can be expanded using the elastic moduli in equation (2.4) to yield

$$\delta \int [\mu^2 h(\overline{\overline{\overline{m}}}:\overline{\overline{\overline{\varepsilon}}})^2 - 2\overline{\overline{\overline{\sigma}}}:\overline{\overline{\overline{\varepsilon}}}^{\bullet}\overline{\overline{\overline{\varepsilon}}} + \overline{\overline{\overline{\sigma}}}:\overline{\overline{\overline{L}}}^{T}\cdot\overline{\overline{\overline{L}}}] \, dV = 0. \qquad (2.42)$$

It should be noted that (2.42) applies only when there is no unloading anywhere in the material, and for plane stress conditions $(\delta\tau_{33}/\delta\tau)^J$ is set equal to zero throughout. It transpires that

$$\varepsilon_{33} = A_1\varepsilon_{11} + A_2\varepsilon_{22} \, , \qquad (2.43)$$

where
$$A_1 = -\frac{\nu-\mu(1-2\nu)m_{11}m_{33}}{(1-\nu)-\mu(1-2\nu)m_{33}^2} \, , \qquad (2.44a)$$

and
$$A_2 = -\frac{\nu-\mu(1-2\nu)m_{22}m_{33}}{(1-\nu)-\mu(1-2\nu)m_{33}^2} \, . \qquad (2.44b)$$

Using the Love-Kirchhoff assumptions then, as demonstrated before, the buckling criterion can be reduced to the form

$$\delta(U_m + U_b + W) = 0 \qquad (2.45)$$

In this instance

$$U_m = \int_S t \{\mu^2 h [C_{11}^2 \varepsilon_{11}^{o2} + C_{22}^2 \varepsilon_{22}^{o2} + 2C_{11} C_{22} \varepsilon_{11}^{o} \varepsilon_{22}^{o}]$$

$$- 2 [\sigma_{11}(\varepsilon_{11}^{o2} + \varepsilon_{12}^{o2}) + \sigma_{22}(\varepsilon_{21}^{o2} + \varepsilon_{22}^{o2})]\} \, dS \qquad (2.46)$$

$$U_b = S\int \frac{t^3}{12} \{\mu^2 h [C_{11}^2 k_{11}^2 + C_{22}^2 k_{22}^2 + 2C_{11} C_{22} k_{11} k_{22}]$$

$$- 2 [\sigma_{11}(k_{11}^2 + k_{12}^2) + \sigma_{22}(k_{21}^2 + k_{22}^2)\} dS \qquad (2.47)$$

$$W = S\int t \{\sigma_{11} [(\frac{\partial u}{\partial x_1})^2 + (\frac{\partial v}{\partial x_1})^2 + (\frac{\partial w}{\partial x_1})^2]$$

$$+ \sigma_{22} [(\frac{\partial u}{\partial x_2})^2 + (\frac{\partial v}{\partial x_2})^2 + (\frac{\partial w}{\partial x_2})^2]\} dS \qquad (2.48)$$

$$C_{11} = A_1 m_{33} + m_{11} \qquad (2.49a)$$

$$C_{22} = A_2 m_{33} + m_{22} \qquad (2.49b)$$

As already mentioned, Bruhns and Thermann [7] have queried the order of approximation by neglecting the elastic energy. However, as will be shown in chapter 3, the results of such a model can be in better agreement with experimental data than analyses employing the Prandtl-Reuss equations.

2.3.2 A Re-evaluation of the Prandtl-Reuss Equations in Bifurcation Analyses

Some of the shortcomings of the Prandtl-Reuss equations have been raised in section 2.2. Physically we expect the stress and strain increments to be related in the following way

$$\overset{=}{\dot{\sigma}} = \overset{4}{\overline{D}} : \overset{=}{\dot{\varepsilon}} \quad , \qquad (2.50)$$

where the components of $\overset{4}{\overline{D}}$ correspond to the tangent modulus.

At large plastic strains, in particular, we expect the bracketed quantity in either equations (2.7) or (2.8) to be relatively small and

$$2G\ [\underline{\underline{\underline{\underline{1}}}}+A\underline{\underline{1}}-\mu\ \underline{\underline{\underline{\underline{m}}}}\underline{\underline{m}}]:\underline{\underline{\underline{\underline{\varepsilon}}}} = \underline{\underline{\underline{\underline{D}}}}:\underline{\underline{\underline{\underline{\varepsilon}}}} \tag{2.51}$$

The order of magnitude of the individual moduli in (2.13) was criticized earlier and hence the components of $\underline{\underline{\underline{\underline{D}}}}$ are not in the order of the tangent modulus. On the other hand, not all buckling phenomena occur at relatively low strains, as will be shown for conical dies later in this thesis, and hence an order of approximation suitable for relatively large plastic strains ought to be considered.

At large strains with $h << 2G$, to a good order of approximation we may write

$$\mu = \frac{2G}{h+2G} = \frac{1}{1+\delta} \simeq (1-\delta) \tag{2.52}$$

where

$$\delta = h/2G << 1 \tag{2.53}$$

Now let $\varepsilon_{22} = x\varepsilon_{11}$ and in this case (2.12) can be expressed as,

$$\left(\frac{\delta\tau_{11}}{\delta t}\right)^J = \varepsilon_{11}\ (\alpha_{11} + x\alpha_{12})$$

$$\left(\frac{\delta\tau_{22}}{\delta t}\right)^J = \varepsilon_{11}\ (\alpha_{12} + x\alpha_{22}) \tag{2.54}$$

The use of the above equations is simplified if the assumption of elastic-plastic incompressibility of the solid is invoked. This arises because in general to obtain x, given by

$$x = \frac{\underline{\underline{\varepsilon}} : \bar{e}_2 \bar{e}_2}{\underline{\underline{\varepsilon}} : \bar{e}_1 \bar{e}_1}, \qquad (2.55)$$

it is necessary to solve for $(\frac{\delta \underline{\underline{\tau}}}{\delta t})^J$ in (2.6). However for large plastic strains $||\underline{\underline{\varepsilon}}^p|| >> ||\underline{\underline{\varepsilon}}^e||$

and therefore $\underline{\underline{\varepsilon}}^p \simeq \underline{\underline{\varepsilon}}$ (2.56)

By combining (2.55), (2.56) and (2.5), x may be expressed as

$$x = \frac{m_{22}}{m_{11}} \qquad (2.57)$$

The application of (2.54) to some particular stress systems is demonstrated below

(i) Uniaxial Tension

$$x = -\frac{1}{2}$$

$$\alpha_{11} + x\,\alpha_{12} = h\,[\frac{1+3A}{1+2A-\mu/3}] \qquad (2.58)$$

where A and μ are given by (2.9a) and (2.9b) respectively.

(ii) Equi-Biaxial Tension

$$x = 1$$

$$\alpha_{11} + x\alpha_{12} = \alpha_{12} + x\alpha_{22}$$

$$= h\,[\frac{1+3A}{1+A-2\mu/3}] \qquad (2.59)$$

(iii) Pure Shear

$$x = -1$$

$$\alpha_{11} + x\alpha_{12} = -(\alpha_{12} + x\alpha_{22}) = h \tag{2.60}$$

The above examples illustrate that when the moduli of (2.7), for the normal strain rates, are combined as in (2.54), the final expression will be always in the order of the tangent modulus. Accordingly when the usual thin shell approximations are used we have

$$\left(\frac{\delta \overset{=}{\tau}}{\delta t}\right)^{J} :\varepsilon = \alpha_{11}\varepsilon_{11}^{2} + \alpha_{22}\varepsilon_{22}^{2} + 2\alpha_{12}\varepsilon_{11}\varepsilon_{22} + 2\alpha_{33}\varepsilon_{12}^{2}$$

$$= \varepsilon_{11}^{2}\,[(\alpha_{11}+x\alpha_{12}) + x(\alpha_{12}+x\alpha_{22})] + 2\alpha_{33}\varepsilon_{12}^{2}. \tag{2.61}$$

Substituting from (1.37) into (2.61) gives

$$\left(\frac{\delta \overset{=}{\tau}}{\delta t}\right)^{J} :\varepsilon = [(\alpha_{11}+x\alpha_{12}) + x(\alpha_{12}+x\alpha_{22})]\,(\varepsilon_{11}^{\circ} + zk_{11})^{2}$$

$$+ 2\alpha_{33}(\varepsilon_{12}^{\circ} + zk_{12})^{2}. \tag{2.62}$$

If stretching work is neglected the above equation reduces to

$$\left(\frac{\delta \overset{=}{\tau}}{\delta t}\right)^{J} :\varepsilon = (zk_{11})^{2}\,[(\alpha_{11}+x\alpha_{12}) + x(\alpha_{12}+x\alpha_{22})]$$

$$+ 2(zk_{12})^{2}\,\alpha_{33}\,, \tag{2.63}$$

and in this case

$$x = \frac{\overset{=}{k}:\bar{e}_2\bar{e}_2}{\overset{=}{k}:\bar{e}_1\bar{e}_1} = \frac{k_{22}}{k_{11}}\,. \tag{2.64}$$

Upon substitution in (1.9), with $\bar{v} = \bar{o}$ on S_v, the bifurcation criterion becomes

$$\int \{\varepsilon_{11}^2 [(\alpha_{11}+x\,\alpha_{12}) + x(\alpha_{12}+x\,\alpha_{22}) - 2(\sigma_{11}+x^2\sigma_{22})]$$

$$+ 2\,\varepsilon_{12}^2(\alpha_{33}-\sigma_{11}-\sigma_{22}) + \sigma_{ik}\,w_{j,i}\,w_{j,k}\}\,dV > 0, \qquad (2.65)$$

for all fields vanishing on S_v (but not identically zero) and which satisfy (2.57). All the bracketed quantities in (2.65) are of the order of the modulus h. The exception is the term

$$(\alpha_{33} - \sigma_{11} - \sigma_{22})$$

where, as demonstrated earlier, α_{33} is twice the elastic shear modulus, 2G, as a consequence of the Prandtl-Reuss equations.

In any numerical procedure it is now proposed that h is substituted for 2G in order to avoid the ε_{12}^2 term dominating the calculations. The above reasoning is based on the assumption that ε_{11} and ε_{12} are of the same order of magnitude, since the change in curvature has to obey the Peterson-Mainardi-Codazzi equations for the deformed surface, and hence k_{11} and k_{12} cannot be selected arbitrarily. One might question why immediate recourse was not made to "deformation theory" if in the final analysis the intention is to replace the elastic modulus by a tangent modulus. However, it is considered that the present method demonstrates, in an unambiguous manner, the problems associated with the use of the Prandtl-Reuss equations. It is to be noted that the use of equations (2.57) and (2.64) imposes certain restrictions on the choice of velocity fields, as is demonstrated later.

2.4 Proposed Modification to the Prandtl-Reuss Equations

2.4.1 Introduction

In the present section a modification to the Prandtl-Reuss equations is proposed. The matrix of plastic moduli is chosen to be nonsingular so that the response for an elastic solid and a R-P solid are obtained as limiting cases of an E-P solid. At the same time the modified equation does not suffer a discontinuity in strain during unloading as is the case with the J_2' deformation theory.

It will be shown that the proposed equation meets the continuity requirement and that the boundary value problem is unique, when it is formulated in terms of rates. The maximum work principle is also given for the proposed equation. The application of the proposed equation to buckling problems eases the bifurcation paradox, as demonstrated here-in, for the special case where the stretching work is neglected. However the proposed equation still cannot predict the plastic shear increment for a uniaxially stressed specimen on which an increment of torsion is applied. Further discussion on this aspect is presented later in the thesis.

2.4.2 Proposed Modification

Following the same approach in the development of the incremental theory, as proposed by Hill [44] and Martin [82], a yield function of the following form is assumed

$$f(J_2') = F(W^p) = C. \tag{2.66}$$

In the above expression

$$W^p = \int \bar{\bar{\sigma}} : \bar{\bar{\varepsilon}}^p \tag{2.67}$$

and $$df = dW^p \frac{\partial F}{\partial W^p} ;$$

or to a second order

$$\Delta f = [(\bar{\bar{\sigma}} + \frac{1}{2} \Delta\bar{\bar{\sigma}}) : \bar{\bar{\varepsilon}}^p] F' \tag{2.68}$$

where $$F' = \frac{\partial F}{\partial W^p} .$$

By expressing

$$\bar{\bar{\varepsilon}}^p = \bar{\bar{G}} \Delta f , \tag{2.69}$$

the condition for a neutral change of stress is satisfied if $\bar{\bar{G}}$ is taken as a some symmetric tensor; which is also deviatoric in order to satisfy plastic incompressibility. Here it is assumed that

$$\bar{\bar{G}} = \bar{\bar{G}} (\bar{\bar{\sigma}} , \int \bar{\bar{\varepsilon}} , \bar{\bar{\sigma}}') \tag{2.70}$$

Equation (2.70) is a departure from the existing theories, since $\bar{\bar{G}}$, amongst other things, is taken as a function of $\bar{\bar{\sigma}}'$ (or $\Delta\bar{\bar{\sigma}}$). The notion of a plastic potential, $g(\bar{\bar{\sigma}}')$, - which is a quadratic function of the stresses - is still retained and from which the plastic strain increment can be obtained in the FINAL CONFIGURATION i.e. after the increment is applied. In this case

$$\overset{=}{G} = b \frac{\partial g}{\partial \overset{=}{\sigma}} \Big|_{\overset{=}{\sigma}+\Delta\overset{=}{\sigma}} , \tag{2.71}$$

where b is a scalar function of the stress invariants and possibly also of the strain history.

Upon combining (2.68), (2.69), (2.71) and contracting with $(\sigma + \Delta\sigma)$, it follows that

$$(\overset{=}{\sigma}+\Delta\overset{=}{\sigma}) : \overset{=}{\epsilon}^{p} = b(\overset{=}{\sigma}+\Delta\overset{=}{\sigma}) : \frac{\partial g}{\partial \overset{=}{\sigma}} \Big|_{\overset{=}{\sigma}+\Delta\overset{=}{\sigma}} [(\overset{=}{\sigma} + \frac{1}{2} \Delta\overset{=}{\sigma}) : \overset{=}{\epsilon}^{p}] F' . \tag{2.72}$$

From Euler's theorem of homogeneous functions

$$(\overset{=}{\sigma} + \Delta\overset{=}{\sigma}) : \frac{\partial g}{\partial \overset{=}{\sigma}} \Big|_{\overset{=}{\sigma}+\Delta\overset{=}{\sigma}} = 2,$$

and it is reasonable to assume

$$|| \Delta\overset{=}{\sigma} || << || \overset{=}{\sigma} || .$$

Equation (2.72) therefore provides the following relationship

$$2F' bg(\overset{=}{\sigma} + \Delta\overset{=}{\sigma}) = 1 . \tag{2.73}$$

Substituting from (2.71), (2.68) into (2.69) and eliminating b from (2.73), the plastic strain increment (rate) can be expressed as

$$\overset{=}{\epsilon}^{p} = \frac{1}{2F' g} \frac{\partial g}{\partial \overset{=}{\sigma}} \Big|_{\overset{=}{\sigma}+\Delta\overset{=}{\sigma}} \Delta f . \tag{2.74}$$

The above equation takes a special form with the von Mises yield criterion, since in this case

$$\bar{\sigma} = f = \sqrt{3J_2'} , \tag{2.75}$$

and

$$F' = \frac{H'}{\bar{\sigma}} \tag{2.76}$$

where H' is the rate of change of the equivalent stress with respect to equivalent strain. Substituting (2.75) and (2.76) into (2.74), the plastic strain increment may be expressed as

$$\overset{=}{\varepsilon}^p = \overset{=}{m}^* \frac{\overset{=}{m} : \overset{=}{\Delta\sigma}}{h} , \quad (\overset{=}{m} : \overset{=}{\Delta\sigma}) > 0 \tag{2.77}$$

where

$$\overset{=}{m}^* = \frac{\overset{=}{\sigma}' + \overset{=}{\Delta\sigma}'}{\| \overset{=}{\sigma}' + \overset{=}{\Delta\sigma}' \|} , \tag{2.78}$$

and is the unit normal to the deviatoric yield surface at the final configuration, see Figure 2.5,

and

$$h = H' \left\| \frac{\overset{=}{\sigma}' + \overset{=}{\Delta\sigma}'}{\| \overset{=}{\sigma}' \|} \right\| = H' \tag{2.79}$$

For a R-P solid, (2.77) takes the form

$$\overset{=}{\varepsilon} = \frac{1}{B} (\overset{=}{\sigma}' + \overset{=}{\Delta\sigma}') . \tag{2.80}$$

The inverse of (2.80) is demonstrated in Appendix B, and the result is

$$\overset{=}{\Delta\sigma}' = B \overset{=}{\varepsilon} - \overset{=}{\sigma}' \tag{2.81}$$

where $$\frac{1}{B} = \frac{\overset{=}{\sigma}' : \overset{=}{\epsilon}}{2J_2' + h(\overset{=}{\sigma}' : \overset{=}{\epsilon})} \quad . \tag{2.82}$$

The quantity 1/B could be interpreted as a local reduced modulus, see Figure 2.6. Equations (2.80) and (2.81) show that the directions of the plastic strain increment are coincident with those of the total deviatoric stress (after the increment) and therefore express the directional dependence of $\overset{=}{\epsilon}^p$ on the stress increment $\overset{=}{\Delta\sigma}$. It should be noted that $\overset{=}{\epsilon}^p$ in (2.80) or (2.81) is to be understood as an increment of strain and not strain rate and that the approximation of the scalar quantity, $h \simeq H'$ in (2.79), helps in the inversion of (2.80) and is adopted primarily to provide a nonsingular relation between $\overset{=}{\epsilon}$ and $\overset{=}{\Delta\sigma}$.

For an elastic-plastic solid equations (2.2), (2.3) and (2.77) are combined and following some lengthy algebraic manipulations, given in Appendix B, the inverse is found to be

$$\overset{=}{\Delta\sigma} = X\,(\overset{=}{\epsilon} - L\overset{=}{\sigma}') + Y\,(\overset{=}{\epsilon}:\overset{=}{1})\,\overset{=}{1}\,, \tag{2.83}$$

where X, L and Y are defined in the Appendix B. As demonstrated in Appendix B, equations (2.81) can be derived as a limiting case of (2.83) when the modulus of rigidity goes to infinity. Furthermore, the result for an elastic solid is recovered when the hardening rate h approaches infinity.

Figure (2.7) shows a schematic representation of the strain response to a given stress path according to the Prandtl-Reuss

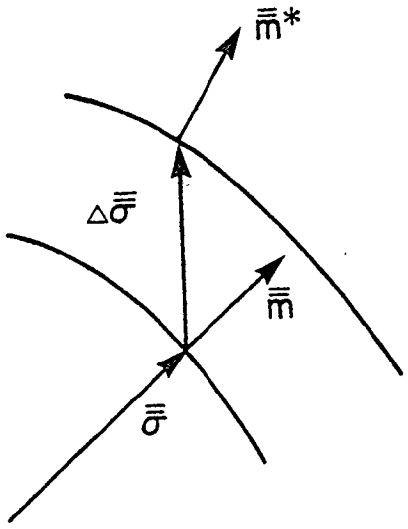

Figure 2.5 Normality principle at final configuration

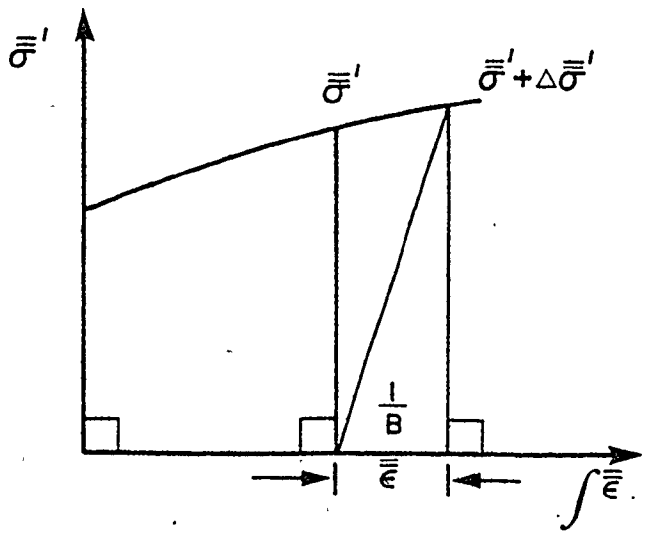

Figure 2.6 Local reduced modulus

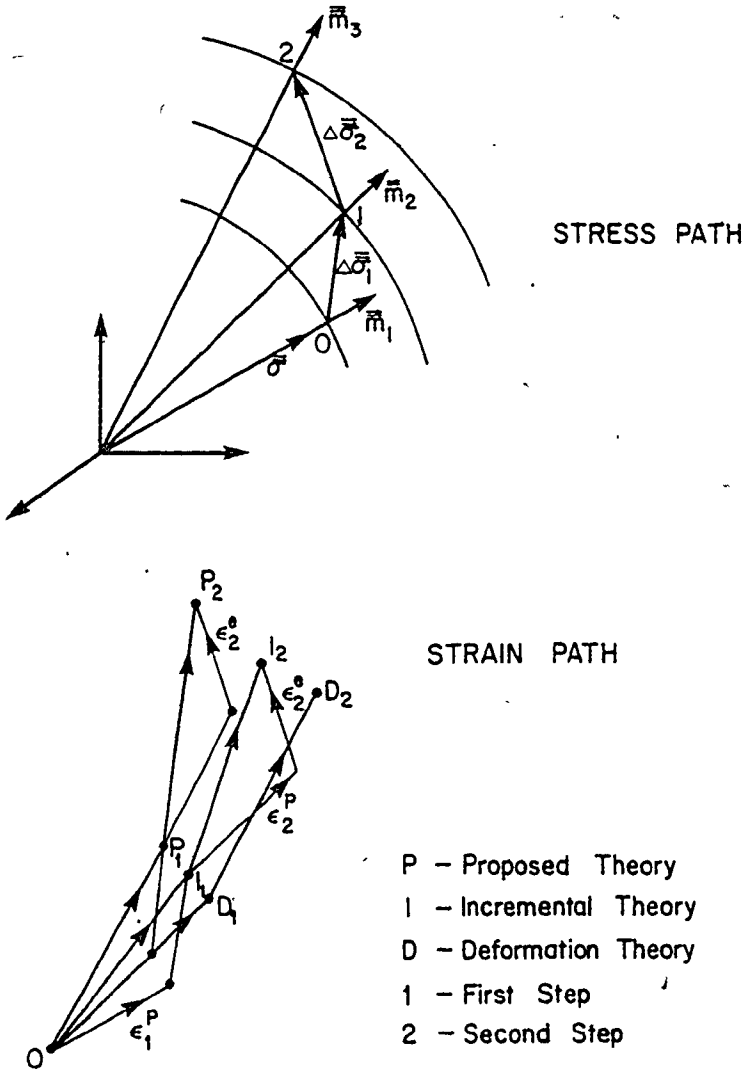

Figure 2.7 Comparison between the strain path for materials obeying the J_2' deformation, J_2' flow theory and the proposed modification to Prandtl-Reuss equations.

equations, the deformation theory and the proposed modification to the Prandtl-Reuss equations.

It is clear that the proposed equation does not suffer the disadvantage of a strain discontinuity which can arise when unloading and reloading when the deformation theory is employed.

The figure also illustrates that the proposed equation is more sensitive to the change of stress rate than the others.
In fact certain experiments do show a larger sensitivity of plastic strain rate directions than that predicted by the J_2' flow theory, witness the work of Peters et al [117]. In Figure 2.8 the difference between the Prandtl-Reuss and the proposed equation is shown for a one-step and two-step stress increment. Here again the final increment will always be more sensitive to the direction of the stress increment, with the proposed equation.

For the particular case of proportional loading

$$\underset{=}{\Delta\sigma}' = C\underset{=}{\sigma}',$$

and when the above is substituted in (2.77), we obtain

$$\underset{=}{\dot{\varepsilon}}^p = \frac{\underset{=}{\sigma}' + C\underset{=}{\sigma}'}{\| \underset{=}{\sigma}' + C\underset{=}{\sigma}' \|} \frac{\underset{=}{m} : \underset{=}{\Delta\sigma}}{h}, \qquad C > 0$$

$$= \underset{=}{m} \frac{\underset{=}{m} : \underset{=}{\Delta\sigma}}{h}, \tag{2.84}$$

and the proposed equations (2.77) reduce to the Prandtl-Reuss equations. In terms of stress increments, (2.84) can be rewritten as

$$\underset{=}{\dot{\varepsilon}}^p = C_1 \underset{=}{m} = C_2 \underset{=}{\sigma}' \tag{2.85}$$

where $$C_1 = \frac{\underset{=}{m} : \underset{=}{\Delta\sigma}}{h}$$

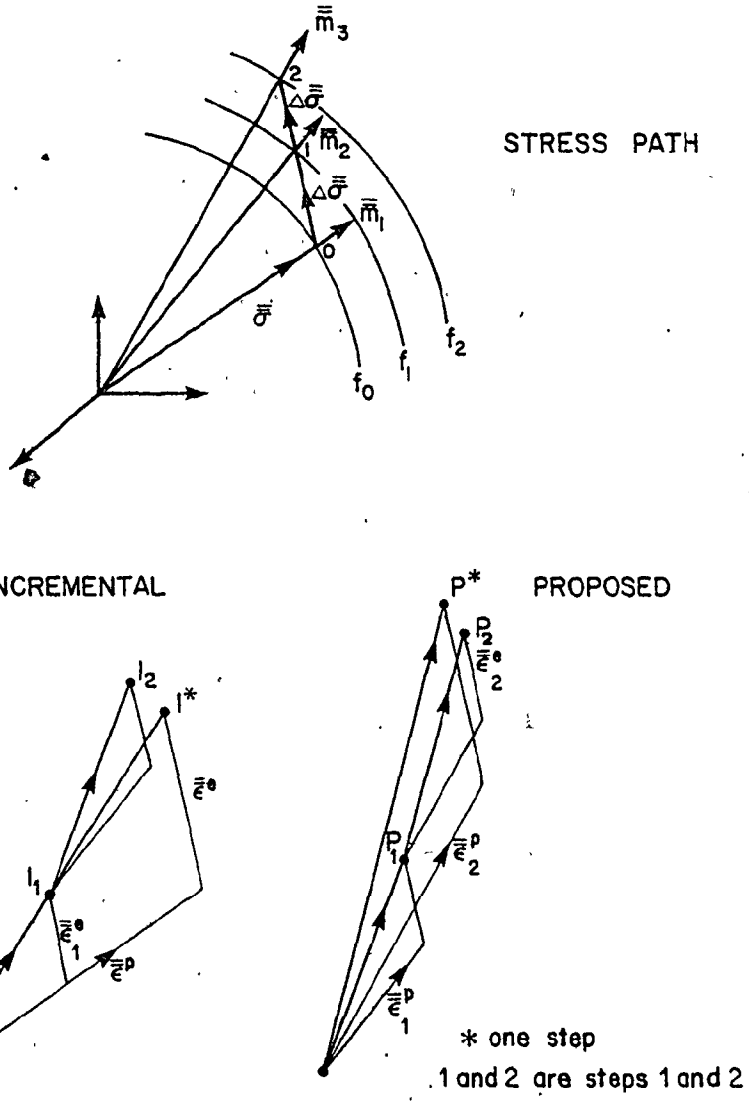

Figure 2.8 J_2' flow theory and its proposed modification for a two-steps increment.

and $$C_2 = \frac{C_1}{\| \sigma' \|}$$

By substituting (2.85) into (2.81), it follows that

$$\overset{=}{\Delta\sigma}' = (B - \frac{1}{C_2}) \overset{=}{\varepsilon} . \tag{2.86}$$

Equation (2.86) shows the simplest inverse for a R-P solid, in a proportional loading process. It is to be noted that such an inverse was not possible with the Prandtl-Reuss equations.

One might expect that the norm of the plastic strain increment calculated through the proposed equations (2.77) would approximate to the norm of (2.5) because $|| \overset{=}{\Delta\sigma}' || << || \overset{=}{\sigma}' ||$ in (2.78). Hence it follows that

$$|| \overset{=}{\varepsilon}^p ||_{(2.5)} \simeq || \overset{=}{\varepsilon}^p ||_{(2.77)}$$

However the advantage of (2.77) is the well conditioned matrix of the plastic moduli. Another advantage which becomes obvious upon comparing (2.8) and (2.83) is that the 2G term disappears from (2.83) and consequently it is expected that the moduli will be of the order of the tangent modulus. On the other hand the main disadvantage of (2.81) and (2.83) is that the relations between stress increments and strain increments are nonlinear.

From (2.78), it is permissible to write

$$\overset{=}{m}^* = \overset{=}{m} + \overset{=}{\Delta m} \tag{2.78a}$$

where $$\overset{=}{\Delta m} = \frac{1}{\sqrt{2J_2'}} \{-(\overset{=}{m} : \overset{=}{\Delta\sigma}) \overset{=}{m} + \overset{=}{\Delta\sigma}'\} \tag{2.87}$$

or $$\overset{=}{m}^{*} = \overset{=}{m}\left[1 - \frac{\overset{=}{m}:\Delta\overset{=}{\sigma}}{\sqrt{2J_2'}}\right] + \frac{\Delta\overset{=}{\sigma}}{\sqrt{2J_2'}} \qquad (2.78b)$$

which shows that the direction of plastic strain increment depends on the direction of stress increment. As a check on the linearity of the increment, we have $\overset{=}{m}:\Delta\overset{=}{m} = 0$.

Substituting from (2.78b) into (2.77)

$$\Delta\overset{=}{\varepsilon}^{P} = [C_3\,\overset{=}{m}\,\overset{=}{m} + C_4\,\Delta\overset{=}{\sigma}'\,\overset{=}{m}] : \Delta\overset{=}{\sigma} \qquad (2.88)$$

where $$C_3 = \frac{1}{h}\left[1 - \frac{\overset{=}{m}:\Delta\overset{=}{\sigma}}{\sqrt{2J_2'}}\right] ,$$

and $$C_4 = \frac{1}{h\sqrt{2J_2'}} \qquad (2.89)$$

From (2.87)

$$\Delta\overset{=}{m}\,(x\,\Delta\overset{=}{\sigma}) = x\,\Delta\overset{=}{m}\,(\Delta\overset{=}{\sigma}) \quad .$$

However, $$\overset{=}{m}^{*}\,(x\,\Delta\overset{=}{\sigma}) \neq x\,\overset{=}{m}^{*}\,(\Delta\overset{=}{\sigma})$$

In this sense and since the moduli of (2.88) depend upon the increment of stress, the relations in (2.88) are non-linear.

In order to compare the degree of approximation involved in the Prandtl-Reuss equations, consider the difference between the plastic strain calculated through a one step or two step solution (for equal final increments of stress) for the proposed and the Prandtl-Reuss equations; refer to Figure 2.8.

(A) Proposed Equation

(i) One Step (increment $2\Delta\bar{\bar{\sigma}}$):-

$$\bar{\bar{\varepsilon}}^t = m_3 \frac{\bar{\bar{m}}_1 : 2\Delta\bar{\bar{\sigma}}}{h}$$

or

$$\bar{\bar{\varepsilon}}^t = 2(\bar{\bar{m}}_1 + 2\Delta m) \frac{\bar{\bar{m}}_1 : \Delta\bar{\bar{\sigma}}}{h}$$

$$= \frac{2}{h} \{\bar{\bar{m}}_1(\bar{\bar{m}}_1 : \Delta\bar{\bar{\sigma}}) + 2\Delta m\ \bar{\bar{m}}_1 : \Delta\bar{\bar{\sigma}}\}$$

(ii) Two Steps:-

For constant h, the strain increment is

$$\bar{\bar{\varepsilon}}_{12} = m_2 \frac{\bar{\bar{m}}_1 : \Delta\bar{\bar{\sigma}}}{h} + m_3 \frac{\bar{\bar{m}}_2 : \Delta\bar{\bar{\sigma}}}{h}$$

$$= \frac{1}{h} \{2\bar{\bar{m}}_1(\bar{\bar{m}}_1 : \Delta\bar{\bar{\sigma}}) + 3\Delta m(\bar{\bar{m}}_1 : \Delta\bar{\bar{\sigma}})$$

$$+ \bar{\bar{m}}_1(\Delta\bar{\bar{m}} : \Delta\bar{\bar{\sigma}}) + 2\Delta m(\Delta\bar{\bar{m}} : \Delta\bar{\bar{\sigma}})\}$$

Hence

$$\bar{\bar{\varepsilon}}^t - \bar{\bar{\varepsilon}}_{12} = \frac{1}{h} \{\Delta m(\bar{\bar{m}}_1 : \Delta\bar{\bar{\sigma}}) - \bar{\bar{m}}_1(\Delta\bar{\bar{m}} : \Delta\bar{\bar{\sigma}})$$

$$- 2\Delta m(\Delta\bar{\bar{m}} : \Delta\bar{\bar{\sigma}})\} \qquad (2.90)$$

Therefore

$$||(\bar{\bar{\varepsilon}}^t - \bar{\bar{\varepsilon}}_{12})|| = \frac{1}{h} \{\Delta m^2(m\Delta\sigma)^2 + (\Delta m\Delta\sigma)^2$$

$$+ 4\Delta m^2[(\Delta m\Delta\sigma)^2 - (m\Delta\sigma)(\Delta m\Delta\sigma)]\}^{1/2} \qquad (2.90a)$$

(B) Prandtl-Reuss Equations

(i) One Step (Increment $2\Delta\bar{\bar{\sigma}}$):-

$$\bar{\bar{\varepsilon}}^t = m_1 \frac{\bar{\bar{m}}_1 : 2\Delta\bar{\bar{\sigma}}}{h}$$

$$= 2m_1 \frac{\bar{\bar{m}}_1 : \Delta\bar{\bar{\sigma}}}{h}$$

(ii) Two Steps:-

$$\bar{\bar{\varepsilon}}_{12} = m_1 \frac{\bar{\bar{m}}_1 : \Delta\bar{\bar{\sigma}}}{h} + m_2 \frac{\bar{\bar{m}}_2 : \Delta\bar{\bar{\sigma}}}{h}$$

$$= \frac{1}{h}\{2m_1(\bar{\bar{m}}_1 : \Delta\bar{\bar{\sigma}}) + \Delta m(\bar{\bar{m}} : \Delta\bar{\bar{\sigma}}) + m_1(\Delta\bar{\bar{m}} : \Delta\bar{\bar{\sigma}})$$

$$+ \Delta m(\Delta\bar{\bar{m}} : \Delta\bar{\bar{\sigma}})\}$$

Therefore $$\bar{\bar{\varepsilon}}^t - \bar{\bar{\varepsilon}}_{12} = -\frac{1}{h}\{\Delta m(\bar{\bar{m}}_1 : \Delta\bar{\bar{\sigma}}) + m_1(\Delta\bar{\bar{m}} : \Delta\bar{\bar{\sigma}})$$

$$+ \Delta m(\Delta\bar{\bar{m}} : \Delta\bar{\bar{\sigma}})\} \qquad (2.91)$$

and hence $$||(\bar{\bar{\varepsilon}}^t - \bar{\bar{\varepsilon}}_{12})|| = \frac{1}{h}\{\Delta m^2(m\Delta\sigma)^2 + (\Delta m\Delta\sigma)^2$$

$$+ 2\Delta m^2[(\Delta m\Delta\sigma)^2 + (m\Delta\sigma)(\Delta m\Delta\sigma)^2]\}^{1/2} \qquad (2.91a)$$

By comparing (2.90) and (2.91), we can observe that

$$||\bar{\bar{\varepsilon}}^t - \bar{\bar{\varepsilon}}_{12}|| \quad > \quad ||\bar{\bar{\varepsilon}}^t - \bar{\bar{\varepsilon}}_{12}||$$

Prandtl-Reuss proposed

Similarly there is little difference in the final direction of the plastic strain increment following a one or two stress increment when using the proposed equations. Hence less numerical deviation might be expected when the proposed equations are used in conjunction with a numerical technique and larger step sizes could well be permitted in the computational procedures.

2.4.3 Uniqueness Criterion for Rigid-Plastic Solids (Infinitesimal Strain)

Given the boundary value problem defined in section 1.1, we have

$$\bar{F}^{\cdot} = \bar{F}^{\cdot *} \qquad \text{on } S_F \tag{2.92}$$

$$\bar{v} = \bar{v}^{*} \qquad \text{on } S_V \tag{2.93}$$

We assume two solutions, to the B.V.P., given by

$$\overset{=}{\sigma}_1^{\cdot} \text{ and } \overset{=}{\varepsilon}_1$$

$$\overset{=}{\sigma}_2^{\cdot} \text{ and } \overset{=}{\varepsilon}_2$$

Following a procedure identical to that given in section 1.1.1, the uniqueness criterion can be expressed as

$$I = \int \overset{=}{\Delta\sigma}^{\cdot} : \overset{=}{\Delta\varepsilon}\, dV \neq 0 \tag{2.94}$$

where $\overset{=}{\Delta\sigma}^{\cdot} = \overset{=}{\sigma}_1^{\cdot} - \overset{=}{\sigma}_2^{\cdot}$

$$\Delta\underline{\underline{\varepsilon}} = \underline{\underline{\varepsilon}}_1 - \underline{\underline{\varepsilon}}_2$$

From (2.88), $\Delta\underline{\underline{\varepsilon}}$ could be given by

$$\Delta\underline{\underline{\varepsilon}} = \frac{1}{h\sqrt{2J_2'}} \{ \underline{\underline{m}}\, A + \underline{\underline{B}} \} \qquad (2.95)$$

where $A = \underline{\underline{C}}_{31}(\underline{\underline{m}}:\underline{\underline{\sigma}}_1') - \underline{\underline{C}}_{32}(\underline{\underline{m}}:\underline{\underline{\sigma}}_2')$

$$= [\underline{\underline{m}}:(\underline{\underline{\sigma}}_1'-\underline{\underline{\sigma}}_2')]\,[\sqrt{2J_2'} - \underline{\underline{m}}:(\underline{\underline{\sigma}}_1'+\underline{\underline{\sigma}}_2')] \quad , \qquad (2.96)$$

and $B = \sigma_1'\,'(\underline{\underline{m}}:\underline{\underline{\sigma}}_1') - \sigma_2'\,'(\underline{\underline{m}}:\underline{\underline{\sigma}}_2')$. $\qquad (2.97)$

Hence $I = \int \Delta\underline{\underline{\sigma}}':\Delta\underline{\underline{\varepsilon}}\, dV = \int \frac{1}{h\sqrt{2J_2'}} \{ D + E \}\, dV \qquad (2.98)$

where $D = A(\Delta\underline{\underline{\sigma}}':\underline{\underline{m}})$

$$= (\underline{\underline{m}}:\Delta\underline{\underline{\sigma}}')^2\,[\sqrt{2J_2'} - \underline{\underline{m}}:(\underline{\underline{\sigma}}_1'+\underline{\underline{\sigma}}_2')] \qquad (2.99)$$

and $E = \Delta\underline{\underline{\sigma}}':\underline{\underline{B}}$

$$= (\Delta\underline{\underline{\sigma}}':\underline{\underline{\sigma}}_1'')(\underline{\underline{m}}:\underline{\underline{\sigma}}_1') - (\Delta\underline{\underline{\sigma}}':\underline{\underline{\sigma}}_2'')(\underline{\underline{m}}:\underline{\underline{\sigma}}_2') \quad . \qquad (2.100)$$

The quantity D is comprised of terms of second and third order, whereas E contains only third order terms, therefore

$$D \gg E \qquad (2.101)$$

In testing for uniqueness, the following four cases will be considered

(i) $\overset{=}{\varepsilon}_1 \neq 0$ and $\overset{=}{\varepsilon}_2 \neq 0$

$I \geq 0$, with equality if $\overset{=}{\sigma}_1^{\cdot} = \overset{=}{\sigma}_2^{\cdot}$

(ii) $\overset{=}{\varepsilon}_1 \neq 0$ and $\overset{=}{\varepsilon}_2 = 0$

$$I = \int (\Delta\overset{=}{\sigma}^{\cdot} : \overset{=}{m}_1^{*}) \left(\frac{\overset{=}{m} : \overset{=}{\sigma}_1^{\cdot}}{h}\right) dV > 0$$

(iii) $\overset{=}{\varepsilon}_1 = 0$ and $\overset{=}{\varepsilon}_2 \neq 0$

$$I = -\int (\Delta\overset{=}{\sigma}^{\cdot} : \overset{=}{m}_2^{*}) \left(\frac{\overset{=}{m} : \overset{=}{\sigma}_2^{\cdot}}{h}\right) dV > 0$$

(iv) $\overset{=}{\varepsilon}_1 = \overset{=}{\varepsilon}_2 = 0$

$I = 0$ for any $\overset{=}{\sigma}_1^{\cdot}$ and $\overset{=}{\sigma}_2^{\cdot}$.

In view of the boundary conditions on S_F and S_V,

$$0 = \int \Delta\bar{F}^{\cdot} \cdot \Delta\bar{v}\, dS = \int \Delta\overset{=}{\sigma}^{\cdot} : \Delta\overset{=}{\varepsilon}\, dV \quad ,$$

and it follows that $\bar{\varepsilon}_1 = \bar{\varepsilon}_2$ in (i) and that regions (ii) and (iii) cannot exist since their contributions would be definitely positive. In other words, only one mode of deformation is compatible with the boundary conditions for $\bar{F}^{\cdot}$. On the other

hand, the stress rate is unique in the zone of deformation.

It should be noted that for the Prandtl-Reuss equations $\overline{\overline{m}}_1^* = \overline{\overline{m}}_2^* = \overline{\overline{m}}$, and hence

$$\underset{\sim}{I} = \frac{1}{h} [\overline{\overline{m}}:(\dot{\sigma}_1-\dot{\sigma}_2)]^2 \, dV \geq 0 \quad ,$$

$$\text{for } \overline{\overline{\varepsilon}}_1 \neq 0 \text{ and } \overline{\overline{\varepsilon}}_2 \neq 0 \quad ,$$

and in this case the combination of STRESS RATE COMPONENTS involved in $\overline{\overline{m}}:\dot{\overline{\overline{\sigma}}}$ and not the components individually, is necessarily unique in the zone of deformation.

It should also be noted that the sufficient criterion of uniqueness (1.6) is valid for any statically admissible set ($\Delta\bar{F}$ and $\Delta\bar{\bar{S}}$) and for any kinematically admissible set ($\Delta\bar{v}$ and $\Delta\bar{\bar{L}}$) as long as the force equilibrium equations and strain-displacement relations are linear. Equation (1.6) is therefore valid regardless of the form of the CONSTITUTIVE EQUATIONS.

2.4.4 Extremum Principles

(A) Lower Bound for Elastic-Plastic Solids

Let $(\Delta\overline{\overline{\sigma}}_1, \overline{\overline{\varepsilon}}_1)$ be the actual increment of stress and strain produced by given external stress increments $\Delta\bar{F}_1$ over a part S_F of the surface, and by given displacement-increments over the remainder S_u, see Figure 1.1. Let $(\Delta\overline{\overline{\sigma}}_2, \overline{\overline{\varepsilon}}_2)$ be any increments which satisfy the stress-strain relations, the stress boundary conditions, and the equations of equilibrium, but such that $\overline{\overline{\varepsilon}}_2$ is

not necessarily derivable from a continuous displacement. It may be shown, through the principle of virtual work, that

$$\int (\Delta\underline{\underline{\sigma}}_2 - \Delta\underline{\underline{\sigma}}_1) : \underline{\underline{\varepsilon}}_1 \, dV = \int_{S_u} (\Delta\bar{F}_2 - \Delta\bar{F}_1) \cdot \Delta\bar{u} \, dS \qquad (2.102)$$

Now $2\,(\Delta\underline{\underline{\sigma}}_2 - \Delta\underline{\underline{\sigma}}_1) : \underline{\underline{\varepsilon}}_1 \equiv$

$$(\Delta\underline{\underline{\sigma}}_2 : \underline{\underline{\varepsilon}}_2 - \Delta\underline{\underline{\sigma}}_1 : \underline{\underline{\varepsilon}}_1) - [\Delta\underline{\underline{\sigma}}_2 : (\underline{\underline{\varepsilon}}_2 - \underline{\underline{\varepsilon}}_1) + \underline{\underline{\varepsilon}}_1 : (\Delta\underline{\underline{\sigma}}_1 - \Delta\underline{\underline{\sigma}}_2)] \qquad (2.103)$$

The terms between square brackets can be divided into $B^e + B^p$, where the elastic part

$$B^e = \Delta\underline{\underline{\sigma}}_2 : (\underline{\underline{\varepsilon}}_2^e - \underline{\underline{\varepsilon}}_1^e) + \underline{\underline{\varepsilon}}_1^e : (\Delta\underline{\underline{\sigma}}_1 - \Delta\underline{\underline{\sigma}}_2)$$

Substituting from (2.3), it can be shown that

$$B^e = (\Delta\underline{\underline{\sigma}}_2 - \Delta\underline{\underline{\sigma}}_1) : \underline{\underline{\underline{\underline{K}}}}^{-1} : (\Delta\underline{\underline{\sigma}}_2 - \Delta\underline{\underline{\sigma}}_1) \qquad (2.104)$$

and since K is positive definite, hence

$$B^e \geq 0 \qquad (2.105)$$

Through the use of (2.88), the plastic part B^p can be shown to yield

$$hB^p = C^2 \{ \alpha_2 \Delta f_2^{\,2} - 2\alpha_1 \Delta f_1 \Delta f_2 + \alpha_1 \Delta f_1^{\,2} \}$$

$$+ \frac{C^3}{\sqrt{2J_2'}} \{-\alpha_2 \Delta f_3^{\,2} + 2\alpha_1 \Delta f_2 \Delta f_1^{\,2} - \alpha_1 \Delta f_1^{\,3}\}$$

$$+ \frac{C}{\sqrt{2J_2'}} \{\alpha_2 \Delta f_2 (\Delta\sigma_2)^2 - 2\alpha_1 \Delta f_1 \Delta\sigma_1 \Delta\sigma_2 + \alpha_1 \Delta f_1 (\Delta\sigma_1)^2\} \tag{2.106}$$

where $C \Delta f_i = \overset{=}{m} : \Delta\overset{=}{\sigma}_i$, $C = \sqrt{\frac{2}{3}}$ (2.107)

$$\alpha_i = 1 \quad , \quad \Delta f_i > 0 \quad ,$$

and

$$\alpha_i = 0 \quad , \quad \Delta f_i \leq 0$$

By considering the four possible combinations of α_1 and α_2, it may be shown that B^p is never negative.

$$\text{i.e. } B^p \geq 0 \tag{2.108}$$

The equality sign in (2.105) and (2.108) is when $\Delta\overset{=}{\sigma}_1 = \Delta\overset{=}{\sigma}_2$. It follows from (2.102), (2.103), (2.105) and (2.108) that unless $\Delta\overset{=}{\sigma}_1 = \Delta\overset{=}{\sigma}_2$ at every point

$$\frac{1}{2} \int \Delta\overset{=}{\sigma}_2 : \overset{=}{\varepsilon}_2 \, dV - \int_{S_u} \Delta\bar{F}_2 \cdot \Delta\bar{u} \, dS > \frac{1}{2} \int \Delta\overset{=}{\sigma}_1 : \overset{=}{\varepsilon}_1 \, dV - \int_{S_u} \Delta\bar{F}_1 \cdot \Delta\bar{u} \, dS$$

$$= \frac{1}{2} \int_{S_F} \Delta\bar{F}_1 \cdot \Delta\bar{u} \, dS - \frac{1}{2} \int_{S_u} \Delta\bar{F}_1 \cdot \Delta\bar{u} \, dS \tag{2.109}$$

(B) Upper Bound

Following Hill [44]* again, there is a second extremum principle for distributions $(\Delta\bar{\bar{\sigma}}_2, \bar{\bar{\varepsilon}}_2)$ where $\bar{\bar{\varepsilon}}_2$ is derivable from a displacement $\Delta\bar{u}_2$ satisfying the boundary conditions but $\Delta\bar{\bar{\sigma}}_2$ is not in equilibrium. In this case we begin with the equation

$$\int (\bar{\bar{\varepsilon}}_2-\bar{\bar{\varepsilon}}_1):\Delta\bar{\bar{\sigma}}_1 \, dV = \int_{S_F} (\Delta\bar{u}_2-\Delta\bar{u}_1)\cdot \Delta\bar{F}_1 \, dS$$

and the identity $2(\bar{\bar{\varepsilon}}_2-\bar{\bar{\varepsilon}}_1):\Delta\bar{\bar{\sigma}}_1 \equiv$

$$(\Delta\bar{\bar{\sigma}}_2:\bar{\bar{\varepsilon}}_2 - \Delta\bar{\bar{\sigma}}_1:\bar{\bar{\varepsilon}}_1) - [\bar{\bar{\varepsilon}}_2:(\Delta\bar{\bar{\sigma}}_2-\Delta\bar{\bar{\sigma}}_1) + \Delta\bar{\bar{\sigma}}_1:(\bar{\bar{\varepsilon}}_1-\bar{\bar{\varepsilon}}_2)]$$

By the argument employed previously, the term in square brackets can be shown to be positive, unless $\Delta\bar{\bar{\sigma}}_2 = \Delta\bar{\bar{\sigma}}_1$. Hence, unless $\Delta\bar{\bar{\sigma}}_2 = \Delta\bar{\bar{\sigma}}_1$ at every point,

$$\int_{S_F} \Delta\bar{u}_2\cdot\Delta\bar{F}_1 \, dS - \frac{1}{2}\int \Delta\bar{\bar{\sigma}}_2:\bar{\bar{\varepsilon}}_2 \, dV < \int_{S_F} \Delta\bar{u}_1\cdot\Delta\bar{F}_1 dS - \frac{1}{2}\int \Delta\bar{\bar{\sigma}}_1:\bar{\bar{\varepsilon}}_1 \, dV$$

$$= \frac{1}{2}\int_{S_F} \Delta\bar{F}_1\cdot\Delta\bar{u}_1 dS - \frac{1}{2}\int_{S_u} \Delta\bar{F}_1\cdot\Delta\bar{u}_1 dS \qquad (2.110)$$

Comparing this with (2.109) we observe that in the first principle the right hand side is the minimum of one function of $(\Delta\bar{\bar{\sigma}}_2, \bar{\bar{\varepsilon}}_2)$ and in the second the maximum of another.

2.4.5 Application to Bifurcation Analyses of Plates and Shells

The difficulty of applying the proposed equations (2.88) stems from the nonlinear relation between stress increment and strain increment, and therefore a rate potential in the sense described in section 1.4 does not exist. Hence, a variational formulation cannot be found for the proposed equations. However, we can still apply the suggested equations in a manner analogous to that followed by Hill [55], for a rigid-plastic solid. To recapitulate, the rate potential for an elastic-plastic solid in terms of Jaumann's derivative is

$$2V = \left(\frac{\delta \overset{=}{\tau}}{\delta t}\right) : \overset{=}{\varepsilon} = \overset{=}{\varepsilon} : \overset{\overset{4}{=}}{T} : \overset{=}{\varepsilon} \tag{2.111}$$

where $\overset{\overset{4}{=}}{T}$ is given by (1.28b). For rigid-plastic solids, the matrix of plastic moduli is singular, however define

$$2V = \overset{=}{\varepsilon} : \overset{\overset{4}{=}}{h} : \overset{=}{\varepsilon} \quad , \tag{2.112}$$

although V no longer acts as a regular potential since the strain rate direction $\overset{=}{m}$ is pre-determined by the current stress.

Returning back to the proposed equations, rewrite (2.81) as

$$\overset{=}{\Delta\sigma} = \left[\frac{2J_2'}{\overset{=}{\sigma} : \overset{=}{\varepsilon}} + h \right] \overset{=}{\varepsilon} - \overset{=}{\sigma} \tag{2.113}$$

Hence

$$\int \overset{=}{\Delta\sigma} : \overset{=}{\varepsilon} \, dV = \int \left\{ \left[\frac{2J_2'}{\overset{=}{\sigma} : \overset{=}{\varepsilon}} + h \right] (\overset{=}{\varepsilon} : \overset{=}{\varepsilon}) - \overset{=}{\sigma} : \overset{=}{\varepsilon} \right\} dV \tag{2.114}$$

Substituting from (1.37) and assuming that middle surface strain rates can be neglected then,

$$\underline{\underline{\varepsilon}} = z\underline{\underline{k}}$$

$$\int_{-t/2}^{t/2} \underline{\underline{\sigma}} : \underline{\underline{\varepsilon}}\, dz = \int_{-t/2}^{t/2} z(\underline{\underline{\sigma}} : \underline{\underline{k}})\, dz = 0$$

$$\int_{-t/2}^{t/2} \frac{2J_2'}{\underline{\underline{\sigma}} : \underline{\underline{\varepsilon}}} (\underline{\underline{\varepsilon}} : \underline{\underline{\varepsilon}})\, dz = \int_{-t/2}^{t/2} z \frac{2J_2'}{\underline{\underline{\sigma}} : \underline{\underline{k}}} (\underline{\underline{k}} : \underline{\underline{k}})\, dz = 0$$

and hence the incremental strain energy in (2.114) can be rewritten as

$$\int \Delta\underline{\underline{\sigma}} : \underline{\underline{\varepsilon}}\, dV = z^2 \int \underline{\underline{k}} : \underline{\underline{\underline{\underline{h}}}} : \underline{\underline{k}}\, dV$$

$$= \int \underline{\underline{\varepsilon}} : \underline{\underline{\underline{\underline{h}}}} : \underline{\underline{k}}\, dV \quad . \tag{2.115}$$

The left hand side of (2.115) is interpreted as the "bending energy potential", with

$$2V^* = \underline{\underline{\varepsilon}} : \underline{\underline{\underline{\underline{h}}}} : \underline{\underline{\varepsilon}} \quad . \tag{2.116}$$

The difference between (2.112) and (2.116) is that for the proposed R-P constitutive equations, the inverse is valid, whereas it does not exist for the Prandtl-Reuss equations.

It should be noted that the stretching work is neglected in (2.115) since for bifurcation purposes it is found that for maximum critical thicknesses this condition ought to be enforced, Sewell [125] and Naruse and Takeyama [99, 100].

It is clear from (2.115) that the incremental strain energy

is governed by the tangent modulus and not moduli of the order of the elastic moduli as in (2.12). The same can be demonstrated for elastic-plastic solids.

It is suggested to apply the bifurcation criterion (1.9) with the incremental strain energy $H(\bar{w})$, for rigid plastic solids, in the form shown in (2.115) and $\Sigma(\bar{w})$ still by equation (1.11). The major advantage of the present approach is that there are no restrictions placed on the kinematically admissible velocity fields, aside from incompressibility, and hence a wider set of velocity fields can be selected when compared to the classical case with the Prandtl-Reuss equations. This advantage becomes more obvious in case of rigid-plastic solids, where bifurcation, with the proposed equations, is not ruled out by the constitutive equations alone as is with the Prandtl-Reuss equations, Dubey and Ariaratnam [31] and Kumar [74].

2.5 Some Final Remarks on Constitutive Equations

It was shown that for the J_2' deformation theory, the relation between stress rates and strain rates is linear. Nevertheless the theory suffers from the discontinuity between the elastic and plastic regions, i.e. a change in plastic strain is predicted following elastic unloading. The matrix of plastic moduli is nonsingular and hence solutions could be obtained for the rigid-plastic solid through the potential energy and complementary energy functions.

The case is different for the rigid-plastic solid obeying the Prandtl-Reuss equations, where solutions cannot be obtained in terms of the complementary energy function since the constitutive relations for the rigid-plastic solid cannot be deduced as a limiting case from the elastic-plastic solid when Young's modulus approaches infinity. It is also shown that each modulus separately in (2.13) is in the order of the elastic moduli. This point is crucial for the bifurcation analyses, since there is an often held view that buckling occurs only at very low strain levels and hence moduli of the order of the elastic ones should be used, Hutchison [65]. This is not the general case since with conical dies, as will be shown in chapter 4, wrinkling (buckling) can occur at large plastic strains.

Classical theories of plasticity adhere to the concept of normality of the plastic strain increment to the current yield surface i.e. prior to any stress increment. Thus the direction of the plastic strain increment is determined by the current deviatoric stresses, and hence excludes its dependence on the stress increment. As discussed here-in the classical theory employed in bifurcation analyses can lead to a prediction of plastic moduli which are of the same order as the elastic moduli. This immediately raises doubts as to whether the theoretical model is at all representative of the physical situation.

Similar problems are to be expected with other solids obeying the normality rule at the current configuration such as creep and viscoplastic solids.

It was to avoid some of the disadvantages associated with the Prandtl-Reuss equations that the constitutive equations described in section 2.4, were proposed. The proposed equations provide a non-singular matrix of plastic moduli and include the directional dependence of the plastic strain increment on the increment of stress. However this latter aspect results in the relations being nonlinear. It is also shown that the moduli are in the order of the hardening parameter and is therefore an improvement over the J_2' flow theory. This point is of crucial importance and the consequences are clarified through the following example: - Consider a uniaxially loaded specimen, at large strain levels in the plastic region. When an increment in stress in the longitudinal direction is applied, the incremental work per unit volume is given by

$$W_1 = \frac{1}{2}\left(\frac{\delta \underline{\underline{\tau}}}{\delta t}\right) : \underline{\underline{\underline{\underline{J}}}} : \underline{\underline{\epsilon}}$$

Substituting from (2.58) into (2.61) with $\mu = 1$ and $\nu = 1/3$, we obtain

$$W_1 = \frac{9}{11} h \, \epsilon_{11}^2 \qquad (2.117)$$

When a torsional stress increment $\Delta\sigma_{12}$ is applied, according to the Prandtl-Reuss equations, $\alpha_{33} = 2G$, and the incremental work in

this case is given by

$$W_2 = \frac{9}{11} h \varepsilon_{11}^2 + 2G \varepsilon_{12}^2 \quad . \tag{2.118}$$

Since ε_{11}, ε_{22} and ε_{12} are of the same order and $2G >> h$ (at large plastic strains), we have $W_2 >> W_1$.

For any additional increment of radial stress,

$m_{12} = \sqrt{\frac{3}{2}} \frac{\Delta\sigma_{12}}{\sigma_{11}}$, and from (2.8) and (2.61), we have

$$W_3 = \frac{9}{11} h \varepsilon_{11}^2 + 2G \left[\varepsilon_{12}^2 - m_{12} \varepsilon_{12} \left(m_{12} \varepsilon_{12} + \sqrt{\frac{3}{2}} \varepsilon_{11}\right)\right] \tag{2.119}$$

Hence $$W_2 > W_3 >> W_1 \quad ,$$

i.e. the incremental work per unit volume jumps more than one order of magnitude (depending on the ratio $2G/h$), with a torsional load (wherever small) and remains at that level for any subsequent increment of radial loading. This type of response, according to the J_2 flow theory, is physically difficult to interpret and moreover it is quite difficult to visualize that through a deviation from radial loading, the material would respond such that the stiffness in one direction could be three orders of magnitude higher than the other direction. Such a response have not been experimentally reported and represents our main objection on the use of the Prandtl-Reuss equations in bifurcation analysis.

In the next subsection some of the experimental works, that evaluate the constitutive equations, are reported.

2.5.1 Experimental Evidence of Non-linearity

The tests reported below were carried on tubular specimens, with different combination of axial and torsional loading. Naghdi and Rowley [97] applied tension, followed by torsion, and then permitted varying amounts of accompanying tension. In another investigation by Naghdi et al [98], the loading program was such that the specimens were subjected to an initial tension and torsion followed by increments of tension and torsion. The work of Peters et al [117] consisted of loading the specimens in compression and then adding increments of torsion, while Morrison and Shepherd [94] applied initial tension followed by sequence of torque increments, a further increase in tension and finally where possible a further increase of torque. Feigen [37] carried a test similar to that of Peters et al [117] however one torsional increment is added and then at a different strain level removed. Naghdi and Rowley [97] observed the occurence of the plastic shear strains once the torque is applied and found that the initial shear modulus is less than the elastic modulus by a factor of two. In the other work designed to check the validity of the assumption of linearity, Naghdi et al [98] found experimentally that a strong correlation existed between the direction of both the stress and strain-increment vectors for all the specimens tested. They reported that the directions of the stress increment and strain increment vectors have the same sense along the entire loading path and concluded that this experimental finding proves the

existence of a corner on the yield surface, and rendered invalid the assumption of linearity of the increment of plastic strains during the increment of stresses. Many investigators, see Philips [118], follow the same reasoning in that for a vertex to exist, the plastic strain increments corresponding to two properly directed stress increments should have different directions. The experimental findings of Naghdi et al [98] can be interpreted in the light of the proposed constitutive equations, for clarity see Fig. 2.5, which supports the intuitive feeling that the material response is unlikely to be independent of the external loading. Peters et al [117] reported that the experimentally established curve, see Figure 2.9 taken from their work (Figure 10, p. 136), between the directions of the principal axis of plastic strain increments and the directions of principal stresses, fall above the theoretical line calculated according to both the J_2 deformation and flow theories; the deviation is quite substantial. That last finding was also shown by Morrison and Shephard [94] and no explanation was given in the above two works to interpret the results. In a discussion of the work by Morrison and Shephard [94], Budiansky and Batdorf [94] mentioned that "the location of the principal axes of plastic strain rate appeared to depend markedly on the location of the principal stress rate axes as well as on the location of the principal stress axes. Thus, the experiment afforded evidence that NO LINEAR incremental theory could be of general validity". Morrison and Shephard [94]

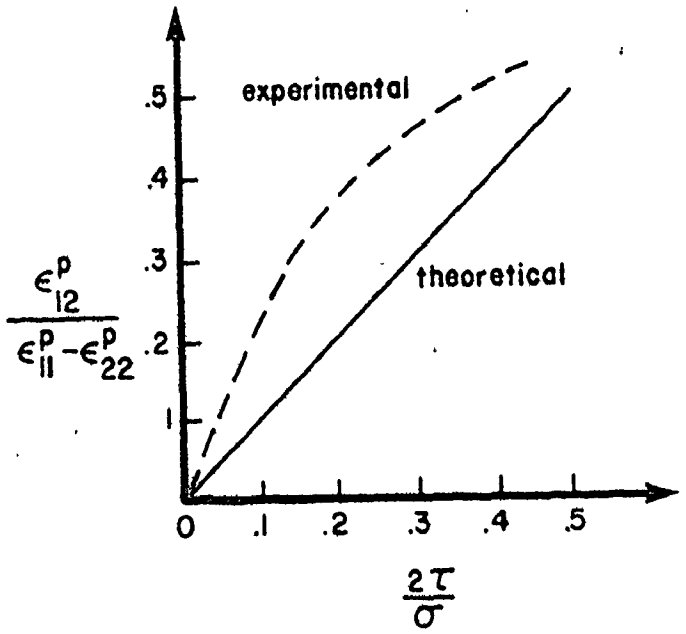

Figure 2.9 Change of the direction of the plastic strain increment with direction of stress

mentioned that the most consistent feature of the behaviour of the material was that the rotation of the incremental plastic strain axes tended to "lead" that of the stress axes and therefore the incremental plastic strain axes would tend to rotate faster than the stress axes. On the other hand Feigen [37] experimentally found that the initial shear modulus decreases with axial strain, in contrast with a constant value as predicted by the flow theory, and a substantially smaller value as predicted by the J_2' deformation theory.

In summary, experiments show a dependence of initial shear modulus on plasticity, a plastic shear strain at the beginning of twist for a uniaxially loaded specimen and evidence of correlation between the stress rate and strain rate axes. In order to follow the of lin the

the presence of a yield vertex. However, this is a supposition and need not be the actual case. The non-linear constitutive equations developed in 2.4 could be another supposition, and more so it explains the experimental observations in Figure 2.9, as shown below:-

The deviatoric stress for uniaxial tension is

$$\sigma'_{ij} = \begin{bmatrix} 2\sigma/3 & 0 & 0 \\ 0 & -\sigma/3 & 0 \\ 0 & 0 & -\sigma/3 \end{bmatrix},$$

upon applying a torsional stress τ the deviatoric components become

$$\sigma'_{ij} = \begin{bmatrix} 2\sigma/3 & \tau & 0 \\ \tau & -\sigma/3 & 0 \\ 0 & 0 & -\sigma/3 \end{bmatrix}.$$

With a further increment $\Delta\tau$, we get

$$\sigma'_{ij} = \begin{bmatrix} 2\sigma/3 & \tau+\Delta\tau & 0 \\ \tau+\Delta\tau & -\sigma/3 & 0 \\ 0 & 0 & -\sigma/3 \end{bmatrix}.$$

The direction of the plastic strain increment in terms of twice the angle of rotation is

$$2\theta = \frac{2\varepsilon_{12}}{\varepsilon_{11}-\varepsilon_{22}} \quad .$$

In the case when the Prandtl-Reuss equations are used

$$2\,\theta_{PR} = \frac{2\,m_{12}}{m_{11}-m_{12}} = \frac{2\tau}{\sigma} \quad .$$

Whereas with the proposed constitutive equations,

$$2\,\theta_{prop.} = \frac{2\,m^{*}_{12}}{m^{*}_{11}-m^{*}_{12}} = \frac{2(\tau+\Delta\tau)}{\sigma} \quad .$$

The directions of the principal axis of the stress is

$$2\,\theta_{\sigma} = \frac{2\tau}{\sigma}$$

Hence
$$\theta_{PR} = \theta_{\sigma} < \theta_{prop.} \qquad (2.120)$$

Equation (2.120) explains the finding in Figure 2.9. Another advantage of the proposed constitutive equations is the prediction of the initial shear modulus decreasing with plasticity as demonstrated below.

The initial shear modulus $2G^{*}$ according to the proposed equations is given by

$$2G^{*} = \frac{\Delta\sigma_{12}}{\varepsilon^{e}_{12} + \varepsilon^{p}_{12}} = \frac{\Delta\sigma_{12}}{\frac{\Delta\sigma_{12}}{2G} + m^{*}_{12}\,\frac{\underline{m}:\Delta\sigma}{h}} \qquad (2.121)$$

For a uniaxially loaded specimen, when an increment of axial and torsional load is applied

$$m_{12}^{*} = \frac{\Delta\sigma_{12}}{\|\underline{\underline{\sigma}}'\|} \propto \frac{\Delta\sigma_{12}}{\sqrt{2J_2'}} \qquad (2.122)$$

$$\underline{\underline{m}} : \underline{\underline{\Delta\sigma}} = \sqrt{\frac{2}{3}}\,\Delta\sigma \quad , \qquad \text{with} \quad \bar{\sigma} = \sqrt{3\,J_2'}$$

Substituting the above in (2.121), we obtain

$$2G^{*} = \frac{1}{\frac{1}{2G} + \frac{\Delta\sigma}{h\bar{\sigma}}} \quad , \qquad (2.123)$$

where it is clear that the initial shear modulus decreases with increasing plasticity and is not a constant value as predicted by the Prandtl-Reuss equations.

According to the deformation theory, the initial shear modulus is given by Peters et al [117] as

$$2G' = \frac{2\,E_s\,E}{3E+(2\mu-1)E_s} \quad . \qquad (2.124)$$

For the experiments by Feigen [37] , $\frac{\Delta\sigma}{\bar{\sigma}} \simeq 10^{-2}$

and hence by comparing (2.123) and (2.124), we get

$$2G > 2G^{*} > 2G' \qquad (2.125)$$

Equation (2.125) is confirmed by the experiments of Feigen, Opt. cit., and therefore the proposed theory explains the experimental findings better than the J_2' deformation and J_2' flow theories.

2.5.2 Effect of Yield Surface Increase on Plastic Strains

None of the above mentioned constitutive equations can predict the first increment of plastic shear strain for a specimen deformed in uniaxial tension and then subjected to torsional loading. Note that for the rigid-plastic solid, according to the J_2' deformation theory, the strain increment is scaled by $(2E_{s/3})$ which is still in the order of elastic moduli for moderate strains.

The reason lies in the approximation used for the increase of the yield surface $\Delta f(\overset{=}{\Delta\sigma})$ as shown below. Upon expanding Δf it follows that

$$\Delta f = \overset{=}{\Delta\sigma} : \frac{\partial f}{\partial \overset{=}{\sigma}} + \frac{1}{2!}\, \overset{=}{\Delta\sigma}\, \overset{=}{\Delta\sigma} : \frac{\partial}{\partial \overset{=}{\sigma}} \frac{\partial f}{\partial \overset{=}{\sigma}} + 0(\overset{=}{\Delta\sigma})^3 \,. \qquad (2.126)$$

Since $f = \sqrt{3J_2'} = \sqrt{\frac{3}{2}\,(\overset{=}{\sigma}' : \overset{=}{\sigma}')}$

then $$\frac{\partial f}{\partial \overset{=}{\sigma}} = \sqrt{\frac{3}{2}}\, \frac{\overset{=}{\sigma}'}{\sqrt{2J_2'}} = \sqrt{\frac{3}{2}}\, \overset{=}{\sigma}'\, (\overset{=}{\sigma}' : \overset{=}{\sigma}')^{-1/2} \,, \qquad (2.127)$$

and $$\frac{\partial}{\partial \overset{=}{\sigma}} \left(\frac{\partial f}{\partial \overset{=}{\sigma}}\right) = \sqrt{\frac{3}{2}} \left[\frac{\partial \overset{=}{\sigma}'}{\partial \overset{=}{\sigma}}\, (\overset{=}{\sigma}' : \overset{=}{\sigma}')^{-1/2} - \overset{=}{\sigma}'\, \overset{=}{\sigma}'\, (\overset{=}{\sigma}' : \overset{=}{\sigma}')^{-3/2} \right]$$

$$= \sqrt{\frac{3}{2}} \left[\frac{\overset{4}{I} - \overset{=}{I}\,\overset{=}{I}}{\sqrt{2J_2'}} - \frac{\overset{=}{\sigma}'\,\overset{=}{\sigma}'}{(2J_2')^{3/2}} \right] \,. \qquad (2.128)$$

Substituting from (2.127) and (2.128) into (2.126), the yield surface expansion becomes

$$\Delta f = \sqrt{\frac{3}{2}} \{ \overset{=}{\Delta\sigma}' : \frac{\overset{=}{\sigma}'}{\sqrt{2J_2'}} + \frac{1}{2!} \frac{1}{\sqrt{2J_2'}} [(\overset{=}{\Delta\sigma}' : \overset{=}{\Delta\sigma}') - \frac{1}{2J_2'} (\overset{=}{\Delta\sigma} : \overset{=}{\sigma}')^2] \}$$

$$+ 0 (\overset{=}{\Delta\sigma})^3 \quad , \tag{2.129}$$

or in terms of the unit normal to the deviatoric yield surface

$$\Delta f = \sqrt{\frac{3}{2}} \{ \overset{=}{m} : \overset{=}{\Delta\sigma} + \frac{1}{2!} \frac{1}{\sqrt{2J_2'}} [(\overset{=}{\Delta\sigma}' : \overset{=}{\Delta\sigma}') - (\overset{=}{m} : \overset{=}{\Delta\sigma})^2] \} + \mathcal{O} (\overset{=}{\Delta\sigma})^3 \quad . \tag{2.130}$$

Within the linear approximation, only first order terms in $\overset{=}{\Delta\sigma}$ are retained and accordingly (2.129) and (2.130) imply that Δf depends on the combination of $(\overset{=}{m} : \overset{=}{\Delta\sigma})$ and not on $\overset{=}{\Delta\sigma}$ alone. Moreover $(\overset{=}{m} : \overset{=}{\Delta\sigma})$ would therefore be zero if no deviatoric components in the direction of the increment were present.

Therefore if the problem of a uniaxially loaded specimen under incremental twist were to be properly modelled, second order terms are inevitable. Furthermore, equation (2.130) illustrates the difficulty of measuring the dependence of the yield surface on the increment of stress, where $||\overset{=}{\Delta\sigma}|| < ||\overset{=}{\sigma}||$ and $||\overset{=}{\Delta\sigma} : \overset{=}{\Delta\sigma}|| \ll ||\overset{=}{\sigma}||$ i.e. very small quantities to detect with respect to $\overset{=}{\sigma}$.

CHAPTER 3

CONVENTIONAL DEEP DRAWING WITHOUT BLANK-HOLDER

3.1 Introduction

Deep drawing is a process in which a thin metal sheet is formed into a cup, box or a shell. It is the principal method by which deep recessed parts are produced. In this chapter, the deep drawing of a cylindrical cup from a flat circular blank is considered, which is shown schematically in Figure 3.1. Note, the blank holder which is usually part of the conventional tooling is not shown in the diagram. In such a process, the metal undergoes the following stages of deformation, Johnson and Mellor [67]: -

(i) Pure radial drawing of the blank in the flange area.

(ii) Bending and sliding over the die profile.

(iii) Stretching between die and punch.

(iv) Bending and sliding over the punch profile radius.

(v) Stretching and sliding over the punch head.

The failure of the drawn part can occur in any of these stages. In practice, the failure takes place either in the flange as buckling due to compressive stresses, or splitting at punch nose caused by tensile stresses.

Wrinkling of the flange can be avoided by applying sufficient blank-holding pressure. However, too high a pressure leads to the splitting failure. Thus, in a practical drawing operation a compromise is sought between these two conditions.

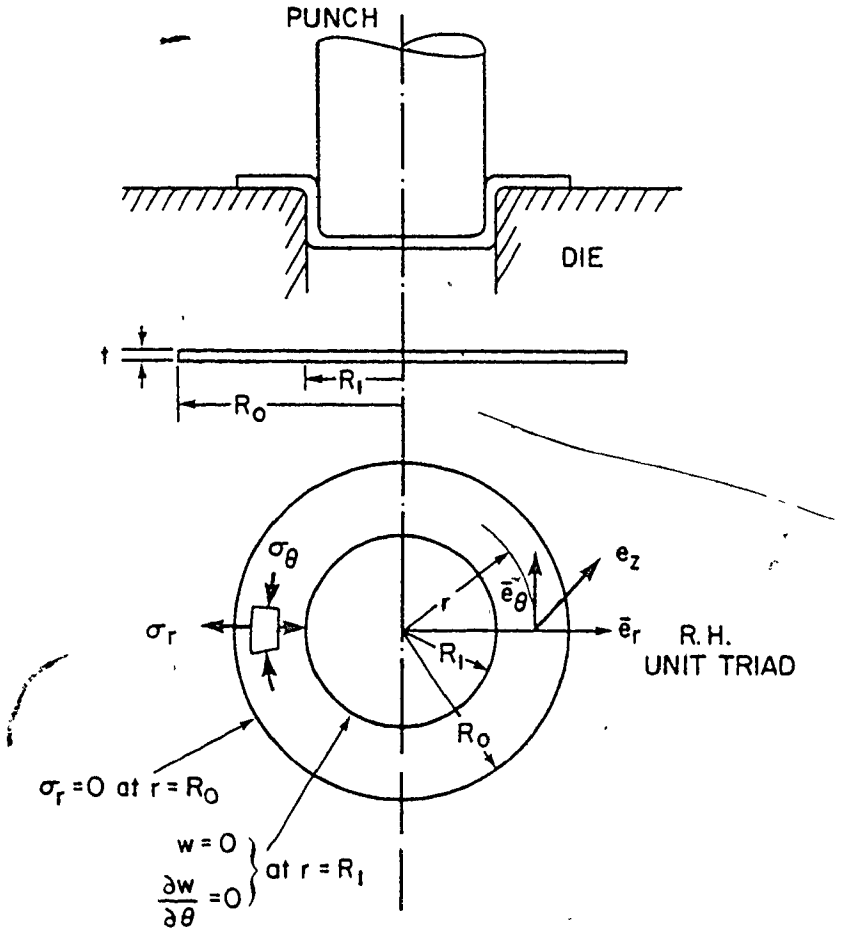

Figure 3.1 Deep drawing: coordinate system and boundary conditions

Only failure due to wrinkling of the flange, in the absence of a blank holder, is considered in this chapter.

In the absence of a blank holder the flange is virtually drawn under a condition of plane stress. The radial stress, σ_r, is tensile and the hoop stress, σ_θ, compressive, see Figure 3.1.

The yield criterion of Tresca and von-Mises is given by

$$\sigma_r - \sigma_\theta = Y = \bar{\sigma}$$

and

$$\sigma_r^2 - \sigma_r\sigma_\theta + \sigma_\theta^2 = Y^2 = \bar{\sigma}^2$$

respectively. During drawing σ_θ is unlikely to go tensile and a limiting case would appear to be $\sigma_\theta = 0$ at the inside radius of the flange; while σ_r is always zero at the outer rim. The range of possible stress states is shown in Figure 3.2.

The wrinkling problem has been studied by Geckeler [39] who treated the wrinkling of the flange as a problem in elastic buckling. Baldwin and Howald [3] applied Geckeler's method to a variety of practical blank geometries. Both Senior [124] and Kawai [70] assumed the flange to buckle in a series of waves, and a half wave segment was treated as a column under axial load. The buckling condition was determined by equating the energy stored in bending to the work done by the axial loads (Senior), or by considering the moment equilibrium over a half wave length (Kawai). The effect of plasticity was introduced through von Karman's reduced modulus. The constraint exerted by the die lip was allowed for by introducing a fictitious line load at the mean radius of the flange. The latter assumption became necessary in order to obtain a reasonable degree of correspondence between the theoretical predictions and the experimental results for blanks drawn without a blank holder.

Neglecting the two dimensional nature of the problem is an

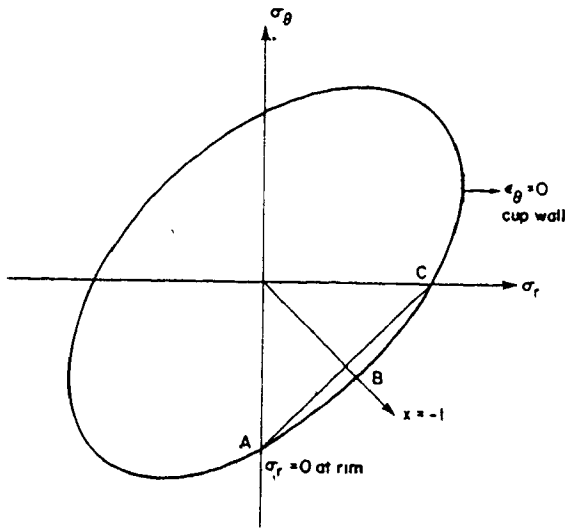

Figure 3.2 Plane stress von-Mises and Tresca yield loci: ABC is the possible range

oversimplification. On the other hand, the adoption of the reduced modulus contradicts the finding that when buckling occurs the material does not unload, as was shown by Shanley [132] and Hill [48]. Shanley proposed that the bending of a column can proceed under increasing axial load without causing any unloading and thus the tangent modulus is the correct effective modulus. On the other hand, the reduced modulus is derived by assuming that upon reaching the critical uniform stress the column bends, which causes the strain to decrease on one side and increase on the other.

Miyagawa [91] determined the buckling stress in the flange from the stationary condition of the total potential energy of the formed wrinkles; the moduli of the elastic energy criterion were replaced by elastic-plastic moduli. However, it is not clear which type of constitutive equations of plasticity were used in the analysis. In an earlier paper Miyagawa [90] had suggested

that an analytical solution of the controlling equations appeared unlikely under the boundary conditions encountered in practice. Kulkarni [73] adopted Hill's bifurcation criterion in a variational form and the problem is posed as the stability of an initial state of stress, and a numerical solution is obtained using Ritz's procedure. It should be noted that this approach is particularly suitable for metal forming problems because in many cases the deformation pattern is known qualitatively from experiments, while the direct solution of differential equations is usually not possible. Some of the details of Kulkarni's approach, opt. cit., are repeated here, since there appeared to be some minor errors in the original work. Naruse and Takeyama [99] considered flange wrinkling, in the absence of a blank holder, and assumed the inner rim to be either fixed or simply supported. The basic differential equations for bifurcation were derived from Hill's uniqueness criterion by means of calculus of variation and were solved numerically. A constitutive equation was proposed in terms of the convected derivative of the Kirchhoff stress, and it was found that the minimum condition at bifurcation corresponds to the case of pure bending. They predicted a critical blank thickness to diameter ratio much less than observed in practice, which implies that the calculated buckling stresses are too high. In a later paper [100] the same authors simulated the blank holder force by introducing spring type loading, and assumed this force to be proportional to the maximum lateral deflection of the

outside edge of the flange. In this case the Jaumann derivative was used but the resulting critical stresses were still very large compared to the experimental ones. Triantafyllidis and Needleman [143] analyzed flange wrinkling as a plastic bifurcation problem of an annular plate made of an orthotropic elastic-plastic material. The critical drawing stress and displacement at the onset of wrinkling was obtained from both a deformation theory and a flow theory of plasticity. It was demonstrated that the critical stress was not a monotonic function of the drawing ratio, and that the limiting drawing ratio increased with increasing values of the normal anisotropy parameter, $\bar{r}$.

In the present work, flange wrinkling during deep drawing without a blank-holder is treated as a problem of elastic-plastic buckling of an annular plate. The application of Hill's uniqueness criterion, along with the Prandtl-Reuss equations, to this particular problem is shown herein to be unsuccessful in predicting the critical dimensions of the blank (when compared with existing experimental data) at which wrinkling first occurs. In an attempt to improve the theoretical predictions a procedure proposed by Dubey and Ariaratnam [31] is adopted, whereby the original elastic-plastic formulation can be approximated by that of a rigid-plastic solid. The method is shown to yield a better comparison with experimental data for the critical dimensions of the blank. A limiting case of the elastic-plastic formulation is also demonstrated namely, the wrinkling of an elastic annulus

under external radial loading. It transpires that the predictions agree quite well with existing experimental results, and also with alternative theoretical treatment given by Rozsa [120].

Later in this chapter the Prandtl-Reuss equations are examined in greater detail, as well as their use in bifurcation analysis. It is shown that by invoking elastic-plastic compressibility, and by introducing some not unreasonable approximations regarding the form of the stress distribution within the flange of the annulus, the degree of correspondence between theoretical predictions and experimental observations is much improved. The results show that a material with a low yield stress and a high rate of hardening has a favourable effect on the prevention of buckling, and that the number of wrinkles into which the annulus collapses depends mainly on the geometric properties of the system.

When the buckling of a rigid-plastic annulus is considered, assuming the classical Levy-Mises flow rule, no buckling mode is predicted in the flange during deep drawing.

Finally the application of the proposed constitutive equation is demonstrated and it is shown that the results compare better with the experiments than all the previously mentioned approaches.

The main conclusion reached in this work is the need for an appropriate constitutive equation.

3.2 Bifurcation Criterion (Classical Approach)

Hill's bifurcation criterion (see chapter 1), for the case where $\bar{v} = \bar{o}$ on S_v, yields

$$H(\bar{v}) - \Sigma(\bar{v}) > 0, \tag{1.9}$$

for all fields vanishing on S_v, but not identically zero. In the above equation,

$$H(\bar{v}) = \int (\frac{\delta \overset{=}{\tau}}{\delta t}) : \overset{=}{J} \cdot \overset{=}{\epsilon} \, dV , \tag{1.10}$$

and

$$\Sigma(\bar{v}) = \int \overset{=}{\sigma} : (2\overset{=}{\epsilon} \cdot \overset{=}{\epsilon} - \overset{=}{L}^T \cdot \overset{=}{L}) \, dV . \tag{1.11}$$

Note that (1.9) is a sufficient but not a necessary condition for bifurcation.

When the usual assumptions of thin plates and shells are adopted the constitutive equations take the form of equations (1.43). For the special case of J_2' flow theory, the equations are expressed by (2.12). Again, μ is given by (2.9b) and the hardening parameter h is expressed as

$$h = \frac{4EE_T}{6(E-E_T)} \tag{3.1}$$

E_T is regarded as the rate of change of the Kirchhoff stress with logarithmic strain, derivable from a tensile test. The quantity E_T can, in general, also be taken as the rate of change of true stress with natural strain to a very good degree of approximation, as was done by Needleman [106] for large plastic strains. The relation between the Kirchhoff stress and true stress is

$$\tau^{\alpha\beta} = \frac{\rho^o}{\rho}\,\sigma^{\alpha\beta}$$

where ρ^o and ρ are the initial and final densities. The yield condition is given in terms of true stress, but for most common metals yielding is essentially independent of pressure and moreover metals are relatively incompressible in the plastic region, therefore little distinction need to be made between the Kirchhoff and true stress, as discussed by Lee [76] and Nemat-Nasser [109].

Substituting from (2.12) and (1.11) into the bifurcation criterion (1.9), it follows that

$$\delta(U_m + U_b + W) = 0 \tag{3.2}$$

The quantities U_m etc. are derived as

$$U_m = \int_S t\,[(\alpha_{11} - 2\sigma_{11})\,\varepsilon_{11}^{o2} + (\alpha_{22} - 2\sigma_{22})\,\varepsilon_{22}^{o2} + 2\alpha_{12}\,\varepsilon_{11}^{o}\,\varepsilon_{22}^{o} + 2(2G - \sigma_{11} - \sigma_{22})\,\varepsilon_{12}^{o2}]\,dS \tag{3.3a}$$

$$U_b = \int_S \frac{t^3}{12}\,[(\alpha_{11} - 2\sigma_{11})\,k_{11}^2 + (\alpha_{22} - 2\sigma_{22})\,k_{22}^2 + 2\alpha_{12}\,k_{11}\,k_{22} + 2(2G - \sigma_{11} - \sigma_{22})\,k_{12}^2]\,dS \tag{3.3b}$$

$$W = \int_S t\{\sigma_{11}\,[(\frac{\partial u}{\partial x_1})^2 + (\frac{\partial v}{\partial x_1})^2 + (\frac{\partial w}{\partial x_1})^2] + \sigma_{22}\,[(\frac{\partial u}{\partial x_2})^2 + (\frac{\partial v}{\partial x_2})^2 + (\frac{\partial w}{\partial x_2})^2]\}\,dS, \tag{3.3c}$$

where S = mid surface area of the shell

t = thickness

σ_{11} and σ_{22} = initial principal stresses

u,v,w = components of velocities along the principal directions.

When σ_{ij} are small compared to the moduli α_{ij}, such that they can be neglected, then U_m, U_b and W reduce to the usual expressions for the energy change due to stretching, bending and rate of change of work done by external loads, respectively, see Timoshenko and Gere [141].

The curvature rates at the middle surface are given by Langhaar [75]

$$k_{rr} = -\frac{\partial^2 w}{\partial r^2} \tag{3.4a}$$

$$k_{\theta\theta} = -\left(\frac{1}{r^2}\frac{\partial^2 w}{\partial \theta^2} + \frac{1}{r}\frac{\partial w}{\partial r}\right) \tag{3.4b}$$

$$k_{\theta r} = k_{r\theta} = -\left(\frac{1}{r}\frac{\partial^2 w}{\partial r \partial \theta} - \frac{1}{r^2}\frac{\partial w}{\partial \theta}\right) \tag{3.4c}$$

The curvatures are illustrated in Figure 3.3.

3.2.1 Application to Deep Drawing

As already mentioned, the problem of flange wrinkling during deep drawing is treated herein as a problem of buckling of an annular plate. Kulkarni [73] considered inextensional buckling

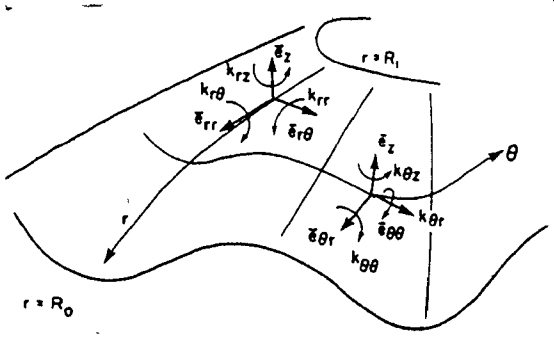

Figure 3.3 Curvature components for the wrinkled flange of an elastic-plastic annulus, where the middle surface strains are neglected, and the stability criterion reduces to the extremum of the functional given by

$$\int_S \{\frac{t^3}{12}[\alpha_{11}(\frac{\partial^2 w}{\partial r^2})^2 + \alpha_{22}(\frac{1}{r^2}\frac{\partial^2 w}{\partial \theta^2} + \frac{1}{r}\frac{\partial w}{\partial r})^2 + 2\alpha_{12}\frac{\partial^2 w}{\partial r^2}(\frac{1}{r^2}\frac{\partial^2 w}{\partial \theta^2} + \frac{1}{r}\frac{\partial w}{\partial r})$$

$$+ 4G(\frac{1}{r}\frac{\partial^2 w}{\partial r \partial \theta} - \frac{1}{r^2}\frac{\partial w}{\partial \theta})^2] dS + \int t[\sigma_{rr}(\frac{\partial w}{\partial r})^2 + \sigma_{\theta\theta}(\frac{1}{r}\frac{\partial w}{\partial \theta})^2]\} dS \quad (3.5)$$

The first variation of (3.5) gives the differential equation governing the buckling problem, together with the boundary conditions to be satisfied by w, see Brush and Almroth [8]. The Euler equation is a fourth order equation with variable coefficients. For the general case of non-symmetric deformations considered, it is not possible to obtain an analytical solution

and hence (3.5) can be minimized directly using a modified Ritz method.

3.2.1 Initial Stresses

Under plane stress conditions the radial equilibrium equation, as given by Hill [44], is

$$\frac{d}{dr}(t\sigma_r) = \frac{t(\sigma_r - \sigma_\theta)}{r} \tag{3.6}$$

The von Mises yield criterion is

$$\sigma_r^2 - \sigma_r \sigma_\theta + \sigma_\theta^2 = \bar{\sigma}^2 , \tag{3.7}$$

and the Levy-Mises flow rule and the condition of incompressibility give respectively

$$\frac{\partial u}{\partial r} = \frac{u}{r} \frac{2\sigma_r - \sigma_\theta}{2\sigma_\theta - \sigma_r} , \tag{3.8}$$

and

$$\frac{1}{t}\frac{\partial t}{\partial b} + \frac{u}{t}\frac{\partial t}{\partial r} + \frac{\partial u}{\partial r} + \frac{u}{r} = 0 . \tag{3.9}$$

In the above equation b is the current free edge radius, t is the current thickness and u the radial inward velocity.

The system of equations is hyperbolic and their solution will give σ_r, σ_θ, t and u at any point at any instant; the time being characterized by the current radius of the free edge. Solutions of these equations using various numerical techniques have been obtained, see for example Budiansky and Wang [12] and Woo [147].

The use of the above equations in conjunction with the Rayleigh-Ritz method makes the terms unwieldy, and since the main object of this work is to evaluate the appropriateness of the Prandtl-Reuss equations for bifurcation analysis, a simpler model is used. The model neglects the variation of the yield stress and the thickness across the flange and adopts the Tresca yield criterion. The stress distribution, as approximated by Kawai [70], is

$$\sigma_r = -\bar{\sigma} \ln \frac{r}{R_o} \tag{3.10}$$

$$\sigma_\theta = -\bar{\sigma} \left(1 + \ln \frac{r}{R_o}\right) \tag{3.11}$$

Strain hardening can be considered in an approximate manner by taking an average value of $\bar{\sigma}$. Fukui et al [38] showed that when the simpler model is used the maximum deviation of σ_r is 10%, whereas the maximum deviation of σ_θ is 25%, but this occurs only in the region very close to the inner edge. Since the partial restraint close to the inner edge is significant and the magnitude of the hoop stress at this location is relatively small compared to the value at the outer edge, and moreover since the critical thickness is proportional to the square root of the stresses, the difference in the two models for bifurcation purposes is expected to be small.

3.2.3 Elastic-Plastic Moduli

Tresca's yield criterion gives

$$\sigma_r - \sigma_\theta = \bar{\sigma} \ , \tag{3.12}$$

and for all practical stress states the components m_{ij} of the unit normal will remain constant throughout the plate. They are given by

$$m_{11} = \frac{1}{\sqrt{2}}$$

$$m_{22} = \frac{-1}{\sqrt{2}} \tag{3.13}$$

$$m_{33} = 0$$

Substituting (3.13) into (2.13), the values of the elastic-plastic moduli are obtained as

$$\alpha_{11} = \frac{E}{1-\nu^2}\left[1 - \frac{\mu}{2}(1-\nu)\right]$$

$$\alpha_{22} = \alpha_{11} \tag{3.14}$$

$$\alpha_{12} = \frac{E}{1-\nu^2}\left[\nu + \frac{\mu}{2}(1-\nu)\right]$$

The variation of μ with η (where $\eta = E/E_T$) is shown in Figure 3.4. Kulkarni [73] in his analysis treated μ as a constant, without specifying the selected value.

3.2.4 Boundary Conditions

The only boundary conditions imposed on w by virtue of the

geometry are

$$w = 0 \text{ at } r = R_1 , \qquad (3.15)$$

and

$$\frac{\partial w}{\partial \theta} = 0 \text{ at } r = R_1 . \qquad (3.16)$$

There is a partial restraint at the inner edge R_1 which causes the

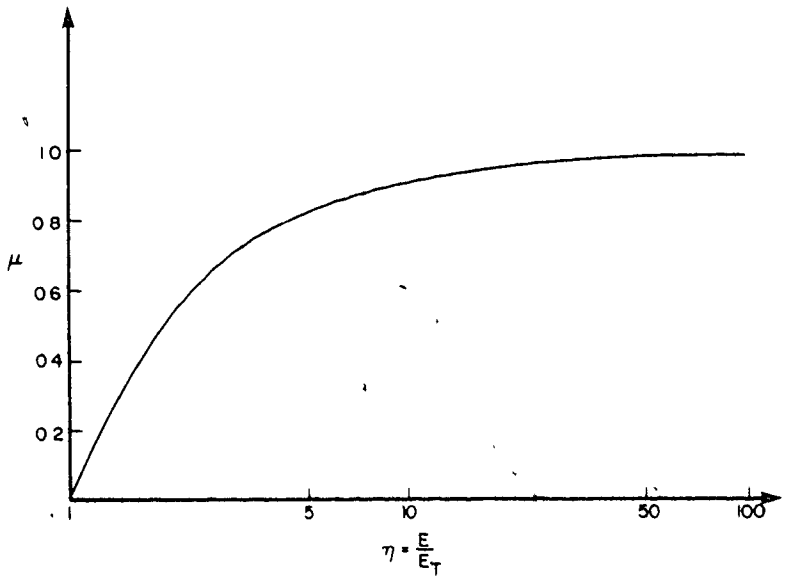

Figure 3.4 - Variation of $\bar{\mu}$ with η

slope $\frac{\partial w}{\partial r}$ at $r = R_1$ to lie between zero and the value corresponding to a freely supported edge defined here as $(\frac{\partial w}{\partial r})_o$

i.e.

$$0 \leq \frac{\partial w}{\partial r} \leq (\frac{\partial w}{\partial r})_o \text{ at } r = R_1$$

The outer edge, $r = R_o$, is free, thus no forced boundary condition is imposed on w at this edge. Other than (3.15) and (3.16), the

remaining boundary conditions occur as natural conditions obtained from the first variation of (3.2). These need not be satisfied by the trial function chosen to minimize (3.2) by the Ritz method.

3.2.5 The Trial Displacement Function

The minimization of (3.2), taken as the condition for stability, is carried out by assuming a trial function w given by

$$w = f(r) \cos n\theta \tag{3.17}$$

In the above equation n is an integer and the function of r contains a number of undetermined coefficients and is such that (3.15) and (3.16) are satisfied. Substituting (3.17) into (3.2) and differentiating the expression with respect to the unknown coefficients of f(r), results in a set of linear equations analogous to Ritz's equations. The usual condition for the existence of non-trivial solutions i.e. the vanishing of the determinant of the coefficients, provides a value for the critical thickness. The largest of these, corresponding to the smallest eigenvalue, is of interest. The calculation is repeated for increasing values of n, in order to reveal an overall maximum value of critical thickness. The particular value of n at which this occurs gives the number of waves into which the plate buckles.

3.2.6 An Illustrative Example

To determine the feasibility of using (3.17) as a trial

function and also to assess the speed of convergence, the buckling of an elastic annular disc was considered. A solution to the same problem has also been given by Rozsa [120], using an alternative analytical procedure.

The disc is assumed to have a uniform thickness and is subjected to a uniformly distributed pressure of σ_o per unit area of the outer edge.

$r = 1$ is taken as outer edge

and $r = R_1$ is the inner edge and $0 \leq R_1 \leq 1$

The stress distribution within the disc, as given by Sokolnikoff [136], is

$$\sigma_r = -\sigma_o \frac{1}{1 - R_1^2} \left(1 - \frac{R_1^2}{r^2}\right) \tag{3.18}$$

$$\sigma_\theta = -\sigma_o \frac{1}{1 - R_1^2} \left(1 + \frac{R_1^2}{r^2}\right) \tag{3.19}$$

The disc is assumed clamped at the outer edge, while the inner edge is completely free, as shown in Figure 3.5. The disc buckles into a series of circumferential waves analogous to the buckling of the flange in deep drawing. Thus in (3.17)

$$w = 0 \text{ and } \frac{\partial w}{\partial \bar{n}} = 0 \text{ at } r=1 , \tag{3.20}$$

where $(\partial w/\partial \bar{n})$ is the normal derivative.

Taking into account (3.20), a trial function is selected as,

$$w = (r^2-1)^2 \left(a_1 + a_2 r^2 + a_3 r^4 + \ldots.\right) \cos n\theta \tag{3.21}$$

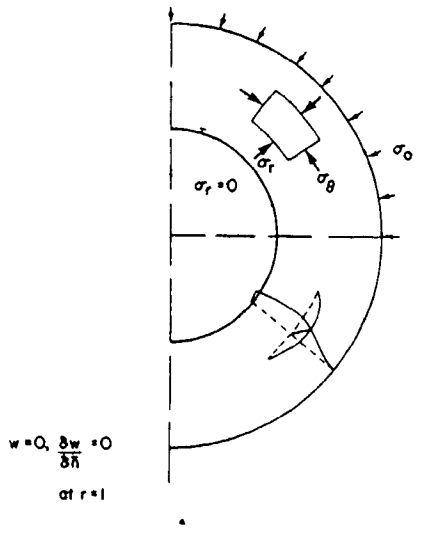

Figure 3.5 Buckling of an annular plate clamped and loaded at the outer edge - inner edge free

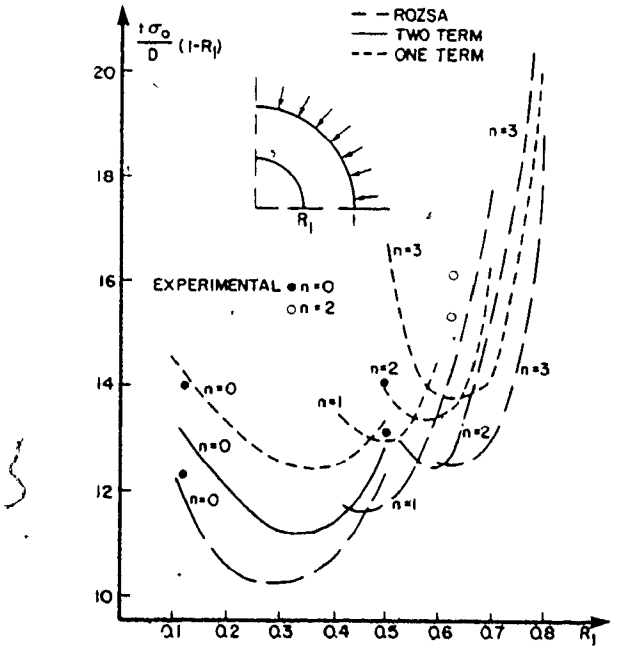

Figure 3.6 Elastic buckling of an annular plate

Since the material of the annular plate is assumed purely elastic, the moduli in (2.13) become

$$\alpha_{11} = \alpha_{22} = \frac{2G}{1-\nu}, \qquad \alpha_{12} = \frac{2\nu G}{1-\nu}. \tag{3.22}$$

From (3.21), (3.22) and (3.2), and carrying out the routine calculations discussed earlier, the critical stress σ_o is obtained as the lowest eigenvalue. Results of the calculations are given in Appendix C and are shown in Figure 3.6. On the same graph, the values obtained by Rozsa [120] are also shown. It is seen that even with only one term in (3.21), the values obtained are within 20% of corresponding results of Rozsa. Two terms give results to within 8%. On the same figure are also shown the experimental points by Majumdar [96]; the figure demonstrates that the present solution agrees well with experiments.

It is clear that the criterion (1.9) reduces to the classical energy criterion and we therefore expect to solve the elastic buckling problem as a special case of (1.9).

3.2.7 Elastic Plastic Analysis of Deep Drawing

For the elastic-plastic annulus, the stability criterion of (3.5) together with the moduli of (3.14) can lead to predictions of the critical thickness.

The condition for an extremum of (3.2) can be written in

the form

$$\delta[L(w) + \frac{1}{t^2} M(w)] = 0 \qquad (3.23)$$

where L(w) contains all the integrals involving E-P moduli and M(w) contains integrals involving initial stresses. Out of these two, L(w) is always positive definite. However, since σ_r and σ_θ are of opposite sign, M(w) may not always be positive definite. When (3.17) is used as a trial function for w, M(w) will be positive only when n is greater than a certain value n_o, indicating that modes of buckling for $n < n_o$ are inadmissible. When n is increased further, the critical thickness calculated gradually increases and reaches a maximum for a certain value of n. This gives the desired buckling mode. Some results arising from this method are shown in Figure 3.7 for R = 1.5, i.e. the ratio of outside to inside diameter of the annulus.

Figure 3.8 shows the variation of the critical thickness t^* (defined as $t/2R_o$) with R, also shown for comparison are the experimental results obtained by Miyagawa [90]. Appendix C gives the expression for t^* plotted in Figure 3.8. From Figure 3.8 it is seen that the predicted critical thickness is considerably less than the experimentally determined values. Figure 3.9 shows the effect of the normalised stress $\sigma^* = \bar{\sigma}/E$, and relative hardening n on the critical thickness. It is clear from the figure that for $n>10$, the relative hardening has little effect. The number of waves into which the blank buckles as determined experimentally by Kawai [70] is shown in Figure 3.10. Also shown in the figure are

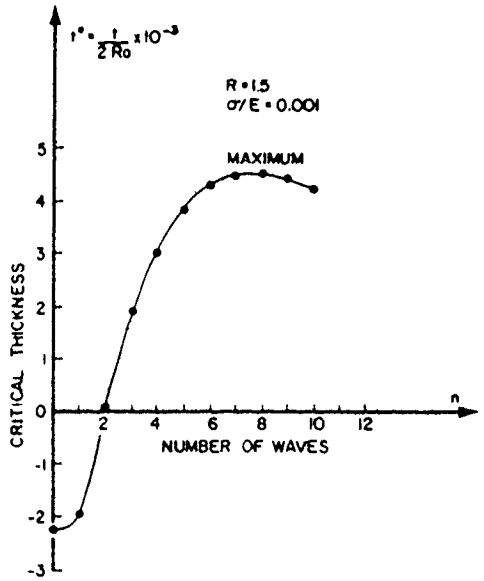

Figure 3.7 Variation of critical thickness ratio with number of waves

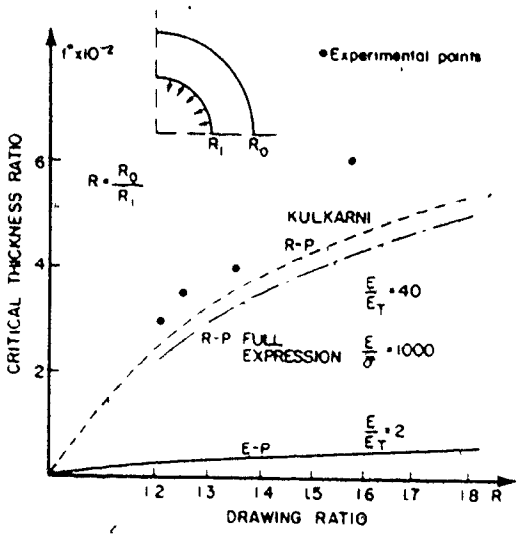

Figure 3.8 Variation of critical thickness ratio with drawing ratio

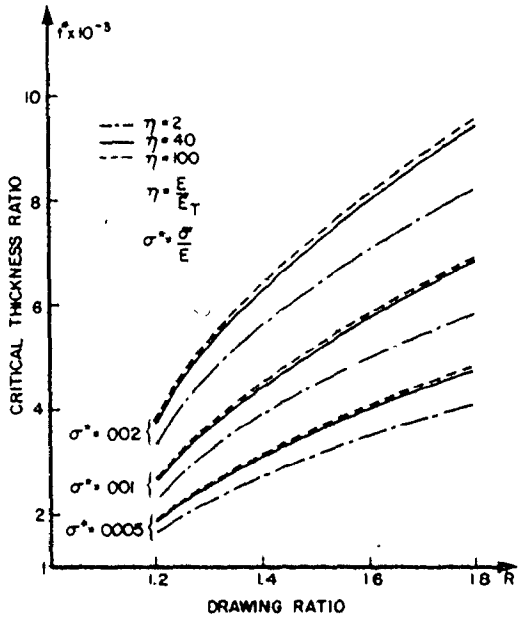

Figure 3.9 Variation of critical thickness ratio with drawing ratio - E-P analysis

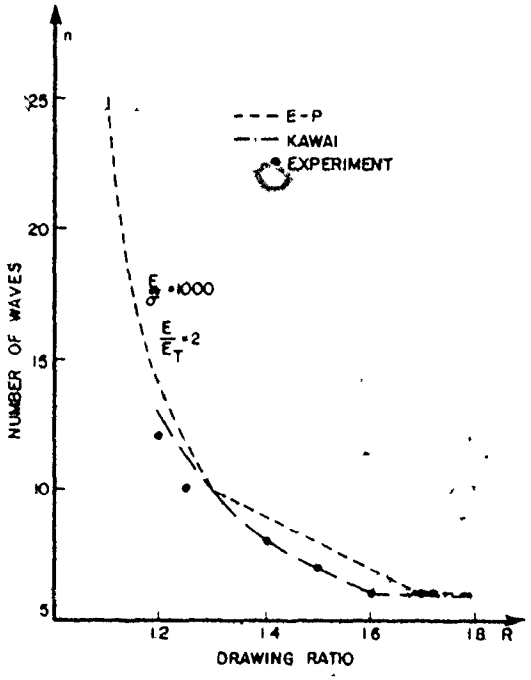

Figure 3.10 Change of number of waves with drawing ratio

the theoretical predictions of Kawai, Opt. cit., and those from the present theory, a reasonable correspondence is obtained in each case.

3.3 A Possible Approach for Rigid-Plastic Solids

It was shown in section 2.3.1 that the bifurcation of a rigid-plastic solid can be approximated by neglecting the incremental elastic work term in the uniqueness criterion, and the final expression is given by (2.45).

In his treatment of the problem, Kulkarni [73] neglected terms of the form σk^2 and $\sigma\varepsilon^{o2}$ with respect to Ck^2 and $C\varepsilon^{o2}$ in (2.47). This is not entirely justified as will be demonstrated later. With the additional assumption of no stretching of the middle surface (2.45) reduces to

$$\delta(U_b + W) = 0 , \tag{3.24}$$

where

$$U_b = \frac{t^3}{12} \frac{3E(\eta-1)}{(3\eta+2\nu-1)^2} \int_S (k_r^2 + k_\theta^2 - 2k_r k_\theta)\, dS , \tag{3.25}$$

and

$$W = t \int_S [\sigma_r \left(\frac{\partial w}{\partial r}\right)^2 + \sigma_\theta \left(\frac{1}{r}\frac{\partial w}{\partial \theta}\right)^2]\, dS . \tag{3.26}$$

The curvatures and stresses in the above expressions are given by (3.4a), (3.4b), (3.10) and (3.11). The trial function for w is again of the form of (3.21) and only one term was retained in Kulkarni's original treatment.

The effect of retaining all the terms in (2.47) on the critical thickness predictions is demonstrated in Figure 3.8. More significant however is that the rigid-plastic analysis can lead to better predictions of critical blank dimensions vis à vis the elastic-plastic analysis. This is somewhat surprising in view of the manipulations that have been performed on the elastic-plastic formulation. In fact Bruhns and Thermann [7] have criticised the accuracy of neglecting the incremental elastic work in (2.39) when this was attempted by Dubey and Ariaratnam [31] in another context.

Figure 3.11 demonstrates the influence of the tangent modulus, E_T, on the critical thickness. It is a controlling influence in the rigid-plastic analysis but apparently plays very little role in the elastic-plastic analysis, as can be seen from the same figure. This again is rather surprising and raises some doubt about the original elastic-plastic formulation. The effect of hardening in each type of analysis is further demonstrated by comparing Figures 3.9 and 3.12, it is certainly more dominant with the rigid-plastic model.

Regardless of the type of analysis employed, the prediction of the number of waves into which the blank buckles is relatively unaffected. This can be seen by comparing Figures 3.10 and 3.13, although the critical thickness changes significantly. Figure 3.14 shows the effect of changing the hardening parameter on the predicted wave formation in the rigid-plastic analysis, again the

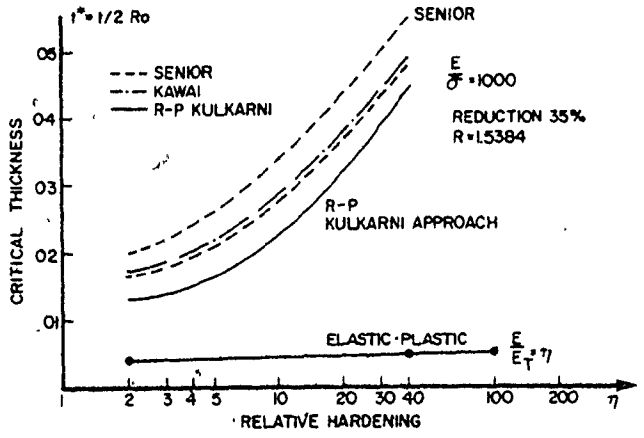

Figure 3.11 Variation of critical thickness ratio with relative hardening

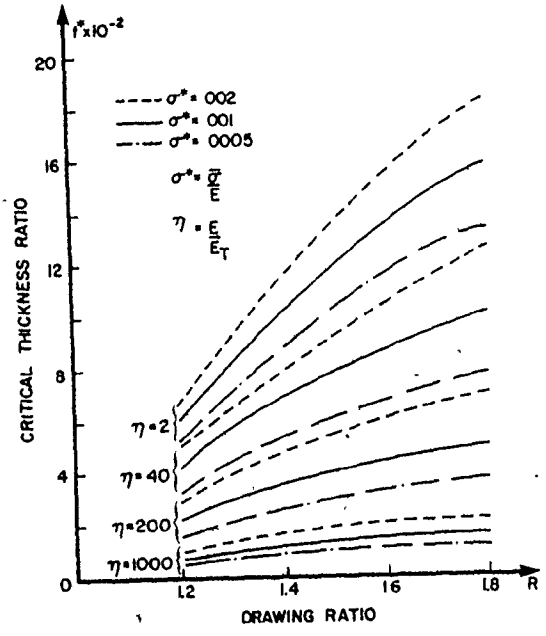

Figure 3.12 Change of critical thickness ratio with drawing ratio - R-P analysis, full expression

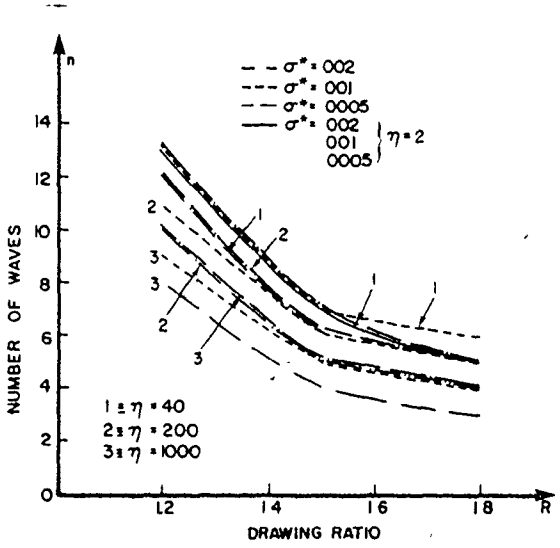

Figure 3.13 Variation of the number of waves with drawing ratio - R-P analysis, full expression

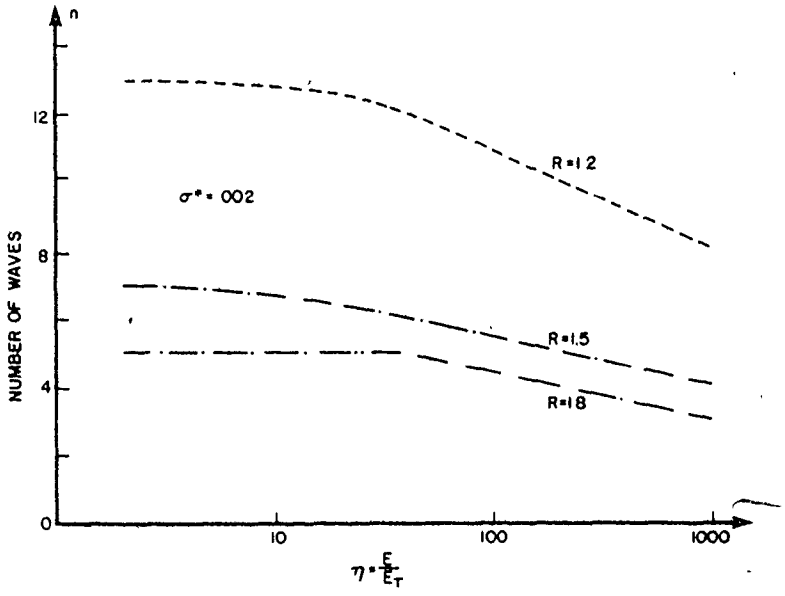

Figure 3.14 Effect of material properties on the number of waves - R-P analysis, full expression

effect is minimal. Further discussion on this point is given later in the chapter.

The final expressions for critical thickness based on (3.25), as assumed by Kulkarni, Opt. cit., and that based on the more complete expression of (2.47), are given in Appendix C.

There still remains an adequate explanation to account for the discrepancy between the predictions based on the elastic-plastic and rigid-plastic models, as presented in the preceding sections. There can be an order of magnitude difference in the predictions of critical thickness based on the respective analyses. It is difficult to imagine that this arises through the neglect of the incremental elastic work contribution (in the rigid-plastic analysis presented here), particularly so if the plastic strains are large. Note that in (2.47) and (3.25) the torsional curvature change $k_{r\theta}$ does not enter into the calculations, as a consequence of the Prandtl-Reuss equations, and it is therefore quite surprising that the R-P approach compares better with experiment than the classical E-P approach. However a closer examination reveals that the term containing $k_{r\theta}$ is the responsible for disparity between theory and experiment, as will be exemplified in the next sections. Therefore, we return to querying the appropriateness of the Prandtl-Reuss equations in the bifurcation analysis notwithstanding their successful application in many numerical procedures.

3.4 Semi Empirical Approach

To further exemplify the shortcomings of the Prandtl-Reuss equations, a semi-empirical approach developed in section 2.3.2 is now applied to the deep drawing problem.

When the appropriate values of strain ratio, $x = -1$, and unit normal m_{ij} are substituted in the bifurcation criterion (2.65), the expression becomes

$$\delta \int \{ 2\varepsilon_{11}^{2}(h - \sigma_{11} - \sigma_{22}) + 2\varepsilon_{12}^{2}(\alpha_{33} - \sigma_{11} - \sigma_{22}) + \sigma_{ik} w_{j,i} w_{j,k} \} dV > 0 \quad (3.27)$$

For large plastic strains, the stresses are in the same order of magnitude as the tangent modulus and cannot therefore be neglected in the first term of (3.27). From (2.13d), $\alpha_{33} = 2G$ and if this were substituted in (3.27) it would be clear that the term multiplied by 2G will be the dominant term, since $2G >> h$ (for large strains), unless the first two terms are of the same order of magnitude. This would imply that

$\int [\varepsilon_{12}^{2} (2G - \sigma_{11} - \sigma_{22})] dS$ and $\int [\varepsilon_{11}^{2} (h - \sigma_{11} - \sigma_{22})] dS$

are of the same order, i.e.

$$\int \varepsilon_{11}^{2} dS >> \int \varepsilon_{12}^{2} dS \quad (3.28)$$

If (3.28) is not satisfied, (3.27) would indicate that whatever the instability mode and the homogeneous stress system, the bifurcation phenomenon is shear predominant, which is physically and mathematically untrue for elastic solids and therefore would appear to be questionable for elastic-plastic solids. It cannot be claimed in general that $\varepsilon_{11} >> \varepsilon_{12}$ since the change in

curvature is governed by the compatibility equations for the deformed middle surface.

In evaluating the strain rates at bifurcation, equations (2.10) are used, where as emphasized before the plastic strain increment is independent of the direction of stress increment. In other words, according to the Prandtl-Reuss equations, the shear part of the plastic strain rate at bifurcation is insensitive to the bifurcation mode, which is a serious deficiency for this type of analysis.

The section immediately following provides details of the semi-empirical method as applied to the flange wrinkling problem.

3.4.1 Application to Deep Drawing

As mentioned earlier the hoop stress in the flange is unlikely to go tensile and a limiting case could appear to be $\sigma_\theta = 0$ at the inside radius of the flange; while σ_r is always zero at the rim. Accordingly the range of possible stress states is shown in Figure 3.2. From (2.57) the range of x for the case of deep drawing is

$$-2 \leq x \leq -1/2 \ .$$

Hill [44] states that the variation of thickness across the blank at any instant can be neglected in the equation of equilibrium, with at most a 5 per cent error in σ_r for drawing ratios less than 2. Furthermore, wrinkling occurs early in the drawing process so that the thickness variation across the flange can be neglected.

In this case the problem simplify significantly and we have a plane stress and plane strain condition superimposed, so that for the von Mises yield criterion

$$x = -1 \tag{3.29a}$$

$$\sigma_{11} = -\sigma_{22} \tag{3.29b}$$

$$m_{11} = -m_{22} = \frac{1}{\sqrt{2}} \tag{3.29c}$$

$$\varepsilon_{11}^{p} = -\varepsilon_{22}^{p} \tag{3.29d}$$

$$\varepsilon_{12}^{p} = 0 \tag{3.29e}$$

Equations (3.29a), (3.29c) and (3.29d) can also result from the application of the normality condition to the Tresca yield surface, and therefore are consistent with equations (3.10) and (3.11). It is clear that the unit normals to the von Mises and Tresca yield surfaces coincide at this particular stress state and this simplification allows the problem to be solved explicitly. Hence, for large plastic strains from (2.54)

$$\left(\frac{\delta\tau_{11}}{\delta t}\right)^{J} = h\varepsilon_{11} , \tag{3.30a}$$

$$\left(\frac{\delta\tau_{22}}{\delta t}\right)^{J} = -h\varepsilon_{11} = h\varepsilon_{22} , \tag{3.30b}$$

and

$$\left(\frac{\delta\tau_{12}}{\delta t}\right)^{J} = 2G\,\varepsilon_{12} . \tag{3.30c}$$

It is apparent from (3.30) that in general

$$\left(\frac{\delta\tau_{12}}{\delta t}\right)^{J} >> \left(\frac{\delta\tau_{11}}{\delta t}\right)^{J} \text{ and } \left(\frac{\delta\tau_{22}}{\delta t}\right)^{J}, \text{ for } \frac{h}{2G} << 1.$$

This is the result of neglecting the plastic component of the shear strain rate and retaining the elastic component, even though we know that for large plastic strains

$$||\bar{\bar{\varepsilon}}^p|| >> ||\bar{\bar{\varepsilon}}^e|| \quad .$$

The only way the above statement would be contradicted would be if (3.28) applied, and this possibility is examined in the next section. It is now proposed to make the terms between brackets in equation (3.27) of the same order of magnitude by substituting h for 2G. In this case the equation becomes

$$\begin{aligned} \delta \{ & 2 \int (\varepsilon_{11}^2 + \varepsilon_{12}^2)(h - \sigma_{11} - \sigma_{22}) r \, dr d\theta \, dz \\ & + \int \{ \sigma_{11} [(\frac{\partial u}{\partial r})^2 + (\frac{\partial v}{\partial r})^2 + (\frac{\partial w}{\partial r})^2] \\ & + \sigma_{22} [(\frac{1}{r} \frac{\partial u}{\partial \theta})^2 + (\frac{1}{r} \frac{\partial v}{\partial \theta})^2 + (\frac{1}{r} \frac{\partial w}{\partial \theta})^2] \} \, r \, dr d\theta \, dz \} = 0 \end{aligned} \tag{3.31}$$

It should be noted that the simple model given by equations (3.29) makes the expressions in the Rayleigh-Ritz procedure manageable. It is unlikely that the answer will be drastically affected to the extent of an order of magnitude difference that already exists between the E-P theory and the experimental results.

3.4.2 Trial Function

Any kinematically admissible set of velocity fields and strain rate fields has to satisfy the kinematic boundary conditions, the strain compatibility equations and possibly any additional constraints like compressibility. The kinematic

boundary conditions for w are given by (3.15) and (3.16). In the present problem the following constraints are also imposed,

$$\varepsilon_{33} = \varepsilon_{13} = \varepsilon_{31} = \varepsilon_{23} = \varepsilon_{32} = 0 , \tag{3.32a}$$

$$\varepsilon_{11} + \varepsilon_{22} + \varepsilon_{33} = 0 . \tag{3.32b}$$

The strains in terms of displacements are

$$\varepsilon_{33} = \frac{\partial w}{\partial z} = 0 \tag{3.33a}$$

$$2\varepsilon_{13} = \frac{\partial u}{\partial z} + \frac{\partial w}{\partial r} = 0 \tag{3.33b}$$

$$2\varepsilon_{23} = \frac{\partial v}{\partial z} + \frac{1}{r}\frac{\partial w}{\partial \theta} = 0 \tag{3.33c}$$

$$\varepsilon_{11} = \frac{\partial u}{\partial r} + z\, k_{11} \tag{3.33d}$$

$$\varepsilon_{22} = \left(\frac{1}{r}\frac{\partial v}{\partial \theta} + \frac{u}{r}\right) + z\, k_{22} \tag{3.33e}$$

$$\varepsilon_{12} = \frac{1}{2}\left(\frac{\partial v}{\partial r} + \frac{1}{r}\frac{\partial u}{\partial \theta} - \frac{v}{r}\right) + z\, k_{12} \tag{3.33f}$$

The curvature rates k_{11} and k_{22} are given by (3.4). It should be noted that if the curvature terms were excluded, the equations for strains are linear in the velocity components and consequently the solution could be interpreted as the difference between two solutions. This shows that the extent of indeterminancy of the velocity fields is to the extent of an additive multiple of the eigenfield, and this approach is used for bifurcation with symmetric modes such as necking and bulging.

The general solution of (3.32) through (3.33) is

$$u = z \frac{\partial f_1}{\partial r}(r,\theta) + u^*(r,\theta) \tag{3.34a}$$

$$v = \frac{z}{r} \frac{\partial f_1}{\partial \theta}(r,\theta) + v^*(r,\theta) \tag{3.34b}$$

$$w = -f_1(r,\theta) \tag{3.34c}$$

where $f_1(r,\theta)$, $u^*(r,\theta)$ and $v^*(r,\theta)$ are arbitrary functions.

Let $f_1(r,\theta) = f(r) \cos n\theta$ (3.35)

and upon combining (3.32b), (3.33d), (3.33e) and (3.35) it follows that

$$\left[\frac{1}{r} \frac{\partial v^*}{\partial \theta}(r,\theta) + \frac{1}{r} u^*(r,\theta) + \frac{\partial u^*}{\partial r}(r,\theta)\right] +$$

$$2z \cos n\theta \left[-\frac{n^2}{r^2} f(r) + \frac{1}{r} \frac{\partial f}{\partial r}(r) + \frac{\partial^2 f}{\partial r^2}(r)\right] = 0 \tag{3.36}$$

In (3.36) it is evident that the z dependent and z independent parts must vanish separately. This leads to two differential equations, as follows

$$\frac{1}{r} \frac{\partial v^*}{\partial \theta}(r,\theta) + \frac{1}{r} u^*(r,\theta) + \frac{\partial u^*}{\partial r}(r,\theta) = 0 , \tag{3.37}$$

$$\frac{-n^2}{r^2} f(r) + \frac{1}{r} \frac{\partial f}{\partial r}(r) + \frac{\partial^2 f}{\partial r^2}(r) = 0 . \tag{3.38}$$

The solution of (3.37) is subject to the boundary conditions

$$u^*(r,\theta) = v^*(r,\theta) = 0, \text{ at } r=R_1 \text{ and } z=0. \tag{3.39}$$

In what follows the symbols u^* and v^* are used rather than keep writing $u^*(r,\theta)$ etc. The solution of (3.38), subject to the

boundary conditions (3.15) and (3.16), is,

$$f(r) = C_1[r^n - R_1^{2n} r^{-n}] \cos n\theta \ , \qquad (3.40)$$

where C_1 and C_2 are constants to be determined from the boundary conditions. Substituting from (3.40) into (3.34a) leads to

$$u = u^* + z\, C_1\, n\, R_1^{n-1} [(\frac{r}{R_1})^{n-1} + (\frac{r}{R_1})^{-n-1}] \cos n\theta \qquad (3.41a)$$

$$v = v^* - z\, C_1\, n\, R_1^{n-1} [(\frac{r}{R_1})^{n-1} - (\frac{r}{R_1})^{-n-1}] \sin n\theta \qquad (3.41b)$$

$$w = -C_1 R_1^n [(\frac{r}{R_1})^n - (\frac{r}{R_1})^{-n}] \cos n\theta \qquad (3.41c)$$

From (3.33) and (3.41c) it follows that

$$\epsilon_{11} = \epsilon_{11}^o + 2zk_{11} \qquad (3.42a)$$

$$\epsilon_{11}^o = u^*,r \qquad (3.42b)$$

$$\epsilon_{22} = -\epsilon_{11} \qquad (3.42c)$$

$$\epsilon_{22}^o = \frac{1}{r}(u^* + v^*,\theta) \qquad (3.42d)$$

$$\epsilon_{12} = \epsilon_{12}^o + 2zk_{12} \qquad (3.42e)$$

$$\epsilon_{12}^o = \frac{1}{2}[v^*,r + \frac{u^*}{r},\theta - \frac{v^*}{r}] \qquad (3.42f)$$

The k_{11} etc. are as before.

It should be noted that (3.42c) satisfies (2.57) and hence the moduli satisfy (2.60). The constraints on the part S_v of the

edge are supposed satisfied to within a reasonable approximation by requiring u=v=w=o and $\frac{1}{r}\frac{\partial w}{\partial \theta} = 0$ on the middle surface at $r=R_1$. The condition $\frac{\partial w}{\partial r} = 0$ is relaxed here since it does not necessarily simulate the actual case of deep drawing.

3.4.3 Bifurcation with Transverse Velocity only Considered

In this case it is assumed that

$$u = v = o \tag{3.43}$$

and w is given by (3.41a). The bifurcation criterion (3.27) reduces to

$$\delta \{ \int \frac{t^3}{6} [k_{11}^2 (h - \sigma_{11} - \sigma_{22})^2 + k_{12}^2 (\alpha_{33} - \sigma_{11} - \sigma_{22})] \, rdrd\theta$$

$$+ \int t[\sigma_{11}(\frac{\partial w}{\partial r})^2 + \sigma_{22}(\frac{1}{r}\frac{\partial w}{\partial \theta})^2] \, rdrd\theta \} = 0 \tag{3.44}$$

As discussed previously if α_{33} equalled 2G, the bifurcation criterion would be shear predominant unless (3.28) applies or, in this case, when

$$\int k_{11}^2 \, dS >> \int k_{12}^2 \, dS \, . \tag{3.45}$$

To verify this assumption, the ratio Q, where

$$Q = \frac{\int k_{11}^2 \, rdrd\theta}{\int k_{12}^2 \, rdrd\theta} = \frac{x_1}{x_2} \tag{3.46}$$

is plotted in Figure 3.15. It is clear that for the full range considered (3.45) does not apply. The quantities in (3.46) are

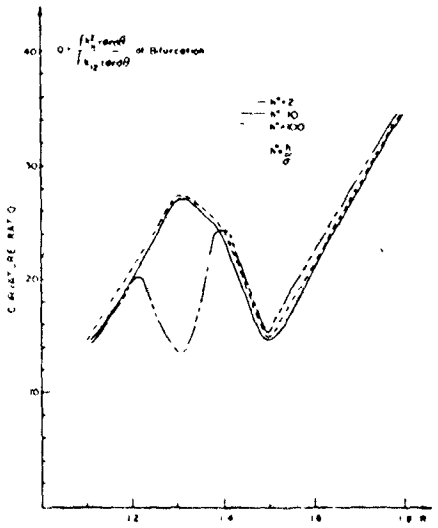

Figure 3.15 Variation of curvature ratio with drawing ratio - proposed E-P model

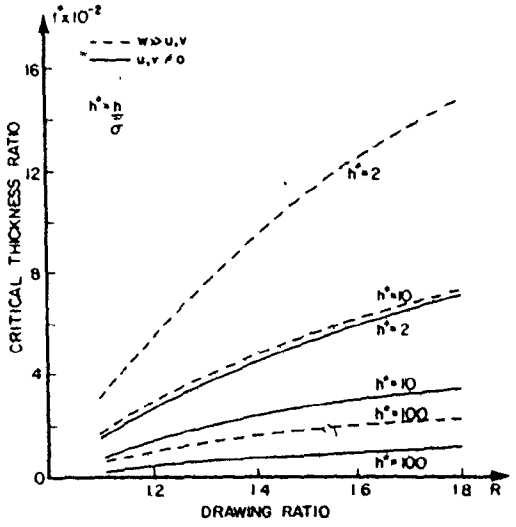

Figure 3.16 Variation of critical thickness ratio with drawing ratio - proposed E-P model

$$x_1 = (\frac{n-1}{2})\, R^{2n-2} - (\frac{n+1}{2})\, R^{-2n-2} + (n^2-1)\, R^2 + (2-n^2) ,$$

$$x_2 = (\frac{n-1}{2})\, R^{2n-2} - (\frac{n+1}{2})\, R^{-2n-2} - (n^2-1)\, R^2 + n^2 ,$$

$$k_{11} = n\, R_1^{\,n-2}\, C_1 \cos n\theta\, [(n-1)x^{n-2} - (n+1)\, x^{-n-2}] , \tag{3.47}$$

and $$k_{12} = -n\, R_1^{\,n-2}\, C_1 \sin n\theta\, [(n-1)x^{n-2} + (n+1)\, x^{-n+2}] .$$

It follows that to avoid the shear component dominating the analysis α_{33} is replaced in (3.44) by a term which is in the order of the tangent modulus. Under these circumstances (3.44) becomes

$$\delta \{\int \frac{t^3}{6} [(k_{11}^{\,2} + k_{12}^{\,2})\, (h - \sigma_{11} - \sigma_{22})]\, r dr d\theta$$

$$+ \int t[\sigma_{11}(\frac{\partial w}{\partial r})^2 + \sigma_{22}(\frac{1}{r}\frac{\partial w}{\partial \theta})^2]\, r dr d\theta\} = 0 \tag{3.48}$$

or

$$t^{*2} = \frac{3}{2}\frac{M}{L} \tag{3.49}$$

where

$$M = \frac{n-1}{2n^2} R^{2n} - \frac{n+1}{2n^2} R^{-2n} + \frac{1}{n^2} - 2 \ln R ,$$

$$L = [(n-1)\, h^* + (n-2)]\, R^{2n} - [(n+1)\, h^* + (n+2)]\, R^{-2n}$$

$$- 4 R^2 \ln R + 2R^2 (h^*+2) , \tag{3.50}$$

and $$h^* = \frac{h}{\bar{\sigma}} .$$

The predictions for critical thickness based on (3.48) are shown in Figure 3.16. It is apparent that the current analysis

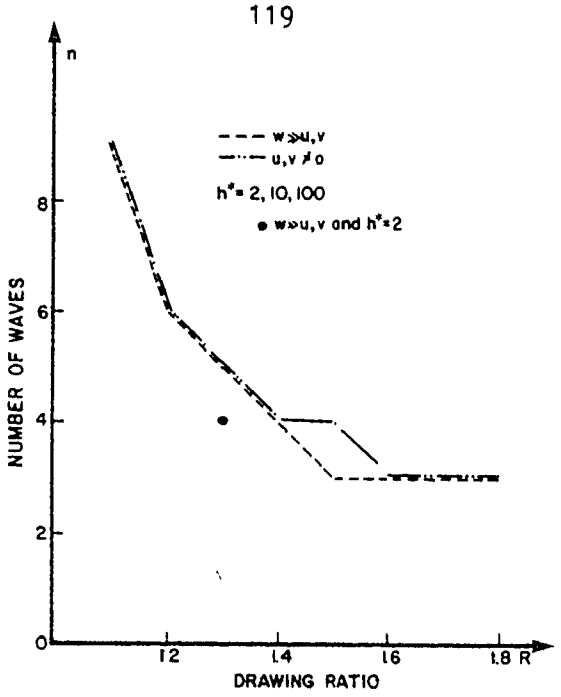

Figure 3.17 Variation of number of waves with drawing ratio - proposed E-P model

can lead to critical blank dimensions more in keeping with experimental observations. For comparison refer to Figure 3.8. The predictions for the wave formation are shown in Figure 3.17.

3.4.4 Bifurcation with Stretching and Bending Included

The analysis of the preceding section can be extended to allow for the stretching work. In this case the displacements are given by (3.41) and the bifurcation criterion becomes

$$\delta \Big[\int 2(\overset{\circ}{\varepsilon}{}^{2}_{11} + \varepsilon^{o2}_{12})\,(h - \sigma_{11} - \sigma_{22})\, dS$$

$$+ \int \frac{2}{3} t^2 \,(k_{11}{}^2 + k_{12}{}^2)\,(h - \sigma_{11} - \sigma_{22})\, dS$$

$$+ \int \frac{1}{t} \Big\{\sigma_{11}\Big[\Big(\frac{\partial u}{\partial r}\Big)^2 + \Big(\frac{\partial v}{\partial r}\Big)^2 + \Big(\frac{\partial w}{\partial r}\Big)^2\Big]$$

$$+ \sigma_{22}\Big[\Big(\frac{1}{r}\frac{\partial u}{\partial \theta}\Big)^2 + \Big(\frac{1}{r}\frac{\partial v}{\partial \theta}\Big)^2 + \Big(\frac{1}{r}\frac{\partial w}{\partial \theta}\Big)^2\Big]\Big\}\, dS\Big] = 0\,, \qquad (3.51)$$

or $$\delta(U_m + U_b + W) = 0 \quad .$$

After performing some lengthy but straight forward manipulations, the critical thickness is given by

$$t^{*2} = \frac{3E_2}{E_3} - \frac{3}{\pi}\left(\frac{1}{R_1 {}^{n}C_1}\right)^2 \frac{E_1}{E_3} \quad , \tag{3.52}$$

where E_1, E_2, and E_3 are given in Appendix C, and the moduli are assumed to be independent of z. Equation (3.52) contains three unknowns u*, v* and C_1 and it is required to maximize the critical thickness with respect to them. It is clear from Appendix C that E_2 and E_3 do not involve u* and v* and moreover E_1, E_2, and E_3 are positive definite. Hence the maximization procedure will furnish

$$u^* = v^* = 0 \quad . \tag{3.53}$$

Therefore for maximum critical thickness, the stretching work of the middle surface has to be equal to zero, see equations (3.41a) and (3.41b). This conclusion was also reached by Sewell [125] for thin plates, and by Naruse and Takeyama [99, 100].

The critical thickness at bifurcation is shown in Figure 3.16 and compared to the case where only the transverse velocity was considered. By comparing the experimental results in Figure 3.8 to the theoretical ones in Figure 3.16, it is obvious that the model which takes the three velocities into account (section 3.4.4) compares better with the experiments than the model which involves only the transverse velocity w, see section 3.4.3. Moreover, the two models proposed in sections 3.4.3 and 3.4.4

compare substantially better with experiment than the E-P model described in section 3.2.7. The number of waves into which the blank buckles, as predicted by the models of sections 3.4.3 and 3.4.4 is shown in Figure 3.17. As can be seen, little difference exists between each model. However, the predicted number of waves from these models is somewhat less than the experimental observations of Kawai, compare Figure 3.17 and Figure 3.10. It should be remembered that the trial function in the proposed models obeys (2.57), whereas there was no such restriction on the trial function used in section 3.2.5. Another difference exists in the kinematic boundary conditions since it was felt, in the proposed model, that the condition $\frac{\partial w}{\partial r} = 0$ at $r=R_1$ is too restrictive and hence it was relaxed.

In general it is more important to predict the critical thickness than the number of waves at wrinkling.

3.5 Rigid Plastic Analysis

When the material is assumed to be R-P from the onset, equation (1.9) together with (2.34) and (2.36) should be applied; the admissible velocity field has to be such that the principal axes of the plastic strain rate coincide with those of the stress. For deep drawing the R-P classical constitutive equations imply

$$\varepsilon_{12} = \varepsilon_{12}^{p} = \varepsilon_{12}^{o} + z\, k_{12} = 0 \qquad (3.54)$$

and equations (3.32) and (3.33) have still to be satisfied.

However equation (3.54) demands that

$$\overset{\circ}{\varepsilon}_{12} = k_{12} = 0 \ . \tag{3.55}$$

Since k_{12} is the twist of the unit triad about the tangent unit vector ($\bar{e}_r$ in Figure 3.3), we therefore cannot have a buckled surface with $k_{12} = 0$. Accordingly, the possibility of wrinkling, in deep drawing for R-P materials, is ruled out by the constitutive equations alone.

3.6 Application of the Proposed Constitutive Equation to the Wrinkling Problem

In section 2.4 a proposed modification to the Prandtl-Reuss equations was first introduced, and the constitutive equations for a R-P solid were given by (2.80). These equations are now employed in the bifurcation criterion to study flange wrinkling. The procedure is to use the bifurcation criterion of equation (1.9) along with $H(\bar{v})$ and $\Sigma(\bar{v})$ given by (2.115) and (1.11) respectively. Note that the proposed constitutive equation no longer requires the plastic strain rate (or increment) to be normal to the yield surface existing just prior to the stress increment, and therefore equation (2.34) does not apply here.

Since

$$\left(\frac{\delta \overset{=}{\tau}'}{\delta t}\right)^J = \left(\frac{\delta \overset{=}{\tau}}{\delta t}\right)^J - \frac{\overset{=}{1}}{3}\left[\left(\frac{\delta \overset{=}{\tau}}{\delta t}\right)^J : \overset{=}{1}\right]$$

and

$$\overset{=}{\varepsilon} : \overset{=}{1} = 0 \ ,$$

it follows that

$$\left(\frac{\delta \bar{\bar{\tau}}'}{\delta t}\right)^J : \bar{\bar{\epsilon}} = \left(\frac{\delta \bar{\bar{\tau}}}{\delta t}\right)^J : \bar{\bar{\epsilon}} \quad . \tag{3.56}$$

From (2.115) when stretching work is neglected,

$$H(\bar{v}) = \int \left(\frac{\delta \bar{\bar{\tau}}'}{\delta t}\right)^J : \bar{\bar{\epsilon}} \, dV = \int z^2 \bar{\bar{k}} : h\bar{\bar{1}} : \bar{\bar{k}} \, dV$$

$$= h \int_{-t/2}^{t/2} z^2 \, (\bar{\bar{k}} : \bar{\bar{k}}) \, dz \, dS$$

$$= \frac{ht^3}{12} (k_{11}^2 + k_{22}^2 + 2k_{12}^2) \, dS \quad . \tag{3.57}$$

If it is assumed that u and v << w , the bifurcation criterion (1.9) takes the form

$$\delta \{ \int \frac{t^2}{12} [(h - 2\sigma_{11})k_{11}^2 + (h - 2\sigma_{22})k_{22}^2 + 2(h - \sigma_{11} - \sigma_{22})k_{12}^2]$$

$$+ \int (\sigma_{11} v_{3,1}^2 + \sigma_{22} v_{3,2}^2) \} \, dS = 0 \tag{3.58}$$

Two different models of the wrinkling function are used here to illustrate the advantage of the approach.

3.6.1 Constrained Buckling Mode

In this case the buckling mode is selected such that (2.57) is satisfied, and the Tresca yield criterion is assumed. For such a mode, equation (3.58) becomes

$$\delta \{ \int \frac{t^2}{6} (h - \sigma_{11} - \sigma_{22})(k_{11}^2 + k_{12}^2) + \int (\sigma_{11} v_{3,1}^2 + \sigma_{22} v_{3,2}^2) \} dS = 0 , \qquad (3.59)$$

which is identical to (3.48). Note that (3.59) is obtained without enforcing α_{33} to equal h, and therefore it clearly demonstrates that the approach is equivalent to one which is physically acceptable.

The disadvantage of the approach, however is that the buckling mode is highly restricted if (2.57) were to be used.

3.6.2 Unrestricted Buckling Mode

From equation (2.80) it is evident that the plastic strain increment is not restricted to be normal to the INITIAL YIELD SURFACE and therefore large flexibility is offered when (2.80) is used. The only restriction is the internal constraint of incompressibility.

To aid with the comparison to the classical elastic-plastic model of section 3.2.7, the wrinkling mode of (3.21) is again used with one coefficient

$$\text{i.e. } a_i = 0 , \qquad i = 2, 3 \ldots m$$

Substituting (3.21) together with (3.10) and (3.11) in (3.58) and carrying out some straight forward but lengthily manipulations, the critical thickness ratio is given by the maximum of

$$t^{*2} = \frac{L(n,R)}{M(h^*,n,R)} \tag{3.60}$$

where

$$t^* = \frac{t}{2Ro}$$

$$L = 3(C_4 + C_5 n^2) \tag{3.61}$$

$$M = R^2[h^*(D_1+D_2n^2+D_3n^4) + (E_1+E_2n^2+E_3n^4)]$$

The quantities D_i, C_j and E_i are defined in Appendix C for i=1,...3, j=4 and 5. The critical thickness ratio is shown in Figure 3.18 as a function of the drawing ratio, whereas the number of wrinkles is plotted in Figure 3.19.

By comparing 3.8 and 3.18 it is evident that the results based on the proposed constitutive equations are more in keeping with experimental data, than those arising from the conventional elastic-plastic model of section 3.2.7. Even when the modifications to the classical E-P model are carried, as described in section 3.4, the results are still inferior to those arising with the proposed constitutive equations, compare Figures 3.16 and 3.18. Considering the order of approximation arising in the utilisation of the proposed constitutive equations the results are encouraging, at least in the context of the flange wrinkling problem.

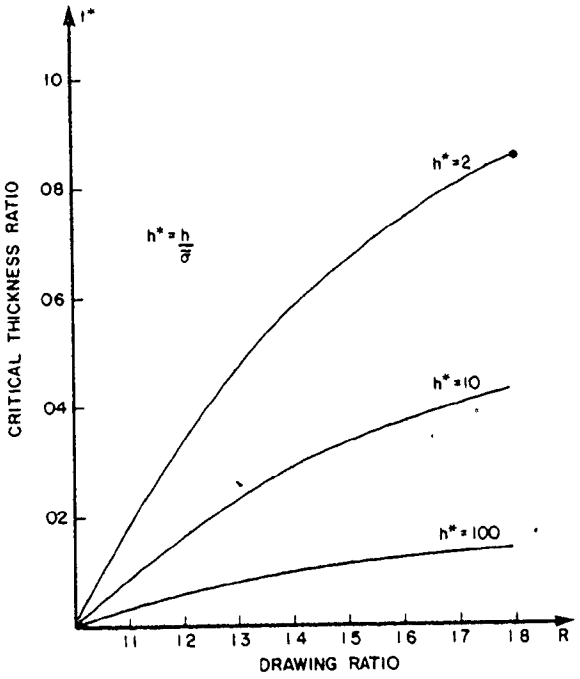

Figure 3.18 Prediction of critical thickness ratio versus drawing ratio using the proposed constitutive equations of section 2.4

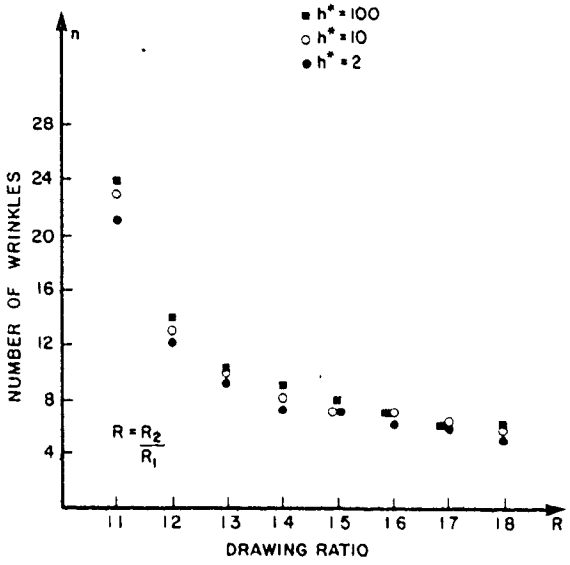

Figure 3.19 Prediction of number of wrinkles (waves) versus drawing ratio using the proposed constitutive equations of section 2.4

3.7 Discussion and Conclusions

3.7.1 Discussion

For all the theoretical models presented in this chapter it is assumed that the yield stress of the flange is constant i.e. the representative stress and the hardening parameter do not vary across the flange. This approach simplifies the resulting equations and is considered acceptable since the main object of this work is to demonstrate that slight modifications to the Prandtl-Reuss equations can lead to predictions for the onset of buckling in deep drawing commensurate with experimental observations.

In principle it would appear that the procedure could be incorporated into more elaborate numerical techniques leading to a more accurate assessment of the stress distribution, such as the finite element method proposed by Wifi [145] for deep drawing. With this knowledge a check on the bifurcation criterion could be made at each stage in the drawing process as shown by Triantafyllidis and Needleman [143] and Chu [19] for cylindrical shells.

The choice of the particular values for the relative normalized stress $\sigma^* = (\bar{\sigma}/E)$ and the relative hardening parameter $\eta = E/E_T$ could be questioned. However, the intention of the work is to demonstrate the method. It will be noted that a practical range of interest has been covered for the quantities σ^* and η, and the predictions of the proposed model are sensitive to these

parameters as shown in Figures 3.12, 3.16 and 3.18. This is in contradiction to the classical approach where they apparently exert little influence as seen from Figures 3.9 and 3.11. Since the problem is one of plastic buckling then it is not unreasonable to expect that material properties, as reflected by σ^* and n, should exert some influence.

The R-P model adopted by Kulkarni [73], described in section 2.3.1, is based on a mathematical manipulation of the classical E-P formulation which results in the incremental elastic energy being neglected with respect to the incremental plastic energy. At first sight this may not appear unreasonable but no justification is demonstrated for ignoring the incremental elastic energy term in the context of the present problem. As mentioned in the text the approach has been criticised when employed in the study of the necking instabilities of plates. While recognizing that the present R-P analysis leads to predictions for buckling in deep drawing more in keeping with experimental observations, it does resolve the shortcomings of the classical E-P formulation.

It should also be noted that the trial function of the R-P model of Kulkarni, Opt. cit., does not obey the Prandtl-Reuss equations since $k_{12} \neq 0$; no bifurcation is possible in properly formulated R-P model when the Prandtl-Reuss equations are used. Some of the shortcomings of the Prandtl-Reuss equations were shown in chapter 2, mainly that the plastic component of the shear strain rate tensor was excluded and only the elastic component was

retained and as was demonstrated by equations (3.27) and (3.30), this resulted in a shear dominated bifurcation criterion and moreover is the reason for ruling out the possibility of bifurcation for a R-P solid as discussed in section 2.4. It was suggested in section 2.2.1 that these shortcomings appear because of the singularity of the matrix of plastic moduli, i.e. there is no inverse relation between the stress rate and strain rate for the R-P solid. An attempt was made in section 2.4 to modify the Prandtl-Reuss equations to produce E-P constitutive equations which could be inverted and reduced to the special cases of either the R-P or elastic solid. This property is not shared by the Prandtl-Reuss equations.

In section 3.6 the proposed constitutive equations is employed in the study of flange wrinkling and the results are more in keeping with experimental observations vis à vis the predictions arising with the classical E-P model from section 3.2.7 and the modified E-P model of section 3.4. However, the use of the proposed constitutive equations may be limited to bifurcation analyses, because of the non-linear relationship between the stress increment and strain increment. It would appear that its adoption would necessitate a numerical procedure for other types of plasticity problems.

It is surprising at first glance to observe that the number of waves into which the blank wrinkles is essentially independent of material properties, i.e. yield stress, hardening rate etc.,

and the type of material model employed, either E-P or R-P. On the other hand a closer look would indicate that for any system, the critical eigenvalue is a function of the mass and material properties of the system, whereas the corresponding eigenvector is affected only by the geometry of the system (for e.g. kinematic boundary conditions). This is exemplified for the buckling of a column with hinged ends.

Figure 3.20 illustrates that for a column with hinged ends the critical eigenvector is always a half sine wave and it is independent of the material properties of the column. Figure 3.21 shows that the eigenvector is quite sensitive to the boundary conditions but again independent of the column material.

It was shown that the number of waves into which the blank buckles as predicted by the models of sections 3.4.3, 3.4.4 and 3.6.1 is half the number calculated by the models of sections 3.2.7, 3.3 and 3.6.2. The difference stems from the different boundary conditions, where in sections 3.4.3, 3.4.4 and 3.6.1 the blank is simply supported at the inner edge whereas it is clamped in the latter cases. It should be noted that the factor of two, in the number of waves, also exists between the columns with fixed and hinged ends, and this simple example may be analogous to the observed difference in the results of deep drawing.

Figures 3.9, 3.16 and 3.18 show that the critical thickness at bifurcation decreases with the increase of the hardening rate, i.e. a large rate of hardening helps in the prevention of

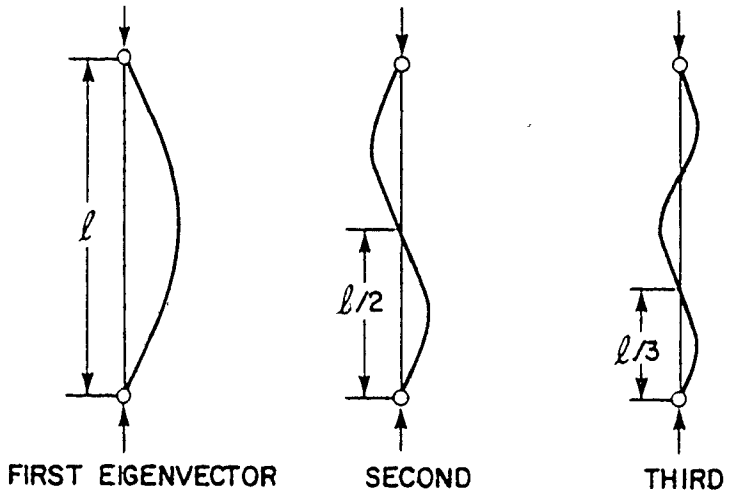

Figure 3.20 Eigenvectors and column material

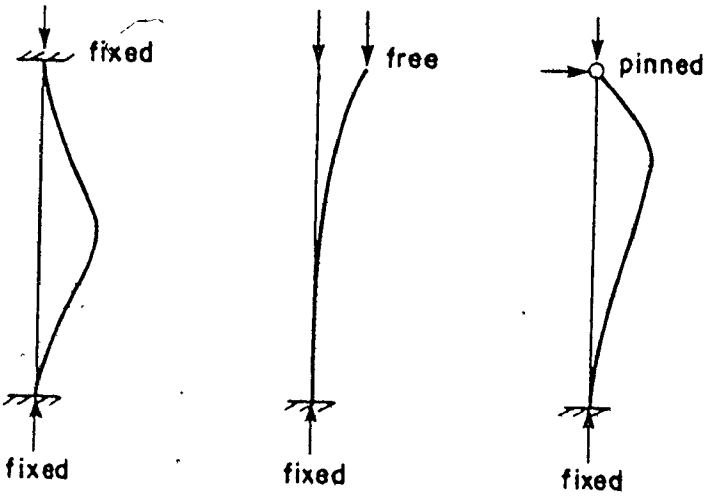

Figure 3.21 Effect of boundary conditions on first eigenvector

wrinkling. An opposite effect is shown in Figure 3.13 for the R-P model, section 3.3, but as already mentioned certain terms have been excluded in the model without justification.

Figures 3.9, 3.12, 3.16 and 3.18 illustrate that the higher the relative hardening $h^*(h^* = h/\bar{\sigma})$, the larger will be the critical thickness at bifurcation or in other words the higher yield stress $\bar{\sigma}$ or the lower the hardening parameter h has a detrimental effect. This can be physically interpreted as a high yield stress resulting in an increased potential energy of the system which manifests itself in any perturbation from equilibrium. On the other hand the lower the hardening parameter h, the more likely an adjacent equilibrium configuration could exist.

3.7.2 Conclusions

In summary the following conclusions can be drawn.

1. There is a need for a suitable constitutive equation which is realistic in terms of material description and at the same time analytically tractable. From a mathematical point of view it would be desirable for such an equation to be readily inverted, and that any formulation for an elastic-plastic solid can be reduced to the special cases of elastic and rigid-plastic solids.

2. A possible modification to the Prandtl-Reuss equations has been suggested in section 3.4, and when incorporated into Hill's uniqueness criterion leads to predictions for the onset of flange wrinkling in deep drawing commensurate with experimental

observations. The procedure seems quite general and not restricted to the problem of flange wrinkling.

3. Any kinematically admissible velocity field must satisfy certain constraints placed on the strains (in particular plastic strain rates or increments) as imposed by the constitutive equations.

4. In the present problem of flange wrinkling in deep drawing the analysis indicates that material properties do exert an influence on the critical dimension of the blank at the onset of wrinkling. This would appear to be physically correct since it is hard to imagine that the process is controlled solely by the geometry of the blank. On the other hand the number of waves into which the blank wrinkles is less dependent upon material properties.

5. As a special case of the E-P formulation, the wrinkling of an elastic annulus under external radial loading was considered. The annulus buckles into a series of waves analogous to the wrinkling of a flange in deep drawing. The predictions compare closely with an existing alternative theoretical analysis, and are consistent with some existing experimental data.

6. An existing technique, whereby the classical E-P formulation can be manipulated to lead to a R-P formulation, has also been applied to the wrinkling problem. Adequate predictions for the onset of flange wrinkling are realised, but ignoring terms involving the elastic energy may not be justified in a number of

problems. The imposition of the normality condition of the strain-rate vector to the yield surface can be a liability for a R-P solid, since severe constraints are imposed on the choice of admissible velocity fields.

7. Predictions based on the proposed constitutive equations (discussed in section 3.6) compare better with experimental results than those from the classical J_2' flow theory of section 3.2.7 and the modified flow theory of section 3.4. Furthermore the proposed model allows a wider choice of admissible velocity fields without increasing the amount of computation, and therefore permits a greater flexibility during modelling vis à vis the alternative models described herein.

8. The results of the present work indicate that materials with a low yield strength but a high rate of hardening should be desirable in deep drawing, i.e. with a large ratio of relative hardening h^*. Materials possessing these characteristics should allow blanks of a given diameter to be drawn from a thinner gauge (all other things being equal), before the onset of wrinkling.

CHAPTER 4

CONICAL AND TRACTRIX DEEP DRAWING DIES

4.1 Introduction

In a conventional drawing operation (see Figure 3.1) a substantial amount of redundant work occurs, such as bending and unbending of the material over the die radius. A consequence of redundant work (all other things being equal) is an increase in the drawing load, which in turn promotes thinning of the material in the vicinity of the punch nose and enhances the likelihood of fracture there. It has been found experimentally that it is possible to successfully draw circular blanks into cylindrical cups up to a Limiting Drawing Ratio (L.D.R) of between 2.0 and about 2.4; the L.D.R is defined as the ratio of maximum blank diameter to punch diameter for a successful draw, see also chapter 5.

It has also been found (particularly from work performed on steel sheet) that if the normal anisotropy of the material increases (see the discussion in chapter 5) so does the L.D.R. However the increase is not dramatic, being of the order of a few percent corresponding to the control that can be exercised over the level of anisotropy in practical steel making.

In practical terms, if a significant improvement in press performance cannot be attained via material properties per se, then it appears logical to consider the manner in which the material is formed

and the associated tooling. In the context of the deep drawing operation the tractrix (Huygen) die, see Figure 5.14, has been proposed (patented in 1938 by O. May [84]) as one which will minimize redundant work. The tractrix curve has the property that any tangent to the curve and a fixed straight line (in the drawing operation this line is the generator of the circular punch) is of constant length.

Ideally, only the rim of the circular blank touches the die and the cup wall remains straight and unchanged in length during the operation. A plastic hinge forms in the material next to the punch nose. In practice the length of the flange increases by about 30 percent, the length of contact at the material-die interface is finite and the unsupported material does not remain straight. However, the redundant work is much less than that which occurs in the conventional deep drawing operation.

Many different die profiles could be employed in a practical drawing operation. This opens up another possible area of investigation, but one which has not been examined in any depth in the present work. The simplest profile is that which corresponds to a conical die, see Figure 4.1. As shown by Shawki [133] it is possible with both the tractrix and conical dies to raise the L.D.R to about 2.9; but this applies only to thicker gauge material which also possesses good ductility, e.g. drawing quality steel. It will be recognized that wrinkling or puckering is a severe limitation when drawing without a blank holder, and in this situation Oehler [112] reports that 30 is an upper figure for the ratio, punch diameter to material thickness.

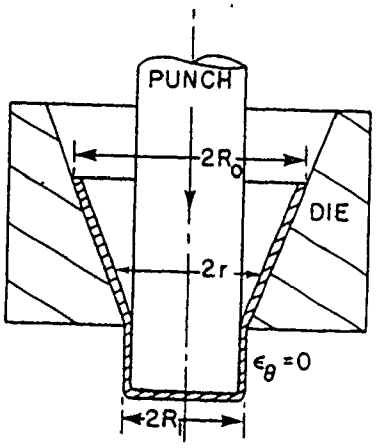

(a)

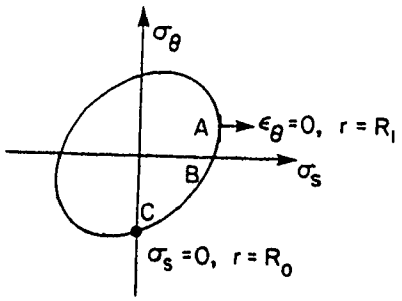

(b)

Figure 4.1 (a) Conical die

(b) von-Mises plane stress yield locus

Nevertheless the tooling is relatively simple and other than a long stroke no special requirements are needed for a press. However, the alignment is rather more critical than with the conventional operation.

Conical and tractrix dies are used in the production of cylinder liners, gas bottles, beverage cans and the like. The drawing process is the first stage in the production of these components. The subsequent stages are ironing processes, where the cup attached to the punch (or ram) is forced through a series of ironing dies which reduce the wall thickness and elongate the cylinder. The drawing and ironing stages are integrated within the body of a single machine, where the ram is usually mounted in a horizontal position. The term D and I can, meaning drawn and ironed, is appearing more and more in the literature.

Shawki [134] has proposed an empirical expression involving punch diameter, d_p, and material thickness, t, viz. $[D_p/t]\sqrt{t}$, as a measure of plate weakness in axially symmetric bending. When this quantity is plotted against the limiting drawing ratio a unique curve for various combinations of punch diameters and blank thicknesses is supposed to exist. Miyagawa [90] identified two types of wrinkling when drawing aluminum through a conical die with 60° die angle. The first type occurs at the beginning of the process whereas the second appears just after the punch has arrived at the exit part of the die and much of the blank fills the conical portion of the die. Miyagawa, Opt. cit., reported that the latter wrinkles can appear locally without necessarily spreading around the whole circumference and he noted that such wrinkles control the process. Miyagawa [90] determined the buckling stress for

the conical shell from the minimum stability condition of the total potential energy of the formed wrinkles. However as with deep drawing it is not clear which type of constitutive equation was used. He showed that the critical thickness ratio (see chapter 3 for definition) tends to increase with increasing the drawing ratio and decreasing cone angle.

In the main, previous investigators have defined material properties imprecisely and terms such as good ductility, soft materials and hard materials have been used to classify material response to deformation. In addition to material properties, this author believes that the mode of wrinkling is also very much dependent upon the mode of deformation of the blank, and this has not been reported in detail in many of the previous studies.

The present work has been undertaken with the aim of identifying material properties which may delay wrinkling, and to classify the wrinkling behaviour in conjunction with the deformation history in order to arrive at a more precise mathematical model of the process. From the present experimental study, described in chapter 5, it was observed that bending at the periphery of the blank dominated the early stages of deformation, and this was followed by a form of tube sinking operation as the punch stroke is increased. A not unreasonable hypothesis is that the buckling mode is dependent on the way the material deforms in the pre-buckled state. A further hypothesis is that in the initial stages, where bending is dominant, the bifurcation mode is controlled by the geometry such as snap through buckling of shells. While in the later stages of deformation - the tube sinking stage - wrinkling is initiated

by excessive compressive hoop stresses. The first type of wrinkling is not amenable to analysis because of the complicated nature of the contact stresses and boundary conditions. Instead an attempt is made to analyse the bifurcation arising during the tube sinking stage. The material is assumed to be rigid-plastic and two distinct models are employed. One is based on the heuristic hypothesis of section 2.3.2, while the second utilises the proposed constitutive equations described in section 2.4.5.

4.2 Initial State in Tube Sinking

The stress distribution in the initial pre-buckled state is obtained based on the following assumptions:-

(i) The wall thickness is small in comparison with the diameter of the tube and the length of contact with the die.

(ii) The stress across the thickness, σ_z, is small compared to the current yield stress of the material and can be neglected. So are the shearing stresses σ_{rz} and $\sigma_{\theta z}$.

(iii) Elastic strains are negligible.

The first two are the standard assumptions in thin shell theory, see Novozhilov [111] and the third assumption is usually made in forming processes which involve large plastic deformation. The coordinate system adopted in this section is shown in Figure D.1 of Appendix D and the following notation is employed:-

σ_s and σ_θ are the longitudinal and circumferential principal stresses respectively,

v is the inward radial velocity,

ϕ is the die semi angle,

$\bar{\mu}$ is the coefficient of Coulomb friction, and

$\bar{\sigma}$ and $\bar{e}$ are the effective stress and total effective strain respectively.

The stress distribution within the conical region of the cup is obtained as follows, see also Figure 4.1. The equilibrium equations for an element of the cup can be written, according to Hill [44], as

$$\frac{d}{dr}(\sigma_s rt) - \sigma_\theta t (1 + \bar{\mu} \cot \phi) = 0 . \tag{4.1}$$

The material is assumed to obey von Mises' yield condition, and for plane stress this is given by

$$\sigma_s^2 + \sigma_\theta^2 - \sigma_s\sigma_\theta = \bar{\sigma}^2 , \tag{4.2}$$

where

$$\bar{\sigma} = f(\bar{e}) . \tag{4.3}$$

The function $f(\bar{e})$ can be obtained from a simple tension test. The strain increments are given by

$$de_\theta = \frac{dr}{r} , \tag{4.4a}$$

$$de_s = \frac{dv}{v} , \tag{4.4b}$$

and

$$de_z = \frac{dh}{h} . \tag{4.4c}$$

The condition of plastic incompressibility is

$$dc_s + de_\theta + de_z = 0 . \tag{4.5}$$

The flow rule associated with (4.2) together with (4.4) and (4.5) gives

$$\frac{dv}{dr} = \frac{v}{r} \frac{2\sigma_s - \sigma_\theta}{2\sigma_\theta - \sigma_s} , \tag{4.6}$$

and

$$\frac{dt}{dr} = \frac{t}{r} \frac{\sigma_s + \sigma_\theta}{\sigma_s - 2\sigma_\theta} . \tag{4.7}$$

Upon substituting (4.7) into (4.1) the following equilibrium equation is obtained

$$\frac{d\sigma_s}{dr} = \frac{1}{r} \frac{2\bar{\sigma}^2 - \sigma_\theta(\sigma_s - \sigma_\theta)\,\bar{\mu}\cot\phi}{\sigma_s - 2\sigma_\theta} \tag{4.8}$$

Equations (4.6), (4.7) and (4.8) together with the appropriate boundary conditions determine the stresses and the strains in the cup. The boundary conditions at $r = R_o$ are

$$\begin{aligned} t &= t_o \\ \sigma_s &= o \\ v &= v_o \end{aligned} \tag{4.9}$$

Kulkarni [73] solved the above equations numerically however, it was claimed, Opt. cit, that little difference existed between the numerical procedure and an approximate analytical method (to be described below) insofar as the results from the bifurcation analysis were affected.

The von Mises yield criterion given by (4.2) is shown plotted in Figure 4.1. It is assumed that the stress state at any point in the partially drawn shell lies within the arc ABC. At point A, $\varepsilon_{\theta\theta} = 0$ and this corresponds to an element of the cylindrical shell at $r = R_i$. While at point C, $\sigma_s = 0$ and thus represents the boundary condition at $r = R_o$. The stresses at other points in the material are located along

the arc AC.

Following the procedure adopted for the conventional deep drawing process a number of simplifying assumptions are now made. Friction and any variation in thickness of the wall of the cup is ignored. The Tresca yield condition is adopted instead of (4.2) and this is expressed in the following manner

$$\sigma_s - \sigma_\theta = m\bar{\sigma} \ , \tag{4.10}$$

where m is a numerical factor. The stresses are given by

$$\sigma_s = -m\bar{\sigma} \ln \frac{s}{s_o} \tag{4.11}$$

$$\sigma_\theta = -m\bar{\sigma} \ (1 + \ln \frac{s}{s_o}) \tag{4.12}$$

The influence of strain hardening is accounted for in an approximate way only, by considering same average value of $\bar{\sigma}$. In the conventional manner the numerical coefficient, m, in (4.10) is 1.15.

4.3 Bifurcation Analysis

The strain rates arising in the problem are given in Appendix D, and for the case where u^o and v^o << w, we have

$$\varepsilon_{11} = -z \frac{\partial^2 w}{\partial s^2} \ , \tag{4.13a}$$

$$\varepsilon_{22} = \frac{w}{s} \cot \phi - \frac{z}{(s \sin\phi)^2} \left(\frac{\partial^2 w}{\partial \theta^2} + \frac{1}{s} \frac{\partial w}{\partial s}\right) \ , \tag{4.13b}$$

$$\varepsilon_{12} = - \frac{z}{s \sin\phi} \left(\frac{\partial^2 w}{\partial s \partial \theta} - \frac{1}{s} \frac{\partial w}{\partial \theta}\right) \ . \tag{4.13c}$$

4.3.1 Semi Empirical Approach

The blank is assumed to deform as a conical shell as shown in Figure 4.2. The analysis procedes along identical lines to that given in section 2.3.2 and section 3.4 etc. The expressions for stress are given by (4.11) and (4.12), and equations (3.29), (3.32) and (3.44) still apply with $dS = r\sin\phi\, ds d\theta$.

In order to apply the above equations, the bifurcation mode has to satisfy (2.57) as well as the boundary conditions. For conical shells and for the chosen stress system (2.57) becomes

$$x = \frac{\varepsilon_{22}}{\varepsilon_{11}} = \frac{\overset{o}{\varepsilon}_{22} + zk_{22}}{\overset{o}{\varepsilon}_{11} + zk_{11}} = -1$$

or
$$(\overset{o}{\varepsilon}_{11} + \overset{o}{\varepsilon}_{22}) + z(k_{11} + k_{22}) = 0 \quad . \tag{4.14}$$

In (4.14) it is evident that the z dependent and z independent parts must vanish separately. This leads to the following equations

$$\frac{\partial^2 w}{\partial s^2} + \frac{1}{(s\sin\phi)^2}\left(\frac{1}{s}\frac{\partial w}{\partial s} + \frac{\partial^2 w}{\partial \theta^2}\right) = 0, \tag{4.15}$$

and

$$\overset{o}{\varepsilon}_{11} + \overset{o}{\varepsilon}_{22} = 0 \quad . \tag{4.16}$$

Equation (4.16) is identically satisfied by neglecting stretching work. It is assumed that the wrinkling mode is given by

$$w = f(s)\cos n\theta \ . \tag{4.17}$$

Upon substituting (4.17) into (4.15) these results in

$$s^2 f''(s) + s f'(s) - \left(\frac{n}{\sin\phi}\right)^2 f(s) = 0 \ , \tag{4.18}$$

which has the general solution

$$f(s) = C_1 s^m + C_2 s^{-m} \quad . \tag{4.19}$$

In the above equation, $m = \frac{n}{\sin\phi}$, and C_1 and C_2 are constants. At $s = s_1$, (see Figure D.1) the boundary conditions are

$$f(s) = 0, \tag{4.20a}$$

and

$$\frac{\partial w}{\partial \theta} = 0 \quad . \tag{4.20b}$$

By substituting from (4.20) into (4.19) and (4.17), the wrinkling mode can be rewritten as

$$w = C_1[s^m - s_1^{2m} s^{-m}] \cos n\theta \quad . \tag{4.21}$$

Note that by having to satisfy (2.57) the wrinkling mode is highly restricted and not all wrinkling modes can be modelled.

Equation (4.21) is now substituted into (3.44), and with $\alpha_{33} = h$ and $dS = r \sin\phi \, ds d\theta$, the bifurcation criterion can be expressed as

$$\delta \int \{\frac{t^2}{6} (k_{11}^2 + k_{12}^2)(h - \sigma_{11} - \sigma_{22}) + (\sigma_{11} v_{3,1}^2 + \sigma_{22} v_{3,2}^2)\} dS = 0. \tag{4.22}$$

Alternatively the criterion can be expressed in terms of a critical thickness ratio (in the manner of section 3.4.2) as the maximum of

$$t^{*2} = \frac{3M}{2L} \quad , \tag{4.23}$$

where

$$M = \frac{S_o^{2m}(m-1)}{2m^2} - S_o^{-2m} \frac{m+1}{2m^2} + \frac{1}{m^2} - 2\ln S_o \quad , \tag{4.24}$$

$$L = S_o^{2m}\,[(m-1)h^* + (m-2)] - S_o^{-2m}\,[(m+1)h^* + (m+2)]$$

$$- 4S_o^2 \ln S_o + 2S_o^2\,(h^* + 2)\,, \qquad (4.25)$$

$$h^* = \frac{h}{\sigma}$$

$$t^* = \frac{t}{2s_2}\,,$$

and

$$S_o = \frac{s_2}{s_1} \geq 1\,.$$

For the conventional deep drawing, $\phi = 90^o$ and $m = n$ and we recover equation (3.49). The relation between the critical thickness ratio t^* and S_o is shown in Figure 4.2 for $\phi = 85^o$, whereas the critical number of wrinkles is shown in Figure 4.3.

4.3.2 An Alternative Wrinkling Mode Based on the Proposed Constitutive Equations

The material is assumed to be rigid-plastic and the proposed constitutive equations are given by (2.80). The pre-bifurcation deformation mode is considered to be as shown in Figure 4.4. Wrinkling is taken to occur in the domain AB only, which is contiguous with the die wall. An additional assumption is that one wrinkle only will form in this region as illustrated in Figure 4.5. The boundary conditions are (see Figures 4.4 and 4.5):-

(i) at $s = s_{oA}$, $\quad w = o\,,$

and $\quad \dfrac{\partial w}{\partial n} = 0\,,$

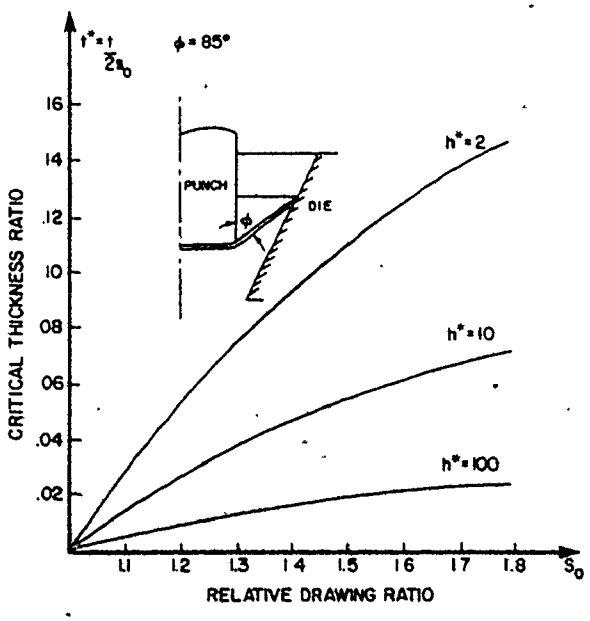

Figure 4.2 Variation of the critical thickness ratio with relative drawing ratio - modified bifurcation criterion

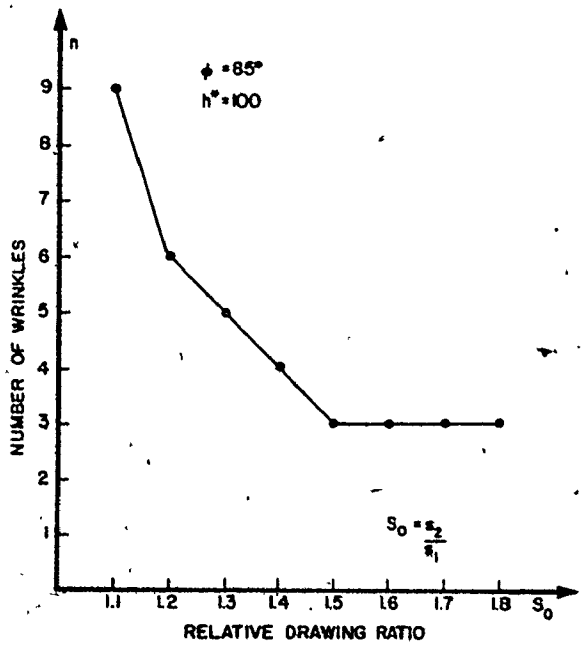

Figure 4.3 Variation of number of wrinkles with relative drawing ratio

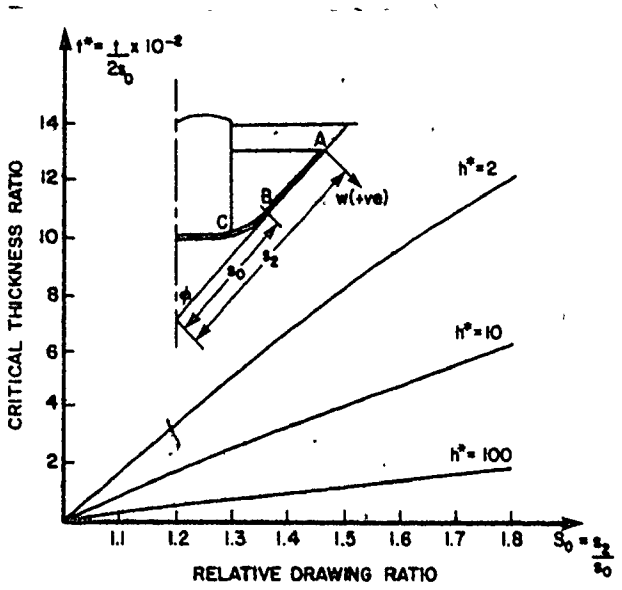

Figure 4.4 Prediction of critical thickness ratio with relative drawing ratio–proposed constitutive equations

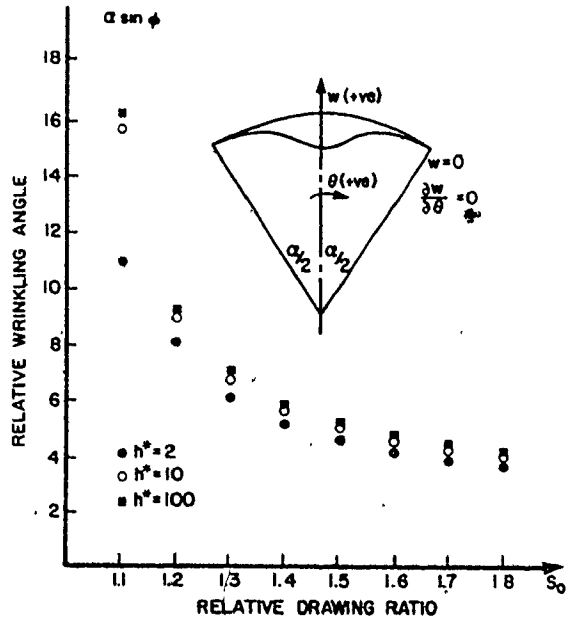

Figure 4.5 Prediction of relative wrinkling angle with relative drawing ratio

where $\frac{\partial w}{\partial n}$ is the derivative along the normal to the surface.

(ii) For $s_2 \geq s \geq s_o$, $\frac{\partial w}{\partial s} \leq 0$,

and $w_o \leq 0$. (4.26)

(iii) $w(\theta) = w(-\theta)$.

(iv) At $\theta = \pm\alpha/2$, $w = 0$,

and $\frac{\partial w}{\partial \theta} = 0$.

(v) At $\theta = 0$, $\frac{\partial w}{\partial \theta} = 0$.

A possible wave form which satisfies (4.26) is

$$w = -w_o (s^2 - s_o^2)^2 (1 + \cos \frac{2\pi\theta}{\alpha}) , \quad w_o > 0. \tag{4.27}$$

Note that the proposed constitutive equations do not impose constraints on the buckling mode in the manner of the Prandtl-Reuss equations, as demonstrated in section 4.3.1.

The bifurcation criterion is again given by (3.58) with $dS = r \sin\phi \, ds d\theta$. If the stress distribution from (4.11) and (4.12) together with (4.27) is substituted into (3.58), the critical thickness ratio $(t/2 s_o)$ is given by the maximum of

$$t^{*2} = \frac{3L}{M} , \tag{4.28}$$

where $$L = d^4 E_1 + d^2 E_2 , \tag{4.29}$$

$$M = K_1 + d^2 K_2 + d^4 K_3 , \tag{4.30}$$

and $$d = \frac{\alpha \sin\phi}{\pi} . \tag{4.31}$$

The quantities E_i and K_j ($i = 1,2$ and $j = 1,2,3$) are functions of the relative drawing ratio S_o ($S_o = s_2/s_o$) and h^* ($h^* = h/\bar{\sigma}$) only, as defined in Appendix D. The value of α that maximizes t^* is the critical one and is obtained from (4.28) by setting

$$\frac{\partial t^*}{\partial \alpha} = 0 \quad . \tag{4.32}$$

This results in the following relation

$$d^4 + g_1 d^2 + g_2 = 0 \ , \tag{4.33}$$

with

$$g_1 = \frac{2 E_1 K_1}{E_1 K_2 - E_2 K_3} \ , \tag{4.34}$$

and

$$g_2 = \frac{E_2 K_1}{E_1 K_2 - E_2 K_3} \ .$$

The roots of the above equation when substituted back into (4.28) leads to the results displayed in Figures 4.4 and 4.5. Upon comparing Figures 4.2 and 4.4 it will be observed that the critical thickness ratio at bifurcation decreases with an increase in the normalized hardening rate. In other words a high rate of hardening and a low yield stress helps in the prevention of wrinkling.

4.4 Discussion and Conclusions

4.4.1 Discussion

In both the models presented in this chapter a gross approximation to the actual stress distribution in the cup wall was adopted. More elaborate numerical procedures could be employed in an attempt to ascertain the pre-bifurcation stress distribution. However,

any accurate prediction of the stresses and the like depends largely upon a knowledge of the boundary conditions, and the conditions which exist at the rim of the cup (particularly in the early stages of the deformation process); these are not precisely known.

No attempt was made to predict the wrinkling behaviour in the early stages of deformation, and both models apply to a later stage in the process - which has been termed the tube sinking stage. Both models indicate that certain plastic properties, in particular the normalized hardening rate h^*, can exert an appreciable effect upon the buckling behaviour. This is in contradiction to the predictions when the classical Prandtl-Rauss equations are embodied in the bifurcation analysis. It is to be noted that the influence of the hardening rate is supported by the experimental findings described in the next chapter. In fact, wrinkles were seen to occur in a manner not dissimilar to the model of section 4.3.2. However, in practice the wrinkles are formed at a very early stage in the process and consequently no claim is being made here that either model portrays the actual events.

4.2.2 Conclusions

i) The imprecise knowledge of the boundary conditions which exist when drawing a circular blank through a conical die, precludes any accurate analytical models of the wrinkling behaviour.

ii) Both of the simplified analytical models presented in this chapter predict that materials with a high normalized hardening

rate should offer more resistance to wrinkling.

iii) The classical J_2' flow theory when used in bifurcation analyses can impose severe restrictions on permissible bifurcation modes. This problem is not encountered in the present study when using the proposed constitutive equations, as is evident from the discussion of section 4.3.2.

CHAPTER 5

EXPERIMENTAL INVESTIGATION OF THE WRINKLING IN CONICAL AND TRACTRIX DIES

In the work of Shawki [133-135] on both conical and tractrix dies, and that of Miyagawa [90] on conical dies, the material properties were poorly identified. Rather vague terms such as good ductility, soft materials and hard materials were used to classify the material response to deformation. No attempt was made in the afore-mentioned articles to relate the wrinkling mode to the conditions in the pre-buckled state, and in the view of the present author this is of prime importance when attempting to model the wrinkling phenomenon. In fact there appears to be nowhere reported in the literature a material parameter (or parameters), related to the pre-buckled state, which is beneficial in helping to resist buckling in a non-conventional drawing operation. Note that some geometric parameters, e.g. slenderness ratio in column buckling, are quoted but no material parameters given except Young's modulus or some plastic modulus (reduced or tangent modulus).

In general there is no single universal test that can describe formability, i.e. the ability to form. The classification of formability is intimately related to the deformation process itself, such as the Swift cupping test which is regarded as a measure of deep drawability.

In the present experimental study attempts were made to draw circular blanks into cylindrical cups, using a conical and a modified tractrix shaped die. Blanks of different diameter and thickness were produced from a number of different materials. The aim of the study was to reveal the influence of the blank geometry, i.e. diameter and thickness, on the wrinkling behaviour, and also to ascertain material parameters which may be beneficial in inhibiting wrinkling. In addition, the use of two different die profiles might lead to some information on the influence of the deformation mode on the wrinkling behaviour.

5.1 Material Selection

Four materials were selected in order to provide a reasonably wide range of mechanical properties, see Table 5.1 and Figures 5.1 and 5.2. The material thicknesses were 0.78, 1.27 and 1.57 mm for Aluminum, Brass and AKDQ steel. The Dual Phase steel was available in the following thicknesses: - 0.78, 0.97 and 1.17 mm. The aluminum was a commercial utility aluminum, having properties similar to that of a 3003-H14 Al-Manganese alloy. The "as-received" brass was of a half hard temper and in accordance with ASTMB-36, alloy 260. The dual phase steel was classified as high form - 80d and supplied by Inland Steel Corporation.

It transpired, see Table 5.2, that the materials had differing degrees of anisotropy as characterized by the normal ($\bar{r}$) and planar (Δr) anisotropy parameters, which are usually defined

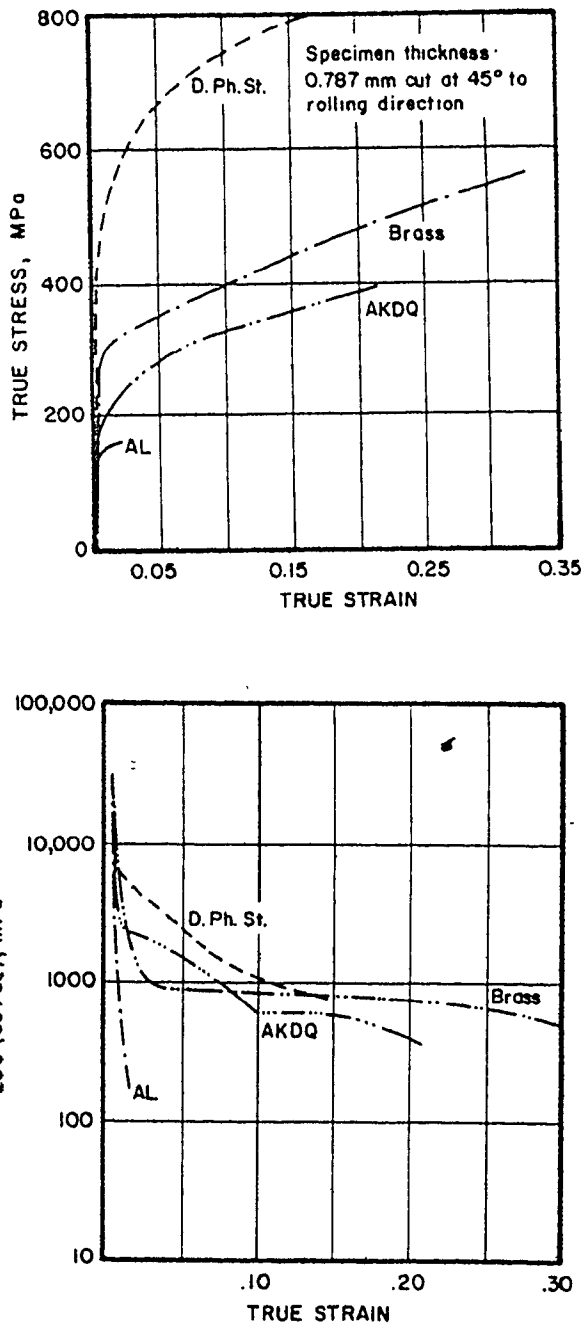

Figure 5.1 Variation of true stress and it's rate of change with true strain in uniaxial tension

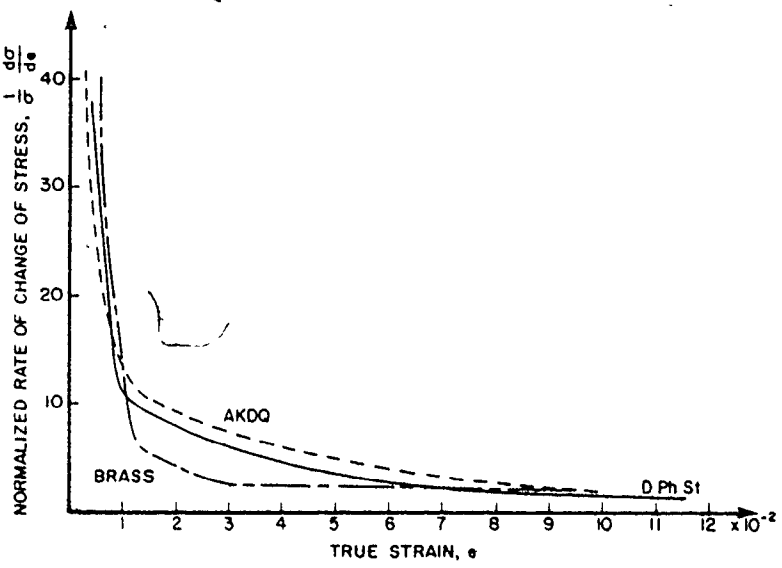

Figure 5.2 Normalized rate of change of stress with strain

by the following empirical expressions

$$\bar{r} = \frac{1}{4}(r_0 + 2r_{45} + r_{90})$$

$$\Delta r = \frac{1}{2}(r_0 + r_{90} - 2r_{45})$$

These parameters have found wide acceptance based on experience gained when drawing sheet steels. In the Swift cupping test the L.D.R. is generally improved, the larger the $\bar{r}$ value, while earing is minimized as $\Delta r \to 0$. How well these findings for steels in this particular test, can be ascribed to other materials (and possibly other types of drawing operations) is a moot point.

Table 5.1

Material Properties

Property	Brass	AKDQ	D.Ph.St.	Aluminum
σ_y, MPa	301.1	179.1	498.0	151.6
σ_{max}, MPa	530.5	372.0	785.0	164.0
ϵ_{max}	0.324	0.271	0.189	0.023
E, 10^3MPa	106.0	206.7	206.7	71.0
ν	0.324	0.292	0.292	0.334

where σ_y yield stress

σ_{max} true stress corresponding to U.T.S.

ϵ_{max} maximum uniform elongation in tensile test

E Young's modulus

ν Poisson's ratio

Table 5.2

Normal and Planar Anisotropy

Material		0°	45°	90°	$\bar{r}$	Δr
Brass	r	0.89	0.85	0.55	0.79	-0.13
	r*	0.79	0.70	0.51	0.67	-0.05
AKDQ	r	1.95	1.58	2.34	1.86	0.56
	r*	1.48	1.16	2.06	1.47	0.60
D.Ph.St.	r	1.29	1.06	1.77	1.29	0.47
	r*	1.00	0.64	1.02	0.82	0.37

where $$r = \frac{e_w}{e_t} = \frac{\ln(w_f/w_o)}{\ln(t_f/t_o)}$$

$$r^* = \frac{-\ln(w_f/w_o)}{\ln(w_f l_f/w_o l_o)}$$

The subscripts o and f denote original and final dimensions respectively of width (w), thickness (t) and length (l). The "r" values in Table 5.2 are the average values of instantaneous r measured at 5% longitudinal strain intervals. These are not available for aluminum since necking occurs at very low strains (approximately 2%). The degree of correspondence between r and r* suggests that the inaccuracies in the "r" values are approximately $\pm$ 0.20.

It was observed from the uniaxial tensile test that the materials showed very different initial hardening rates, i.e. the tangent modulus at low strains. The true stress - true strain curves for the materials are shown in Figure 5.1(a) and their hardening rates in Figure 5.1(b). An attempt was made to fit the tensile data over the entire strain range with the following three empirical relationships: -

$$\sigma = Ke^{n} \tag{5.1}$$

$$\sigma = K_1(e+e_o)^{n_1} \tag{5.2}$$

$$\sigma = S - (S-Y)\exp(-me) \tag{5.3}$$

due to Ludwick, Swift and Voce respectively. The results as shown in Table 5.3 are the average of eighteen specimens from each material. The normalized hardening rate $(\frac{1}{\sigma}\frac{d\sigma}{de})$, as determined from the tensile curves, is plotted against strain in Figure 5.2. The different materials are ranked in a bar chart, in Figure 5.3, according to the mechanical properties considered to have the greatest bearing on the wrinkle behaviour. The usefulness of the various rankings in Figure 5.3 could be questioned since each parameter has some disadvantages. For example, the n value is an average parameter over a wide strain range and may not be appropriate for the region of wrinkling. Similarly, the anisotropic parameters $\bar{r}$ and Δr, are determined at an arbitrary level of tensile strain and they are likely to change with deformation. On the other hand a ratio such as σ_{max}/σ_y does

Table 5.3

Different Parameters in Ludwick, Swift and Voce Expressions

Material	Dual Phase Steel	Brass	AKDQ
K, MPa	996.0	711.5	474.6
Σ_k, MPa	52.3	54.2	16.1
n	0.155	0.169	0.202
Σ_n	0.014	0.009	0.015
K_1, MPa	1038.6	848.5	529.1
Σ_{K_1}, MPa	56.2	109.1	16.7
e_o	.0015	.0374	.0067
Σ_{e_o}	.0018	.0192	.0026
n_1	0.0170	0.314	0.265
Σ_{n_1}	0.017	0.066	0.023
S, MPa	693.5	754.2	379.5
Σ_S, MPa	105.3	86.3	14.6
Y, MPa	366.6	307.1	150.7
Σ_Y, MPa	102.4	27.4	13.5
m	36.95	3.90	10.68
Σ_m	25.89	0.82	1.96

NOTE: Σ denotes the standard deviation

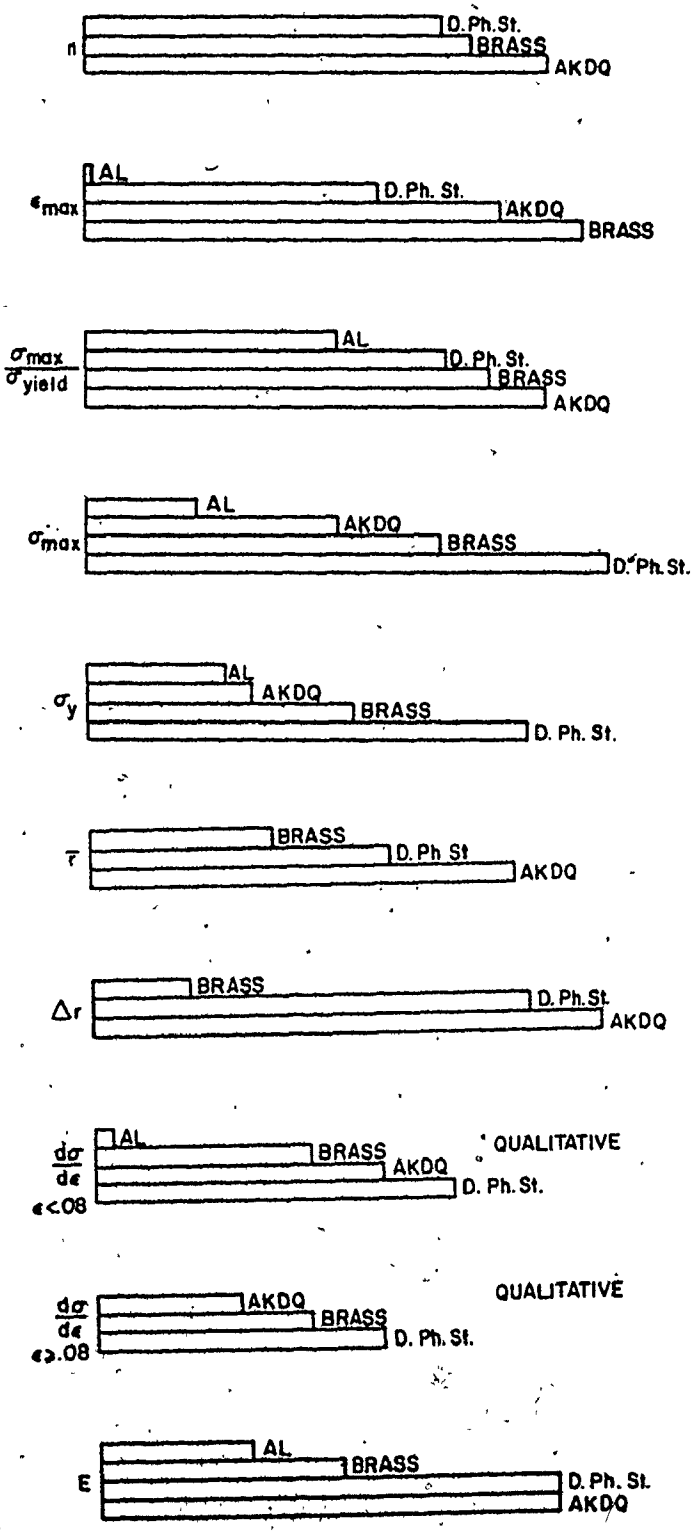

Figure 5.3 Bar chart for material ranking

not really convey the material behaviour between yield and maximum load, in that the stress-strain curve could be quite different in appearance and yet the ratio (σ_{max}/σ_y) is the same. Similar remarks apply to the parameter $\frac{1}{\sigma}\frac{d\sigma}{de}$.

5.2 Experimental Tooling

The experimental arrangement of the tooling for the drawing tests with the conical die is shown in Figure 5.4. The punch and die are made from a case hardened mild steel. The blanks were positioned concentric to the punch and die and also maintained level by fastening them onto the punch. A 6.35 mm diameter hole was drilled and reamed in the centre of each blank. The punch nose radius is 6.35 mm.

A modified tractrix die was also used in the investigation where the approximated tractrix shape was blended into a cone of 30° included angle. The actual tractrix profile results in a die with an unacceptable long axial length. The maximum blank size, D_b, that could be used with the tractrix die was 120.65 mm diameter. The same punch diameter, d_p, was used with both the tractrix and the conical die. Experiments were carried under dry conditions, i.e. no lubricant was used.

5.3 Conical Die

5.3.1 Deformation Pattern and Strain Distribution

A typical load - Punch travel diagram when drawing in the

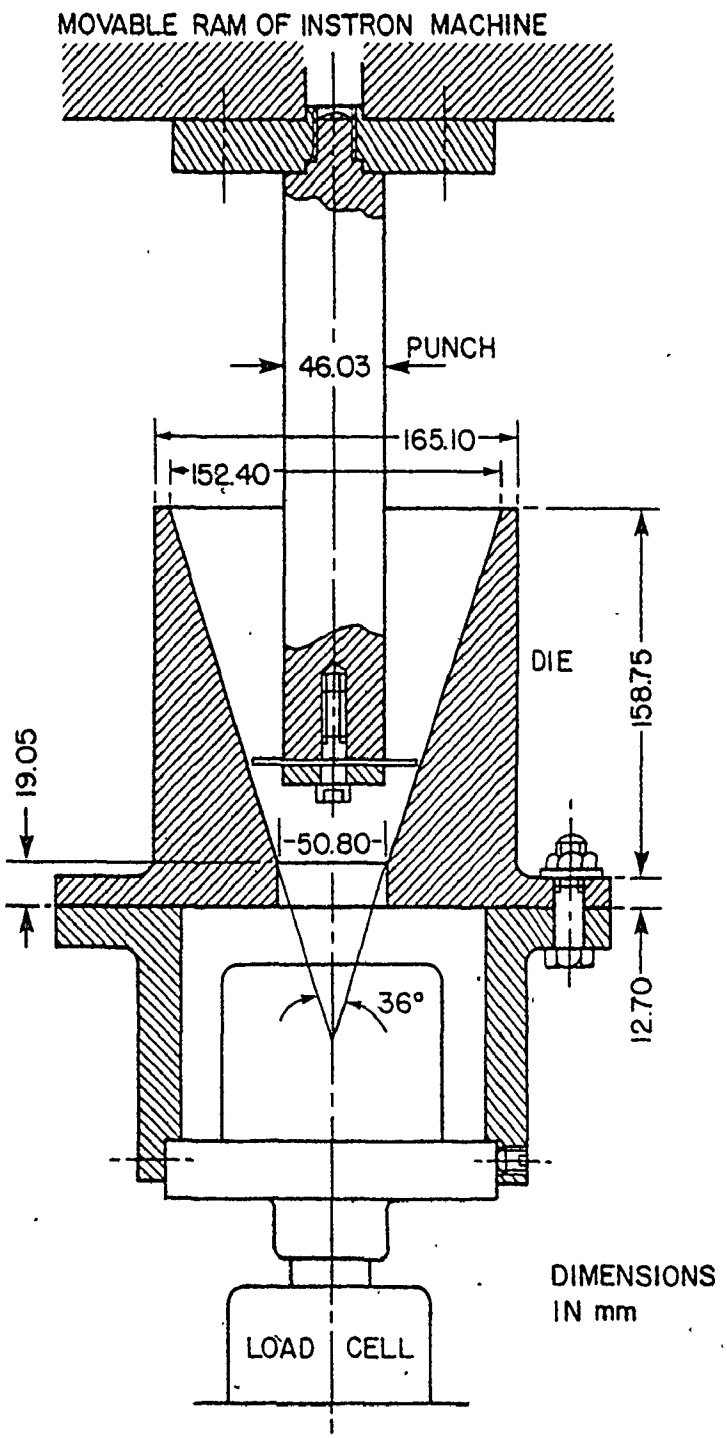

Figure 5.4 Set-up with conical die

conical die, is shown in Figure 5.5. In order to identify the different straining mechanisms, nine specimens were partially drawn and then sectioned using a fine diamond saw in order that a generator could be revealed on a contour projector. The progress of the deformation is shown in Figure 5.6. It is clear that the initial mode of deformation is a dominantly one of bending until the blank side becomes tangent to the die - slightly before step 4. A process typical of tube sinking then starts and can be identified by the large increase in the rate of change of load with respect to punch travel. Between stages 7 and 8 part of the blank is drawn into the cylindrical section of the die and ceases to deform and thereafter the drawing load drops. Between stages 4 and 7, the curvature of the unsupported region changed very little, with bending of the material taking place at the punch nose (a plastic hinge) and also at the point of contact of the material with the die wall.

During the drawing process stretching of the material in the cupwall occured. Figure 5.7 shows the amount of stretch at different deformation stages for a 60.70 mm diameter blank (D_b) of 3003-H14 Al, and is typical of the observations made with other materials and blank sizes.

In order to study the strain path of the different regions of the blank, a circular grid was electrochemically marked on the steel and brass specimens, whereas a photo-printing technique was

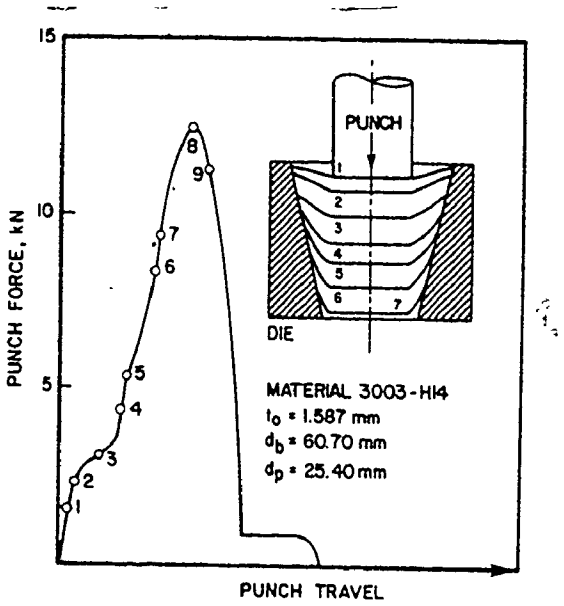

Figure 5.5 Typical punch force - punch travel diagram with conical die

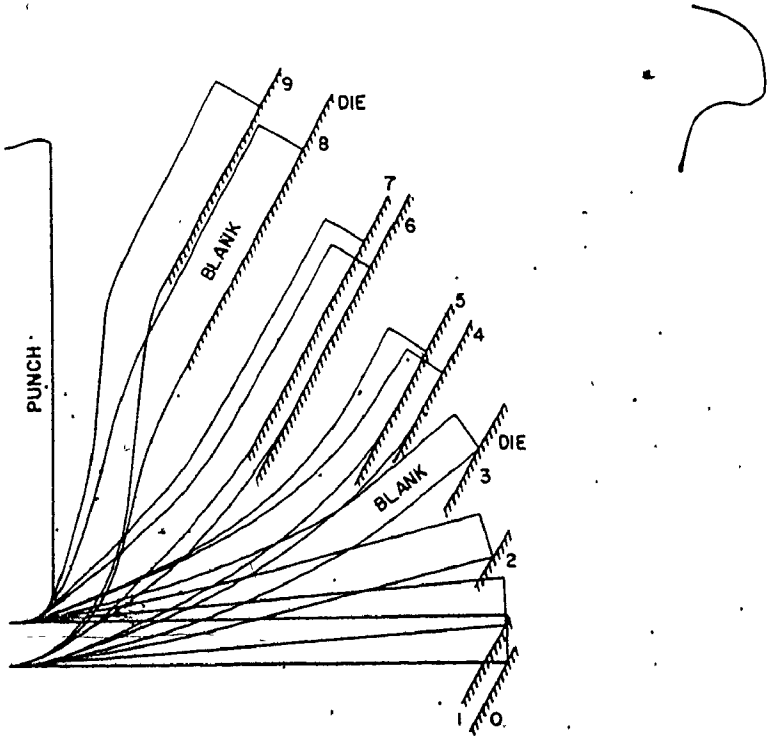

Figure 5.6 Mode of deformation with conical die

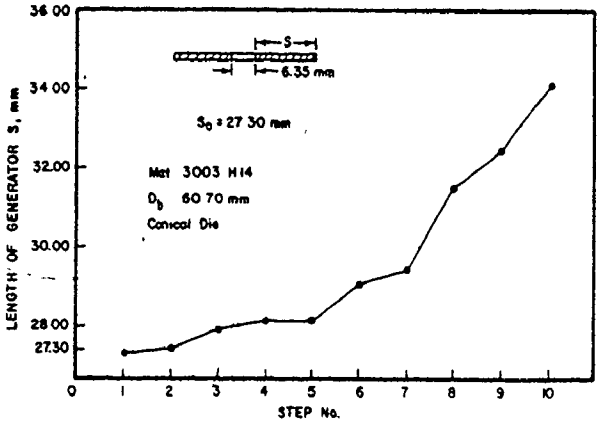

Figure 5.7 Variation of length of generator with drawing process

used for the aluminum specimens. The grid size was 2.5 mm diameter.

The blank can be considered as a thin shell. The deformation process is such that the principal axes of strain change very little during deformation (except perhaps for friction and material anisotropy effects). Thus a circular grid deforms into an ellipse whose major and minor axes are a measure of total in-plane principal strains at that point. The total strain is defined in this work by the logarithmic measure, $e = \ln \frac{l}{d}$, where l is the axes of the ellipse and d is the circle diameter before deformation. The deformed ellipse was measured on an optical microscope, and hence the total principal strains in the radial and circumferential directions were obtained. Some typical results are plotted in Figure 5.10, determined at different stages in the deformation process as characterized by Figure 5.8. At the same time the natural thickness strain was evaluated and some

results are shown in Figure 5.9. Note that at the onset of the process, some small biaxial stretching of the central portion of the blank occurs as the material at the lip feels the wedging action of the die, but ceases as the drawing proceeds. This initial stretching is identified in Figure 5.9 at steps 1 and 2, where thinning of the material takes place. As can be seen from Figure 5.10, a neutral circle, i.e. characterized by zero hoop strain, can always be identified on the part and its location does not change much between stages 3 and 6. The magnitude of the compressive hoop stresses is relatively small with respect to the radial stresses at the neutral circle, and therefore if the unsupported material was to buckle between the punch and the neutral circle then this bifurcation mode is likely to be governed by a geometric type of instability and not a force criterion.

In order to investigate the effect of planar anisotropy, the measurements were carried on two radial lines 45° apart. Some typical results are shown in Figures 5.10(c) and (d), and the variation could be attributed as much to measurement errors as to any differences in material properties.

When examining the blank, it could be easily observed that the edge of the rim curved inwards towards the centre of curvature of the blank. This "EDGE EFFECT" is caused by the shearing stresses at the blank-die interface, as shown in Figure 5.11. On the other hand a close look of the contact surface for a specimen, at stage 6-7 in Figure 5.6, shows that the rim-die interface does

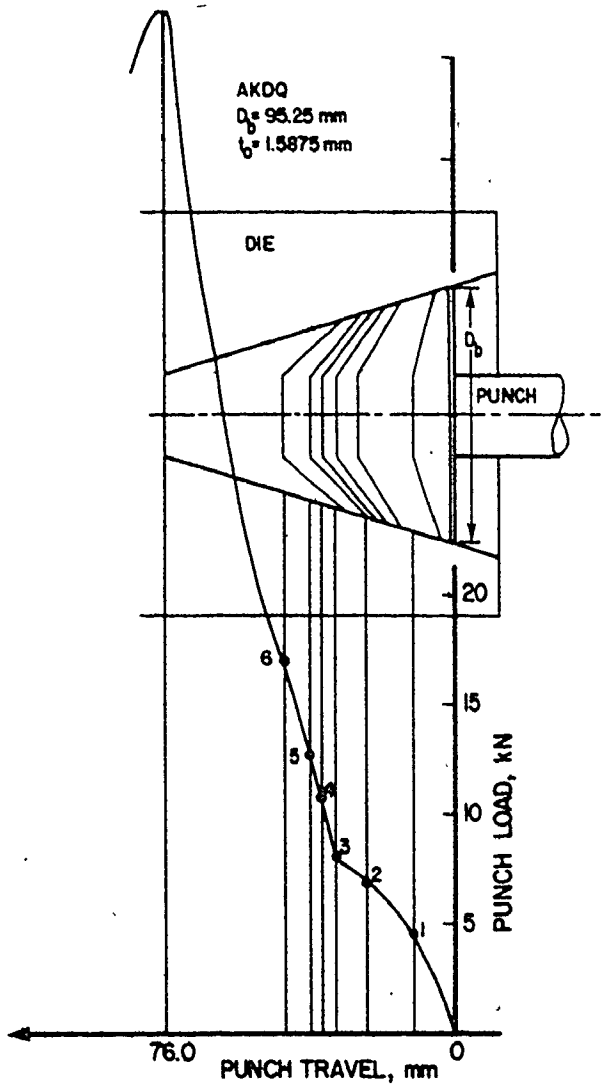

Figure 5.8 Measuring stations with conical die

not have the same brightness. The brightness distribution is shown schematically in Figure 5.11, where the dull region corresponds to the curved lip. Qualitatively, the burnished regions correspond to the regions of higher contact stresses, and therefore the figure shows that the critical bending moments are transferred from the blank's rim, at the beginning of the process, to a region close to the unsupported edge at the stage shown in Figure 5.11.

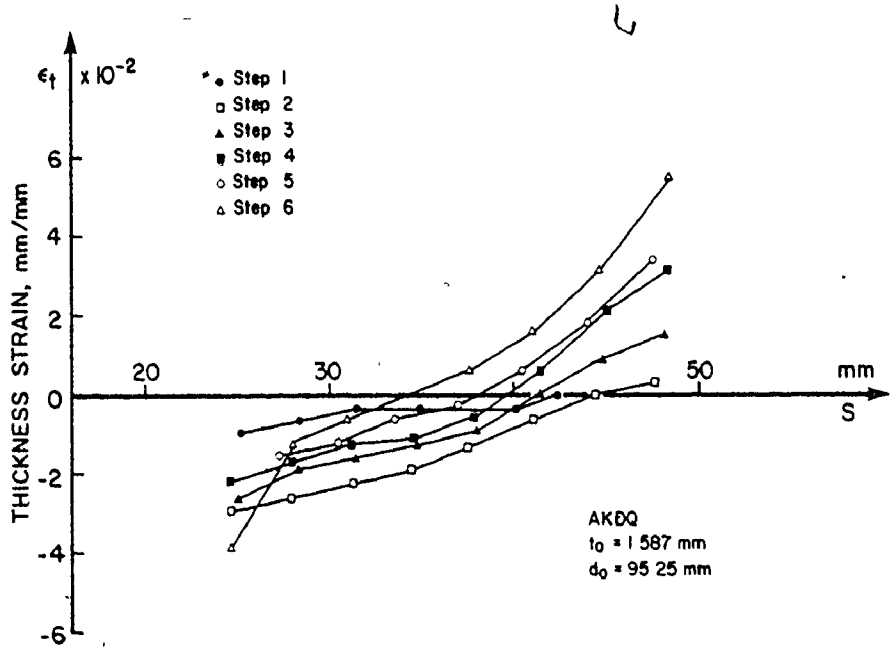

Figure 5.9 Change of thickness strains with drawing process

5.3.2 Identification of Wrinkling Modes

With reference to Figure 5.6, the mode of deformation can be subdivided into 3 stages: -

(i) bending process, steps 1-4, i.e. until the blank becomes tangent to the die.

(ii) tube sinking process, steps 4-7.

(iii) change in curvature of the unsupported section, as can be clearly seen between steps 7 and 8, and is a source of redundant work.

At the same time four types of wrinkling modes can be identified with the process: -

(A) In the bending zone, wrinkling or instability could occur and would be controlled by the bending stiffness which is a

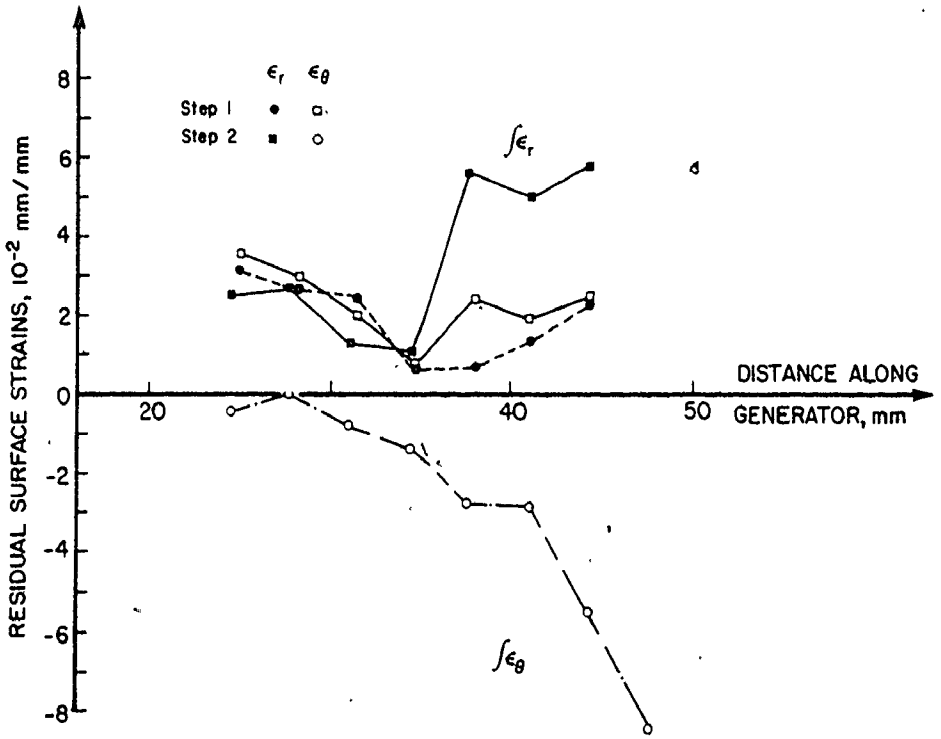

(a)

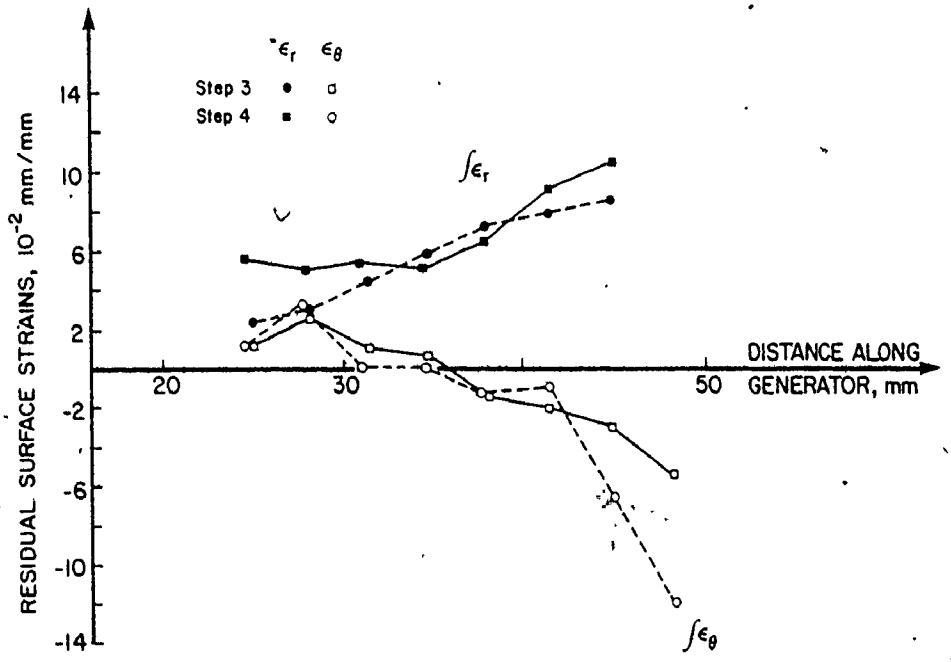

(b)

Figure 5.10 Distribution of radial and circumferential strains

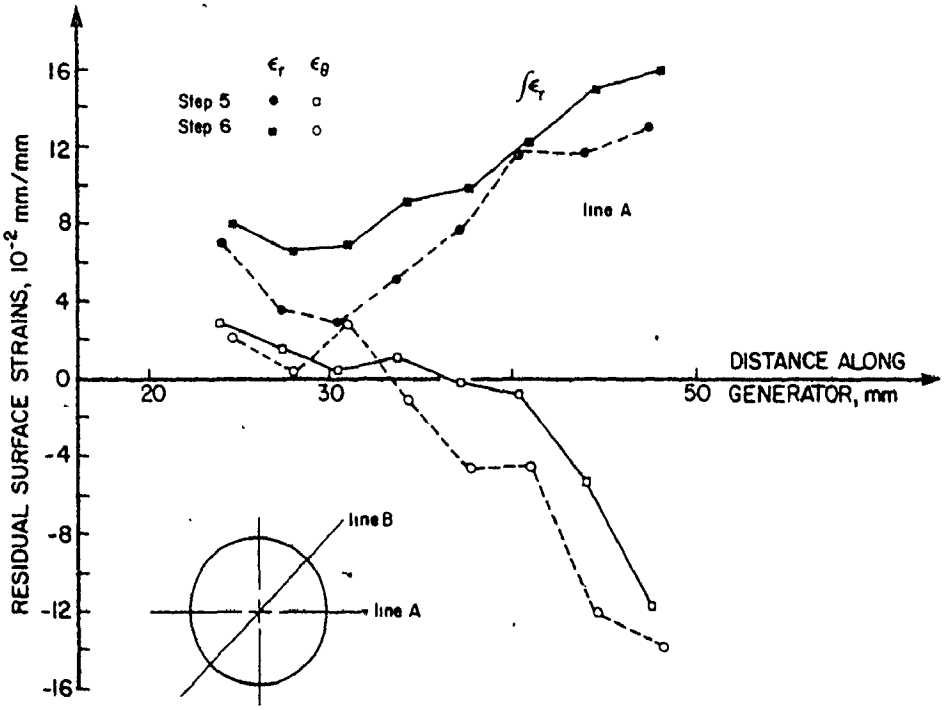

(c)

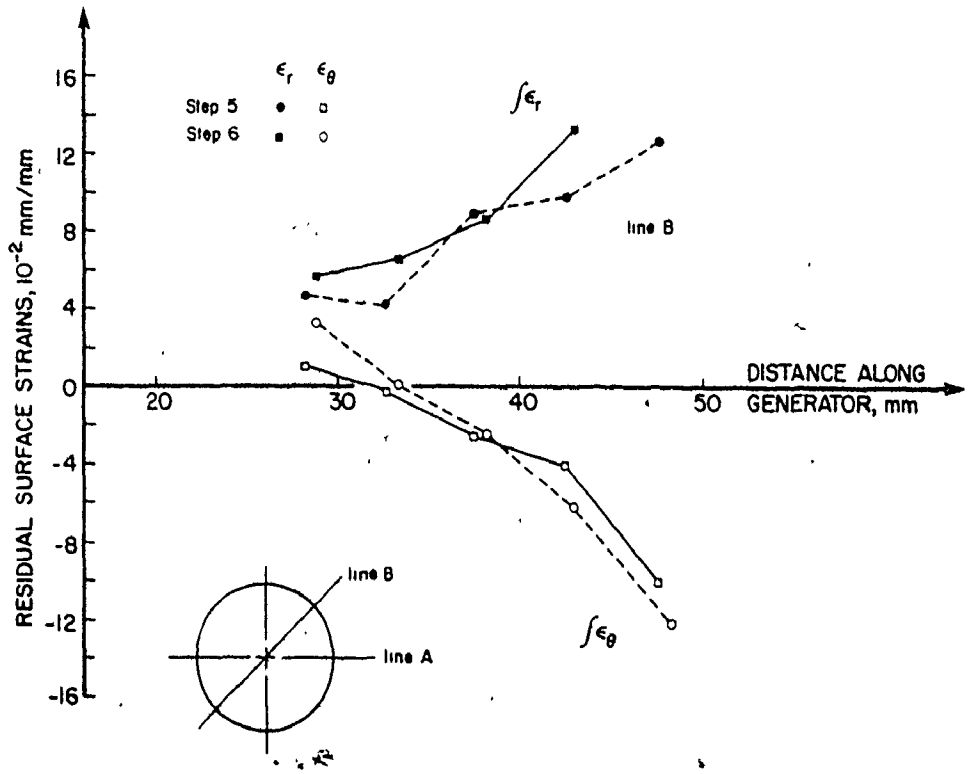

(d)

Figure 5.10 Distribution of radial and circumferential strains

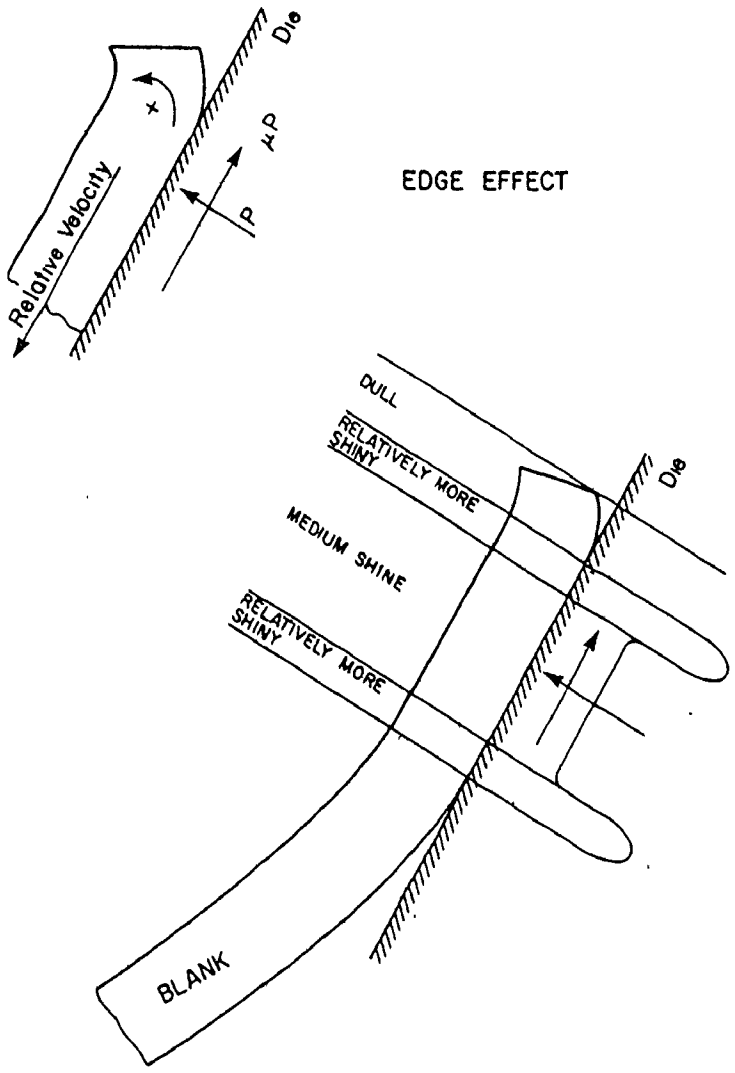

Figure 5.11 Edge effect and distribution of contact stresses

function of the material thickness and not the compressive hoop stresses present in the material. This could be explained by the fact that for synclastic shells, i.e. those shells with positive Gaussian curvature ($K_G = K_{ss}\ K_{\theta\theta} > 0$), transverse bending causes local disturbances near the rim, that dampen out with distance from the point of disturbance. Moreover, the more the

longitudinal generator is made to curve, the shorter is the reach of the boundary disturbance, Oravas [115]. It can be expected that the boundary disturbance would increase in magnitude and dampen out faster with distance when moving from step 1 to 4. Once the blank becomes tangent to the die, i.e. at about step 4 the tube sinking process begins and the rim becomes more constrained and bending disturbance is largely diminished. This suggests that the cone angle could be important, particularly for thin blanks. The influence of the cone angle was not investigated in the present work and although Shawki [112] has quoted an optimum cone angle, $2\alpha = 36^{\circ}$. According to the previous discussion it is clear that the most critical stage for wrinkling due to a bending disturbance is just before the blank becomes tangent to the die. The experiments confirmed this hypotheses and showed that the wrinkling mode is of a kink form inclined towards the centre of curvature of the blank. It is of local nature and in general four kinks were observed with all the materials tested. It seems that this type of bifurcation takes the least amount of energy and in the same time allows additional moments at the rim. Since this mode of wrinkling occurs at very low strains, some type of inextensional circumferential deformation could be expected. It is to be noted that these kinks or folds did not necessarily increase in size as the deformation proceeded, and in certain cases they were erased with continuing deformation. Figures 5.12 show two typical cases where the wrinkles have started at the

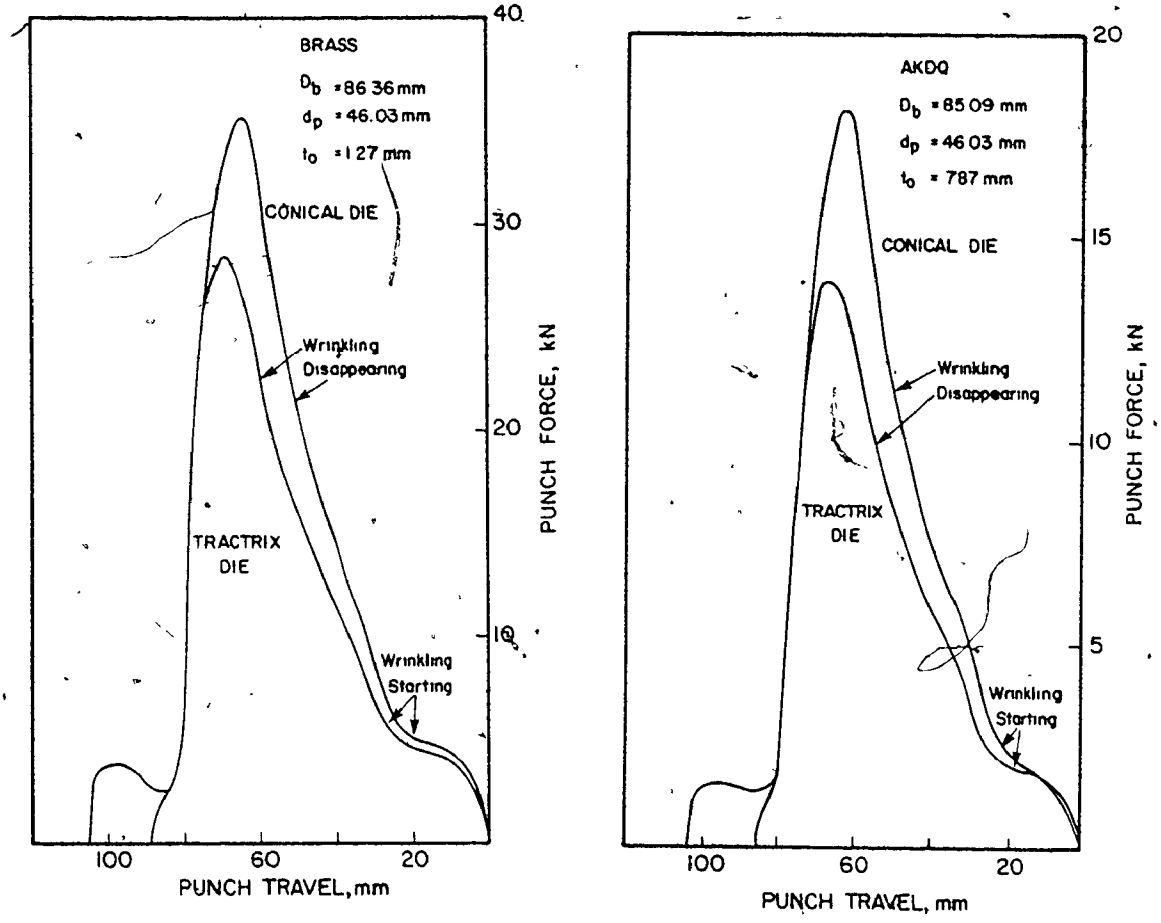

Figure 5.12 Typical location for the start and then disappearance of wrinkles.

transition between bending and tube sinking and also show the stage at which they disappear (i.e. in tube sinking).

As the ratio D_b/t (blank diameter to thickness) increases, wrinkles start to occur earlier in the bending process; these are not normally erased and they rapidly increase in height as the punch descends. It was found that in some cases the wrinkling behaviour could be identified from the load-punch travel diagram. The load could reach a peak value or sometimes a plateau, as was usually observed with low yield strength materials when using relatively large blank diameters, see Figure 5.13a. Materials of increased strength and hardening rate, or when D_b/t decreases,

tend not to show a peak load or plateau once wrinkling starts, see Figure 5.13b. In some special cases a sudden local rate of change of punch load with respect to punch travel can be detected. We can therefore physically understand the difference between uniqueness (bifurcation) and stability and recognize that from the practical point of view we ~~can~~ have a stable bifurcation with the load increasing with deformation.

(B) As can be seen from Figure 5.6, the second type of wrinkling occurs in the tube sinking process (steps 4-7) and the wrinkling is controlled by the compressive hoop stresses as with the case of the conventional deep drawing process. Only in a few cases was this observed in the current experiments; the wrinkles tended to be of a local nature and did not occur around the whole periphery. In most cases one wrinkle appeared and grew with deformation to cause catastrophic wrinkling.

(C) Around stages 6 and 7, where contact stresses at the die-material interface are likely to be large, wrinkles can occur in the unsupported portion between the punch and die. The wrinkles take the form of dimples which are symmetrically located. These caused a discontinuity in curvature at the blank-die interface next to the unsupported region. As the punch advances the dimples can propagate up to the rim causing a catastrophic

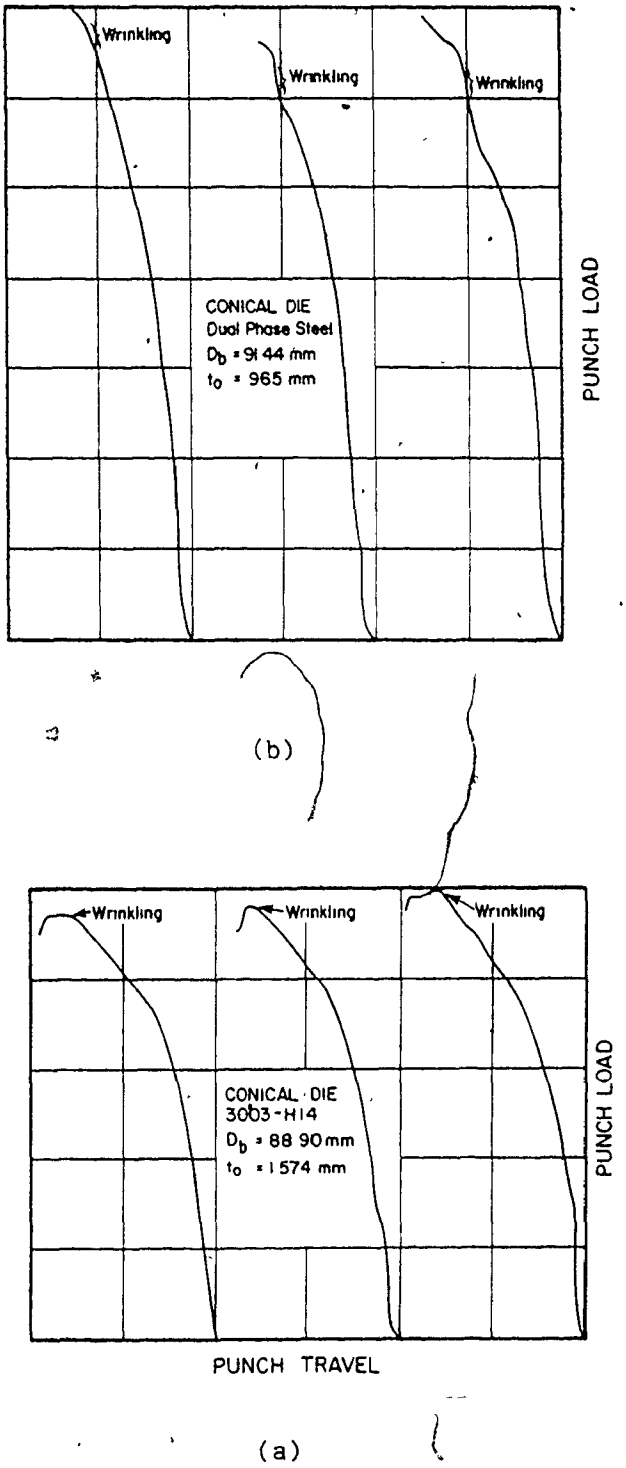

Figure 5.13 Identification of wrinkling behaviour from the load-travel diagram

wrinkle. In all cases eight dimples were formed.

(D) A fourth possibility of wrinkling could occur between stage 7 and 8 because the curvature of the unsupported portion of the blank next to the die is forced to change in sign. This change is not constrained and nothing can be said a priori about the uniqueness around the inflection point. Miyagawa [90] reported that wrinkling could occur "by chance" at this stage. He offered no explanation as to the cause of this type of wrinkling behaviour, but stated that it could be quite crucial when using conical dies.

5.4 The Tractrix Die

The Huygen tractrix die was patented in 1938 by O. May [84]. This die shape was considered to minimize redundant plastic work. Ideally the rim of the blank only would be in contact with the die, and the unsupported wall would remain straight throughout the process with no stretching. In practice the length of the flange increases by about 30 percent. Furthermore the bending resistance at the punch nose prevents the cup wall from remaining straight and the flange shape changes. We therefore can expect some redundant work due to friction and mild bending and unbending. No blankholder is used with this die and accordingly the drawing load is reduced together with a corresponding reduction in localized strain over the punch radii. The

differential equation for the tractrix die is

$$\left(\frac{dy}{dx}\right)^2 = \frac{y^2}{C^2-y^2}$$

where x and y are the coordinates along the punch center line and perpendicular to it respectively, and $x = \pm C$ are the assymptotes to the curve. Figure 5.14 demonstrates how the initial part of the tractrix curve is developed for a mouth diameter of 120.65 mm, as used in the present experiments. It is clear that for a full utilization of the shape of the tractrix die, the die has to be designed for each individual blank size. This was not feasible in our experiments, and the die shown in Figure 5.14 accommodated all the different blank diameters. In order to shorten the die height, the curve in Figure 5.14 was blended into a cone of 30° included angle.

5.4.1 Deformation Pattern

The mode of deformation of the blank is shown in Figure 5.15. In the very early stages the deformation mode is mainly one of bending, similar to events with the conical die. The blank is deformed into a synclastic shell (positive Gaussian curvature) and an edge effect is observed as with conical dies. As the punch descends, the blank rim comes more in contact with the die and the blank begins to form an anticlastic shell (i.e. with negative Gaussian curvature), which is likely to be a major source of redundant work in tractrix dies. At this stage a semi-tube

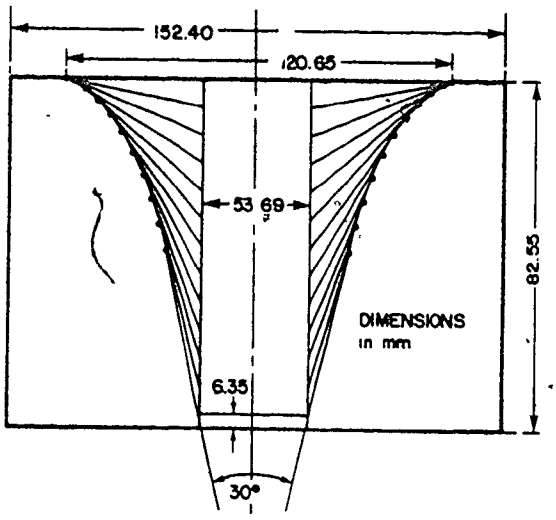

Figure 5.14 Typical generation of tractrix curve

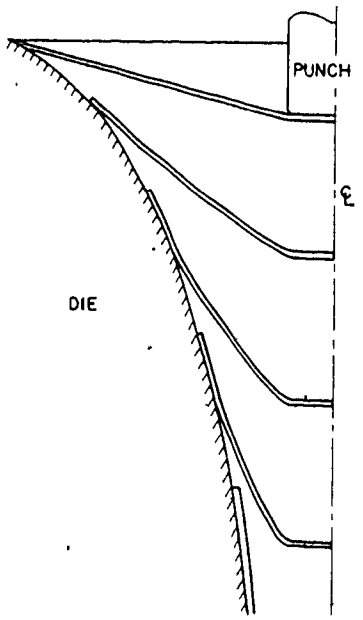

Figure 5.15 Mode of deformation with tractrix die

sinking process starts which constrains the buckling of the shell for the two following reasons: -

(i) it terminates the bending process very early in the deformation process; the bending process being very critical since for anticlastic shells local disturbances penetrate far from the point of disturbance compared with synclastic shells, Oravas [115].

(ii) anticlastic shells have excellent properties against buckling.

Since the blank in contact with the die forms a shell with negative Gaussian curvature and since the region in contact with the punch forms a shell with positive Gaussian curvature, an inflection point on the blank generator is to be expected if no discontinuities in curvature are to be present.

5.4.2 Identification of Wrinkling Modes

According to the mode of deformation, wrinkling can occur in three different regions: -

(A) Kinks can form in the bending process and these are of local nature and are generally symmetric. Four wrinkles are always observed and since this occurs in the beginning, it is for relatively large (D_b/t) blanks.

(B) Wrinkles can form next to the rim in the semi-tube sinking process; they do not have to be symmetrically distributed.

(C) Before the end of the process a discontinuity in the

curvature occcurs in the unsupported part of the blank. This occurs only with relatively thick blanks and the bifurcation mode is in the form of dimples and the drawn part looks rather like a jelly mould. This bifurcation could propagate up to the rim and cause a "catastrophic" wrinkle.

The last one is of similar type to the third form of wrinkling described for conical dies. However, it occurs more frequently with the tractrix die because of the inflection point already existing in the unsupported section of the blank, and this could trigger a discontinuity in curvature. In all cases, eight symmetrically placed dimples were formed and it is considered that this type of bifurcation is relatively insensitive to imperfections, either geometric or material.

5.5 Conical Versus Tractrix Dies

Blanks were drawn in both the conical and tractrix die and the onset of wrinkling was noted. The drawing was continued to determine whether the wrinkles disappeared leading to a successful draw or whether they grew to a catastrophic wrinkle. For a given thickness of sheet, the diameter of the blanks was gradually increased until it was impossible to draw a cup without failure; the limiting diameter was then recorded. The limiting drawing ratio (L.D.R) is defined as

$$\text{L.D.R.} = \frac{\text{maximum blank diameter}}{\text{punch diameter}} = \max \frac{D_b}{d_p} \quad ,$$

for a successful draw. The plot of L.D.R versus the blank thickness for the conical die is shown in Figure 5.16. It is clear that the L.D.R. is a function of the thickness of the material and the type of material. The AKDQ steel shows the largest L.D.R. In Figure 5.17 the experimental plot of the L.D.R. (β) versus d_p/t is shown, and comparison is made with the safe limits determined experimentally by Shawki [112]. No correspondence is obvious. A comparison of the L.D.R. for both the conical and tractrix dies is shown in Table 5.4. It is apparent that the L.D.R. for the tractrix die is not less than that for the conical die and in many cases it is larger. It has to be noted that the lower part of the tractrix die was blended into a cone and therefore little difference between the performance of the two dies can be expected with the smaller blank diameters. Shawki [112] has reported that to maximize the L.D.R., when using a tractrix (or modified tractrix) profile, the full mouth width of the die should be utilised. In other words for each diameter, the die has to be properly designed in order to make full utilization of the tractrix profile. If the blank diameter exceeds the mouth diameter of the die, the rim of the blank deforms in the opposite direction and this will nullify some of the advantages of the process, as reported by Haverbeck [112] and observed in the present set of experiment.

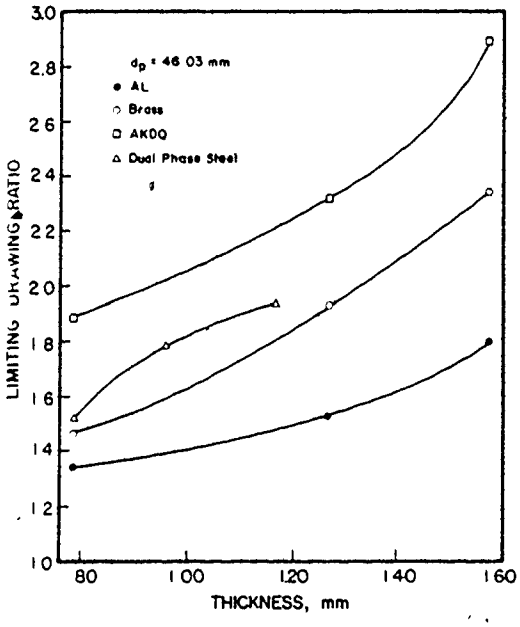

Figure 5.16 Variation of limiting drawing ratio with material thickness in conical die

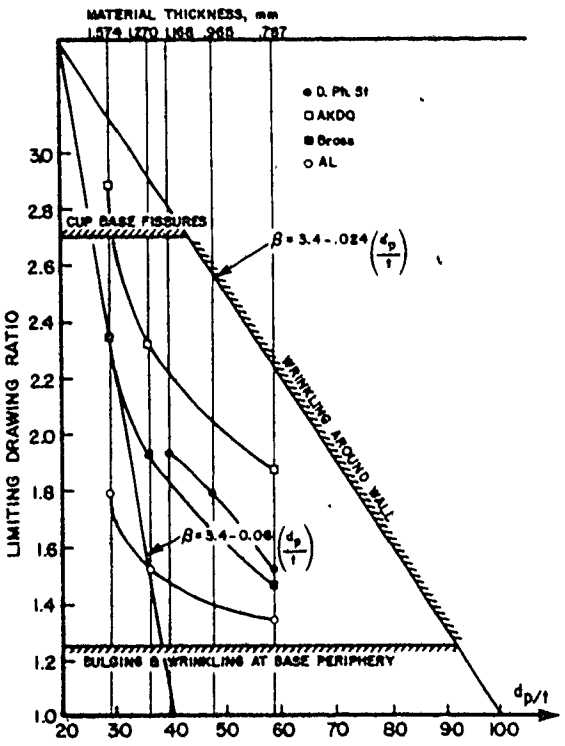

Figure 5.17 Comparison of experimental results with limits set by Shawki [112]

Table 5.4

Comparison Between Conical and Tractrix Dies

Material	Thickness mm	Limit diameter in mm		Maximum load in kN	
		Conical	Tractrix	Conical	Tractrix
Aluminum	0.787	60.96	60.96	1.87	1.11
	1.270	69.85	69.85	5.69	4.31
	1.574	76.20-82.55*	76.20-82.55*	11.57	7.92
Brass	0.787	67.31	67.31	8.63	6.27
	1.270	88.90	$\geq$ 91.44	37.38	29.81
	1.574	107.95	107.95	$\geq$ 40.05	$\geq$ 40.05++
AKDQ	0.787	86.36	$\geq$ 88.90	20.47	18.69
	1.270	106.68	107.95	$\geq$ 40.05	38.27**
	1.574	133.35	+	$\geq$ 44.50	+
D.Ph.St.	0.787	69.85	69.85	14.68	11.12
	0.965	76.20-82.55*	76.20-82.55*	26.70	20.47
	1.168	88.90	$\geq$ 95.25	$\geq$ 44.50	42.72

Punch diameter is 46.03 mm

* Load corresponding to lower limit is shown

\+ Blanks of diameters larger than 120.65 mm cannot be taken by tractrix die

++ The blanks of diameter 114.30 mm wrinkled very early in the process with conical die and quite late with tractrix die

** The blanks of diameter 114.30 mm wrinkled at the beginning of tube sinking in conical die and in a jelly mode fashion with tractrix die.

It is also observed that the maximum load required is considerably less for tractrix dies, and a typical comparison is shown in Table 5.4. Shawki [134] has mentioned that despite the lower maximum load required for the tractrix dies, the work required to draw the cup remains the same. This is not consistent with the present findings as exemplified by the load versus punch travel plots, Figures 5.12. The difference could lie in the actual profile of the die classified as a tractrix in Shawki's work and the present experiments.

It is difficult to provide a quantitative assessment of the frictional work dissipated with each die. The contact area with the tractrix die tends to be larger, thus for comparable contact stresses the frictional work will be larger. Since the total work is less with the tractrix die, it then follows that the plastic work (useful and redundant work) is less. The redundant work will be the consequence of unnecessary bending work. Experiments suggest more total bending work in conical dies.

It has been reported by Shawki [134] and Keeler [71] that the Huygen-tractrix die provides the greatest possible lateral restraint against buckling or wrinkling. This is only true once the semi-tube sinking process begins - which does happen very early in the process - because as mentioned before anticlastic shells have superior buckling resistance compared to synclastic shells. However, it should be noted that just at the very beginning of the process, i.e. in the early bending stage

wrinkling could be quite crucial with the tractrix die, especially for large relative diameter blanks ($D_b/t>>1$). The explanation is schematically illustrated in Figure 5.18. The frictional forces (μP_i), that have a stabilizing effect, are larger with the conical die. On the other hand, the forces that produce the boundary disturbance are larger with the tractrix die. It could therefore be concluded that both effects make the blank less stable in the tractrix die, at the very early stage. This bending process ends up very rapidly but could be quite critical for blanks with large relative diameters, as experimentally observed.

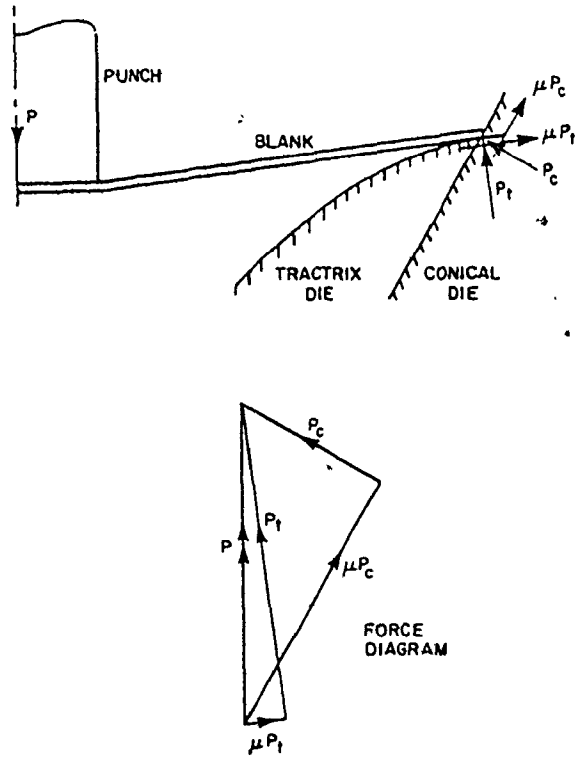

Figure 5.18 Normal and frictional forces with both conical and tractrix dies

5.6 Maximum Load Analysis

Approximate methods of predicting the maximum punch load are presented in this section, following a proposal by Duncan and Johnson [35] for analysing the conventional deep drawing process. The solutions are based on the use of a material true stress-strain curve and the determination of either an instantaneous value of mean yield stress for the process or the plastic work of deformation. The expressions are developed using the basic laws of plasticity, but the actual deformation process has been greatly simplified. The basic model is as follows; the virtual work principle is invoked, i.e.

$$\int \bar{\bar{\sigma}} : \bar{\bar{\epsilon}} \, dV = \int \bar{F} \cdot \bar{v} \, dS$$

or

$$W_I = W_E \quad . \tag{5.4}$$

where W_I and W_E are the internal and external work in the increment of displacement. By integrating both sides of (5.4), we can write

$$\int_0^{\bar{e}} W_I \, d\bar{e} = \int_0^{u} W_E \, du \quad . \tag{5.5}$$

where

$$\int_0^{\bar{e}} W_I \, d\bar{e} = \int_V \int_0^{\bar{e}} \bar{\sigma} \, d\bar{e} \, dV \quad , \tag{5.6}$$

and

$$\int_0^{u} W_E \, du = \int \int \bar{F} \cdot \bar{v} \, du \, dS \quad . \tag{5.7}$$

u and $\bar{e}$ are the total displacement and representative strains respectively.

Internal Work

In order to evaluate (5.6) it is assumed that a flat circular blank is drawn into a flat-bottomed cylindrical cup without change in material thickness. Duncan and Johnson [35] make no attempt to model the actual process, and furthermore frictional effects and the work done in bending and unbending etc., are ignored. They merely compute the plastic work done in converting an annular ring(s) in the flange to a station in the cup wall. The material is assumed to have a true stress-strain relationship of the following form

$$\bar{\sigma} = \bar{\sigma}_o + C\bar{e} \tag{5.8}$$

and two models are proposed for the work done. In the first model an integration procedure is employed resulting in the following expression for the internal work

$$\int_o^{\bar{e}} W_I d\bar{e} = \frac{\pi b^2 t_o}{\sqrt{3}} \bar{\sigma}_o (\beta-1) \{2R^2 \ln R [\frac{\beta \ln R}{\beta-1} -1] + (R^2-1)\} \tag{5.9}$$

where $R = a/b$ is the drawing ratio and $\beta = \frac{C}{\sigma_o \sqrt{3}}$.

The second model uses an averaging procedure in that the work done per unit volume of flange material is assumed equal to that experienced by an element at some mean initial radius $\bar{r}$. The work

expression is given by

$$\int_0^{\bar{e}} W_I d\bar{e} = \frac{\pi b^2}{2\sqrt{3}} t_o (R^2-1)(2\bar{\sigma}_o + C\bar{e}_{\bar{r}}) \ln\left(\frac{R^2+1}{2}\right) , \qquad (5.10)$$

where $$\bar{e}_{\bar{r}} = \frac{1}{\sqrt{3}} \ln\left(\frac{R^2+1}{2}\right) .$$

The original article can be consulted for further details. For convenience equation (5.9) is termed the work analysis (W.A.) and (5.10) the mean work analysis (M.W.A.).

External Work

Equation (5.7) expresses the total external work and it is assumed that this is equal to the area under the punch load-displacement diagram. A not unreasonable assumption is that the shape of the experimental curve can be approximated by two sine waves, see Figure 5.19. The force is accordingly given by

$$P = \begin{cases} P_1 \sin\frac{\pi x}{h_1} + P_2 \sin\frac{\pi x}{h_2} , & x \leq \frac{h_1}{2} \\ P_2 \sin\frac{\pi x}{h_2} , & h_2 \geq x > \frac{h_1}{2} \end{cases} \qquad (5.11)$$

The total work is therefore given as

$$\int_0^u W_E \, du = \int_0^{h_1/2} P_1 \sin\frac{\pi x}{h_1} dx + \int_0^{h_2} P_2 \sin\frac{\pi x}{h_2} dx$$

$$= \frac{1}{\pi} [h_1 P_1 + 2h_2 P_2]$$

Practically $h_1 = .5h_2$ and $P_2 = 4P_1$, and hence

$$\int_0^u W_E \, du = \frac{2.125}{\pi} h_2 P_2 \qquad (5.12)$$

From Figure 5.20, we have

$$h_2 = l_1 + l_2$$

where l_2 is the height of the cup and is obtained from the constancy of volume and thickness assumptions. In the present case the total punch travel is given by

$$h_2 = \frac{b(R^2-1)}{2} + b(R-1)\cot\phi \qquad (5.13)$$

Substituting from (5.13), into (5.12), the total external work is given by

$$\int_0^u W_E \, du = \frac{1.0625}{\pi} b P_2 (R-1)(R+1+2\cot\phi) \qquad (5.14)$$

By equating the total internal and external work, expressions (5.9) and (5.14), the maximum load could be expressed as

$$P_W = \frac{5.36\, bt_o \bar{\sigma}_o (\beta-1)}{(R-1)(R+1+2\cot\phi)} \{2R^2 \ln R \left[\frac{\beta \ln R}{\beta-1} - 1\right] + (R^2-1)\} \qquad (5.15)$$

whereas from the mean work analysis (M.W.A.), equation (5.10) we obtain

$$P_M = 2.68\, b\, t_o \frac{(R+1)}{(R+1+2\cot\phi)} (2\bar{\sigma}_o + C\bar{e}_{\bar{r}}) \ln\left(\frac{R^2+1}{2}\right) \qquad (5.16)$$

The comparison between the experimental points, with $\phi = 18^\circ$, and the theoretical curves for $\phi = 18^\circ$ and 45° is shown in Figures

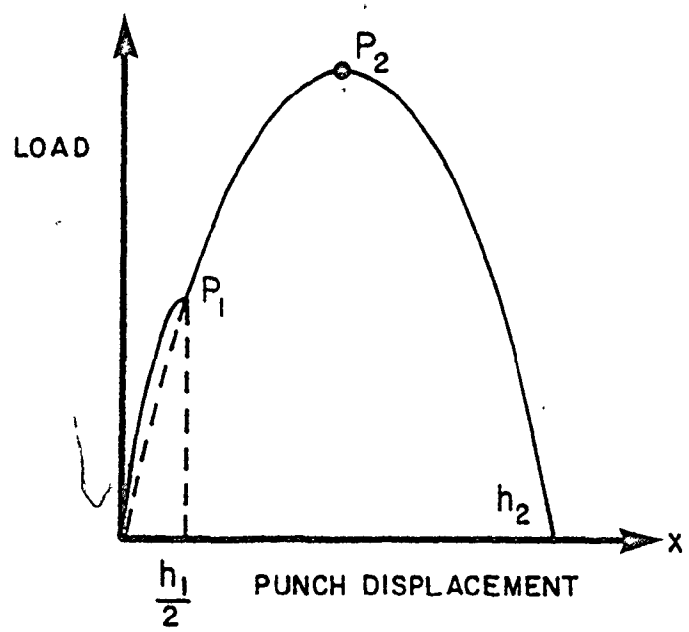

Figure 5.19 Approximation of the shape of the punch load–travel diagram with conical die

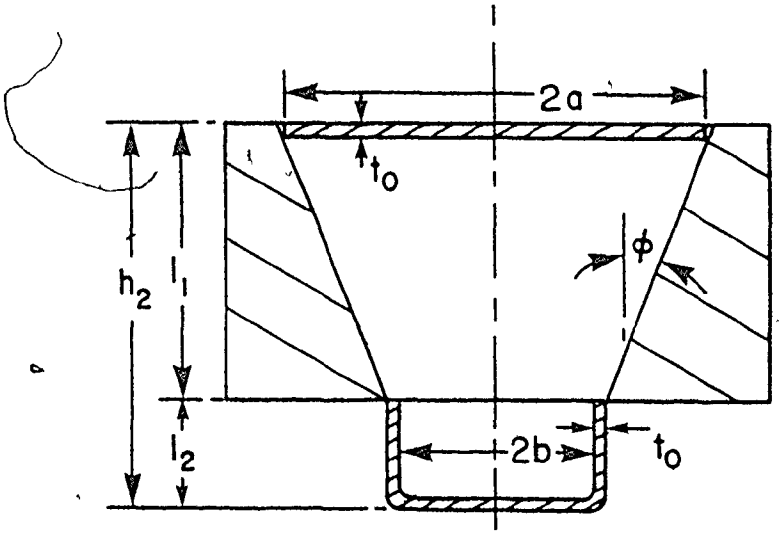

Figure 5.20 Blank and cup geometries

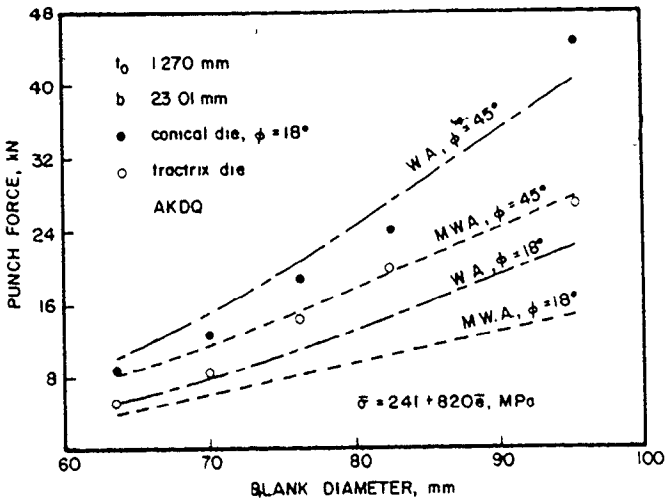

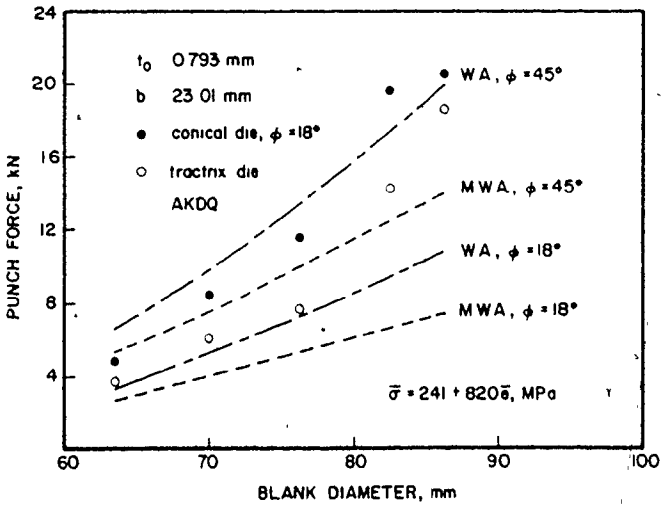

Figure 5.21 Comparison between approximate punch forces and experimental results

5.21. Also given on the same graph, for comparison, are the experimental points obtained with the tractrix die. Figures 5.21 illustrate that the mean work analysis (M.W.A.) load is less than that obtained through the work analysis (W.A.). The theoretical results with $\phi = 18^{\circ}$ do not compare well with the current experimental findings. The differences are not altogether surprising in view of the very simplified model employed, which ignores friction, bending and stretching work. What might be regarded as encouraging is the correspondence in the trend of the results.

In analogy with wire drawing, there may be an optimum cone angle. Shawki [112] reported an optimum cone angle of 36°.

5.7 Discussion and Conclusions

5.7.1 Discussion

The bifurcation approach relies on the theoretical notion that the system is considered to bifurcate if there exists an equilibrium configuration infinitesimally close to the original configuration. It seems therefore difficult to define experimentally the minimum deviation from the steady state configuration. In other words it was difficult to define the minimum wave amplitude to be labelled a definite wrinkle and hence a bifurcation mode. The problem is considerably aggravated by the presence of the edge effect and the earing that could occur with materials of large planar anisotropy Δr.

Because of the complexity of the mode of deformation and the non-homogeneous deformation at the rim, it was a matter of personal judgement to determine the start of the wrinkling process (bifurcation); most experimenters develop their own methods such as the feeling of the curvature of the specimen, use of dial gauges and light reflection from specimen.

A qualitative account of imperfections has not been made in the present study. These imperfections could be in the form of material imperfections, e.g. non-homogeneity of structure or anisotropy, or geometric imperfections caused by variations in material thickness, lack of flatness and errors in the concentricity of the machined blank. Additional geometric imperfections can arise with alignment, e.g. the blank is either not concentric with or perpendicular to the punch at assembly. The real influence of imperfections is often difficult to assess in quantitative terms, other than they are not likely to be beneficial.

From a practical point of view it could be argued that many imperfections will be probabilistic in nature, e.g. random errors in alignment or random errors in machining. Even material imperfections, which may have a degree of regularity in rolled sheets, could take the form of a probabilistic event if blanks are cut in a random manner from the sheet.

The worth of the imperfection approach in bifurcation analysis is the effect it can have in reducing the predicted

critical buckling loads. Therefore it serves as another tool in helping to resolve discrepancies between theoretical predictions and experimental observations.

(i) Conical and Tractrix Dies

It is quite clear in Figures 5.16 and 5.17 as well as in Table 5.4 that the L.D.R. with conical and tractrix dies is substantially larger than that experienced with the conventional deep drawing dies, especially for relatively thick blanks. Typical L.D.R.'s in the conventional process are between 2.0 and 2.4. One of the implications here is in the production of the drawn and ironed can, since when using the conventional deep drawing operation an additional redraw is usually involved before the ironing stage. A deeper cup with the conical die may eliminate the need for the redraw.

The remarks pointed in Table 5.4 indicate that in many cases the wrinkling occurs earlier in the process of deformation with the conical die than with the tractrix die, for the same blank and punch diameters. We therefore deduce that the blanks are more stable in the tractrix die. On the other hand, the wrinkling mode could be quite different in the two dies.

(ii) Material Properties and Wrinkling

Figure 5.16 shows that the limiting drawing ratio (no

catastrophic buckling) increases with thickness. This behaviour is supported by the theoretical models, where the critical thickness ratio is proportional to the square root of the critical stress. As previously mentioned, Figure 5.16 represents the total limiting drawing ratio that in most cases includes the post-buckling behaviour, i.e. the blank could have wrinkled, but because of a complex mechanism involving geometric and material properties, the wrinkles disappear and the final cup is of acceptable appearance. In contrast, the theories presented in the present work can predict only the initial bifurcation and no post-buckling behaviour is given. We therefore cannot directly compare the theoretical and experimental results. However it is clear from Figure 5.16 that the relative material resistance to buckling is higher for AKDQ steel followed by the dual phase steel, then Brass and finally Aluminum. Figures 5.1, 5.2 and 5.3 imply that the only parameters that are ranked in the same order are Young's modulus of elasticity, normalized rate of change of stress with respect to strain $(\frac{1}{\sigma}\frac{d\sigma}{de})$ and normal anisotropy. Accordingly we could expect that some of the above parameters or all of them have a favourable effect for wrinkling resistance. The effect of Young's modulus is quite obvious if the material were to bifurcate in the elastic region. The theory in chapters 3 and 4 predicts that a material with large relative hardening $(h/\bar{\sigma})$ is favourable for deep drawing. We know that $(h/\bar{\sigma})$ is proportional to $\frac{1}{\sigma}\frac{d\sigma}{de}$ and in this sense the normalized rate of

change of stress could be one of the required properties to delay wrinkling. Triantafyllidis and Needleman [143] reported that their model predicts that materials with larger normal anisotropy would have better wrinkling resistance, and Naziri and Pearce [101] observed the effect experimentally; both these investigations were concerned with the conventional drawing operation. In the opinion of the author the effect of $\bar{r}$ is not obvious in terms of the pre-buckled behaviour and can only be explained in terms of the post-buckling response. As an illustration the reader is referred to Figure 5.22 which shows the yield locus for the different stress states in the conical shell, for an isotropic solid ($\bar{r}=1$) and an anisotropic solid with $\bar{r}>1$. The stress points in the conical shell are located along AC and A_1C_1. The drawing mode at the rim is located around D. If it is assumed that the wrinkling behaviour can be simulated by a bending mode in plane strain with $\varepsilon_{\theta\theta}=0$ as suggested in reference [101], this corresponds to point B or B_1 on the locus. The difference between the drawing mode and wrinkling mode is given by the path DB and D_1B_1. It is not clear to the writer how through a very small perturbation, at the critical stage, the stress point at D or D_1 could move to B or B_1, respectively. On the other hand following a post-wrinkling analysis, we could imagine that after local wrinkling, the bifurcation mode is such that the stress system shifts from point D or D_1 to B or B_1 respectively, where these represent catastrophic wrinkling regions. Since the path

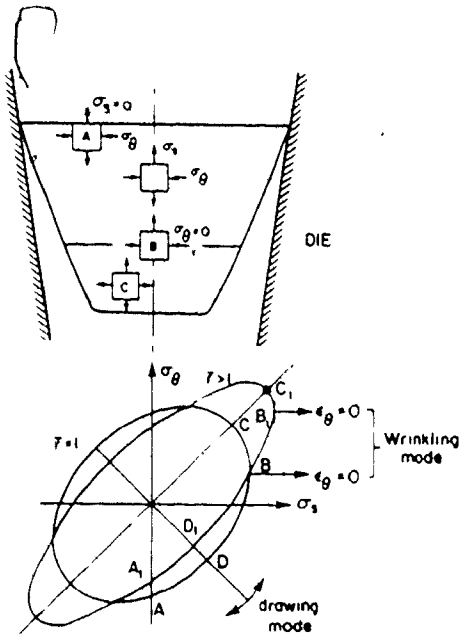

Figure 5.22 Yield locus for wrinkling and drawing modes

$B_1D_1 > BD$, we can expect that it would be easier for a material with a smaller normal anisotropy $\bar{r}$ to shift from a drawing mode to a wrinkling mode and hence fail in a catastrophic way.

(iii) On Optimum Drawing Dies

The advantages and disadvantages of both the conical and tractrix dies were discussed in section 5.5. Some attention might be paid to modifying the tooling, such that in the very early stages of the process some constraint is given to the edge of the blank as indicated schematically in Figure 5.23. This would help to inhibit the early wrinkling mode which as discussed earlier tends to dictate the success or failure of the drawing operation.

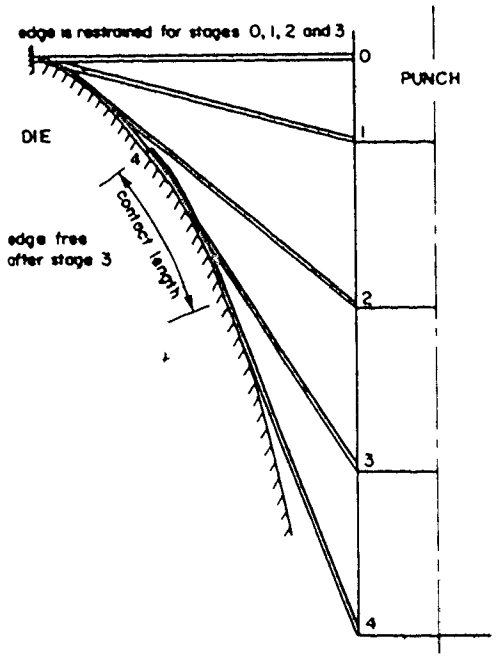

Figure 5.23 Modified tractix die

It should be noted that many die profiles could be employed and it is suggested that consideration should be given to further investigations in this area to determine the shape of an optimum drawing die.

5.7.2 Conclusions

1. The wrinkling behaviour, in the conical and tractrix die, is largely affected by the material properties and the geometry of the deformed blank.

2. The effect of the geometry, with both the conical and tractrix dies, is embodied in the buckling mode, which is primarily dependent on the pre-buckled state of deformation, i.e. stresses and strains that exist prior to buckling.

3. The limiting drawing ratio is higher with the tractrix die,

vis à vis the conical die, while at the same time the maximum punch force is smaller with the tractrix die. This leads to the conclusion that there could be an optimum die profile, and although not investigated here it warrants further study.

4. The limiting drawing ratio, with conical and tractrix dies, is substantially larger than that experienced with the conventional deep drawing dies, especially for relatively thick blanks. The implications of an increased L.D.R. have been discussed in the text in connection with the production of the drawn and ironed can.

5. The blanks wrinkle earlier in the process of deformation with conical than with tractrix dies. Accordingly the blanks are relatively more stable in the tractrix die than in the conical die.

6. More work needs to be done in trying to identify a material parameter (or parameters) that aid in preventing wrinkling. In the present experiments the materials rank according to a normalized work hardening parameter $\frac{1}{\sigma}\frac{d\sigma}{de}$ and this is consistent with the theoretical predictions of earlier chapters.

It was also found that the best material (AKDQ steel) had the highest $\bar{r}$ value. This is consistent with the theoretical predictions of Triantafyllidis and Needleman [143] and also with the experimental findings of Naziri and Pearce [101], for the conventional deep drawing process. The precise role of normal anisotropy needs further elucidation.

APPENDIX A

ERROR ANALYSIS OF PRANDTL-REUSS EQUATIONS

Since $\underline{\underline{\underline{\underline{K}}}} = 2G\ \underline{\underline{\underline{\underline{1}}}} + \lambda\ \underline{\underline{1}}\ \underline{\underline{1}}$, (A.1)

therefore the infinity norm of $\underline{\underline{\underline{\underline{K}}}}$ is given by

$$||\underline{\underline{\underline{\underline{K}}}}||_{\infty} = 3\lambda + 2G \tag{A.2}$$

where $$||K||_{\infty} = \max_{1 \leq i \leq n} \sum_{j=1}^{n} |k_{ij}| \tag{A.3}$$

The inverse of (A.1) is expressed as

$$\underline{\underline{\underline{\underline{K}}}}^{-1} = \frac{\underline{\underline{\underline{\underline{1}}}}}{2G} - \frac{\nu}{E}\ \underline{\underline{1}}\ \underline{\underline{1}}\ , \tag{A.4}$$

and

$$||\underline{\underline{\underline{\underline{K}}}}^{-1}||_{\infty} = \frac{1+2\nu}{E} \tag{A.5}$$

The condition number κ ( ) of the matrix, Bathe and Wilson [5] and Dahlquist and Bjorck [22], is

$$\kappa(\underline{\underline{\underline{\underline{K}}}}) = ||\underline{\underline{\underline{\underline{K}}}}||_{\infty}\ ||\underline{\underline{\underline{\underline{K}}}}^{-1}||_{\infty} = \frac{1+2\nu}{1-2\nu}\ , \tag{A.6}$$

$\kappa(K)$ expresses the degree of ill conditioning of the matrix.

From (2.5) $$\underline{\underline{\varepsilon}}^{P} = \underline{\underline{\underline{\underline{M}}}} : \underline{\underline{\sigma}}.$$

$$||\underline{\underline{\underline{\underline{M}}}}||_{\infty} = \frac{2m_1^2}{h} \max \{\frac{(1+x)}{(1+x)}2\}, \text{ depending on } x$$

Let $$\underline{\underline{\varepsilon}} = \underline{\underline{\underline{\underline{C}}}}_1 : \underline{\underline{\sigma}} = (\underline{\underline{\underline{\underline{K}}}}^{-1} + \underline{\underline{\underline{\underline{M}}}}) : \underline{\underline{\sigma}}\ ,$$

then $$||\underset{\sim}{\bar{C}}_1||_\infty \leq ||\underset{\sim}{\bar{K}}^{-1}||_\infty + ||\underset{\sim}{\bar{M}}||_\infty$$

or $$||\underset{\sim}{\bar{C}}_1||_\infty \leq \frac{1+2\nu}{E} + \frac{2m_1^2}{h} \max\left\{\frac{1+x}{(1+x)^2}\right\} \qquad (A.7)$$

In the above equation m_1 is the $\bar{e}_1$ component of the unit normal to the deviatoric yield surface. Now equation (2.7) can be rewritten as

$$\dot{\bar{\sigma}} = [\underset{\sim}{\bar{K}} - 2\mu G\, \bar{m}\,\bar{m}]: \bar{\varepsilon} = \underset{\sim}{\bar{C}}_1: \bar{\varepsilon}$$

$$= [\underset{\sim}{\bar{K}} - \underset{\sim}{\bar{N}}]: \bar{\varepsilon}$$

Now $$||K-N||_\infty \geq ||K||_\infty - ||N||_\infty ,$$

i.e., $$||\underset{\sim}{\bar{C}}^{-1}||_\infty \geq (3\lambda + 2G) - 2\mu G\, 2m_1^2 \max\left\{\frac{1+x}{(1+x)^2}\right\} \qquad (A.8)$$

Hence $$\kappa(\underset{\sim}{\bar{C}}_1) = ||\underset{\sim}{\bar{C}}_1||_\infty \; ||\underset{\sim}{\bar{C}}_1^{-1}||_\infty$$

$$= \left\{\frac{1+2\nu}{E} + \frac{2m_1^2}{h} \max\left[\frac{1+x}{(1+x)^2}\right]\right\} \left\{(3\lambda+2G) - 2\mu G\, 2m_1^2 \max\left[\frac{1+x}{(1+x)^2}\right]\right\} \qquad (A.9)$$

Since $1 \geq \mu \geq 0$, and $1 \geq m_1^2 \geq 0$, then for the particular case when $E >> h$, equation (A.9) would imply that $\kappa(\underset{\sim}{\bar{C}}_1)$ is in the order of E/h.

The above analysis shows that the ill conditioning of the matrix increases with plastic straining and the matrix becomes extremely ill conditioned with the tangent modulus approaching zero since the condition number in this case would tend to infinity.

APPENDIX B

INVERSION OF THE PROPOSED CONSTITUTIVE RELATIONS

I - Rigid-Plastic Solid

$$\bar{\bar{\varepsilon}} = \bar{\bar{\varepsilon}}^{p} = \frac{(\bar{\bar{m}}:\Delta\bar{\bar{\sigma}})}{h}\,\bar{\bar{m}}^{*} \tag{B.1}$$

where
$$\bar{\bar{m}} = \frac{\bar{\bar{\sigma}}'}{[\bar{\bar{\sigma}}':\bar{\bar{\sigma}}']^{1/2}} \tag{B.2}$$

and
$$\bar{\bar{m}}^{*} = \frac{\bar{\bar{\sigma}}' + \Delta\bar{\bar{\sigma}}'}{\{(\bar{\bar{\sigma}}' + \Delta\bar{\bar{\sigma}}'):(\bar{\bar{\sigma}}' + \Delta\bar{\bar{\sigma}}')\}^{1/2}} \tag{B.3}$$

Substituting into (B.1) then,

$$\bar{\bar{\varepsilon}} = \frac{(\bar{\bar{\sigma}}':\Delta\bar{\bar{\sigma}})\,(\bar{\bar{\sigma}}' + \Delta\bar{\bar{\sigma}}')}{h\{[\bar{\bar{\sigma}}':\bar{\bar{\sigma}}']^{1/2}[(\bar{\bar{\sigma}}'+\Delta\bar{\bar{\sigma}}'):(\bar{\bar{\sigma}}'+\Delta\bar{\bar{\sigma}}')]^{1/2}\}} \tag{B.4}$$

Now
$$\bar{\bar{\sigma}}':\bar{\bar{\sigma}}' = 2J_2' \,,$$

and
$$\bar{\bar{\sigma}}':\Delta\bar{\bar{\sigma}}' = \Delta\bar{\bar{\sigma}}':\bar{\bar{\sigma}}'$$

Hence (B.4) reduces to

$$\bar{\bar{\varepsilon}} = \frac{(\bar{\bar{\sigma}}':\Delta\bar{\bar{\sigma}})\,(\bar{\bar{\sigma}}'+\Delta\bar{\bar{\sigma}}')}{h[2J_2' + (\bar{\bar{\sigma}}':\Delta\bar{\bar{\sigma}}')]} \,. \tag{B.5}$$

$$\bar{\bar{\sigma}}':\bar{\bar{\varepsilon}} = \frac{(\bar{\bar{\sigma}}':\Delta\bar{\bar{\sigma}})[\bar{\bar{\sigma}}':\bar{\bar{\sigma}}' + \bar{\bar{\sigma}}':\Delta\bar{\bar{\sigma}}']}{h[2J_2' + \bar{\bar{\sigma}}':\Delta\bar{\bar{\sigma}}']} \tag{B.6}$$

i.e., $$\bar{\sigma}' : \bar{\varepsilon} = \frac{\bar{\sigma}' : \Delta\bar{\sigma}}{h}$$

Now $$\bar{\sigma}' : \Delta\bar{\sigma}' = \bar{\sigma}' : [\Delta\bar{\sigma} - \frac{1}{3} (\Delta\bar{\sigma} : \bar{1})\bar{1}]$$

$$= \bar{\sigma}' : \Delta\bar{\sigma} \qquad (B.7)$$

Combining (B.5) - (B.7) results in $\bar{\varepsilon} = \frac{1}{B} (\bar{\sigma}' + \Delta\bar{\sigma}')$, whose inverse is

$$\Delta\bar{\sigma}' = B\,\bar{\varepsilon} - \bar{\sigma}' \qquad (B.8)$$

II - Elastic-Plastic Solid

$$\bar{\varepsilon} = \bar{\varepsilon}^e + \bar{\varepsilon}^p \qquad (B.9)$$

where $\bar{\varepsilon}^e$ and $\bar{\varepsilon}^p$ are given by (2.3) and (B.1) respectively.

The constitutive equation is

$$\dot{\bar{\sigma}} = \bar{\bar{K}} : \dot{\bar{\varepsilon}}^e = \bar{\bar{K}} : (\dot{\bar{\varepsilon}} - \dot{\bar{\varepsilon}}^p) \qquad (B.10)$$

Combining (B.10) and (B.5), we get

$$\Delta\bar{\sigma} = \bar{\bar{K}} : \{\bar{\varepsilon} - \frac{(\bar{\sigma}' : \Delta\bar{\sigma})\ (\bar{\sigma}' + \Delta\bar{\sigma}')}{h[2J_2' + (\bar{\sigma}' : \Delta\bar{\sigma}')]}\} \qquad (B.11)$$

and by contracting with $\bar{\sigma}'$

$$\bar{\sigma}' : \Delta\bar{\sigma} = \bar{\sigma}' : \bar{\bar{K}} : \bar{\varepsilon} - \frac{(\bar{\sigma}' : \Delta\bar{\sigma})[\bar{\sigma}' : \bar{\bar{K}} : \bar{\sigma}' + \bar{\sigma}' : \bar{\bar{K}} : \Delta\bar{\sigma}']}{h[2J_2' + \bar{\sigma}' : \Delta\bar{\sigma}]} \qquad (B.12)$$

Since $\bar{\sigma}' : \bar{\bar{K}} : \bar{\sigma}' = 2G.2J_2'$,

$\bar{\sigma}' : \bar{\bar{K}} : \Delta\bar{\sigma}' = 2G(\bar{\sigma}' : \Delta\bar{\sigma}')$,

$\bar{\sigma}' : \Delta\bar{\sigma}' = \bar{\sigma}' : \Delta\bar{\sigma}$,

and $\Delta\bar{\sigma}' = \Delta\bar{\sigma} - \frac{1}{3}(\Delta\bar{\sigma} : \bar{1})\bar{1}$

hence (B.12) reduces to

$$\Delta\bar{\sigma} = \bar{\bar{K}} : \{\bar{\varepsilon} - L[\bar{\sigma}' + \Delta\bar{\sigma} - \frac{1}{3}(\Delta\bar{\sigma} : \bar{1})\bar{1}]\} \qquad (B.13)$$

where $$L = \frac{\delta^*(\bar{\sigma}' : \bar{\varepsilon})}{2J_2^*(1+\delta^*)} \qquad (B.14)$$

$\delta^* = 2G/h$,

and $$2J_2^* = 2J_2' + \frac{2G(\bar{\sigma}' : \bar{\varepsilon})}{1+\delta^*} \qquad (B.15)$$

To cancel $(\Delta\bar{\sigma} : \bar{1})$, obtain the scalar of (B.13) with $\bar{1}$

i.e., $$\Delta\bar{\sigma} : \bar{1} = \bar{\bar{K}} : \bar{\varepsilon} : \bar{1} - L\{\bar{\bar{K}} : \bar{\sigma}' : \bar{1} + \bar{\bar{K}} : \Delta\bar{\sigma} : \bar{1} - \frac{1}{3}\bar{\bar{K}} : \bar{1} : \bar{1}(\Delta\bar{\sigma} : \bar{1})\] \qquad (B.16)$$

Since $\overline{\overline{K}}:\overline{\sigma}':\overline{1} = 0$

$$\overline{\overline{K}}:\Delta\overline{\sigma}:\overline{1} = (2G + 3\lambda)(\Delta\overline{\sigma}:\overline{1}) ,$$

$$\overline{\overline{K}}:\overline{1}:\overline{1} = 3\ (2G + 3\lambda) ,$$

and $\overline{\overline{K}}:\overline{\varepsilon}:\overline{1} = (2G + 3\lambda)(\overline{\varepsilon}:\overline{1})$

therefore $$\Delta\overline{\sigma}:\overline{1} = (2G + 3\lambda)\ (\overline{\varepsilon}:\overline{1}) \qquad (B.17)$$

Substituting back into (B.13) yields

$$\Delta\overline{\sigma} = \overline{\overline{K}}:[\overline{\varepsilon} - L(\overline{\sigma}' + \Delta\overline{\sigma} - Q\overline{1}] \qquad (B.18)$$

where $$Q = \frac{1}{3}\ (2G + 3\lambda)(\overline{\varepsilon}:\overline{1}) \qquad (B.19)$$

or $$[\overline{\overline{1}} + L\overline{\overline{K}}]:\ \Delta\overline{\sigma} = \overline{\overline{K}}:\ [\overline{\varepsilon} - L(\overline{\sigma}' - Q\overline{1}] , \qquad (B.20)$$

therefore $$\Delta\overline{\sigma} = [\overline{\overline{1}} + L\overline{\overline{K}}]^{-1}:\ \overline{\overline{K}}:\ [\overline{\varepsilon} - L(\overline{\sigma}' - Q\overline{1})] \qquad (B.21)$$

The matrix of $[\overline{\overline{1}} + L\overline{\overline{K}}]^{-1}$ is required

where $$[\overline{\overline{1}} + L\overline{\overline{K}}] = (1 + 2GL)\ \overline{\overline{1}} + \lambda L\ \overline{1}\ \overline{1} \qquad (B.22)$$

$$= u^*\ \overline{\overline{1}} + v^*\ \overline{1}\ \overline{1} \qquad (B.23)$$

By assuming a general 4th order tensor

$$[u^*\ \overline{\overline{1}} + v^*\ \overline{1}\ \overline{1}]^{-1} = \overline{\overline{P}} = \bar{A}_r\ \bar{B}_s\ \bar{C}_t\ \bar{D}_u \qquad (B.24)$$

where $$\overline{1}\ \overline{1} = \bar{A}_i\ \bar{A}_i\ \bar{B}_j\ \bar{B}_j , \qquad (B.25)$$

and $$\overline{\overline{1}} = \bar{A}_i\ \bar{B}_j\ \bar{A}_i\ \bar{B}_j \qquad (B.26)$$

we have $$(u^{*}\overline{\overline{I}} + v^{*}\,\overline{\overline{I}}\,\overline{\overline{I}}):\overline{\overline{P}} = \overline{\overline{I}} \qquad (B.27)$$

By substituting from (B.24)-(B.26) in (B.27),

we get $$u^{*}(\overline{\overline{I}}:\overline{\overline{P}}) + v\,\overline{\overline{I}}\,\overline{\overline{I}}:\overline{\overline{P}}=\overline{\overline{I}} \qquad (B.28)$$

or $$\overline{\overline{P}} = \frac{1}{u}^{*}\,[\overline{\overline{I}} - v^{*}\,(\bar{A}_r\cdot\bar{B}_s)\,\overline{\overline{I}}\,\bar{C}_t\,\bar{D}_u] \qquad (B.29)$$

Substituting back into (B.27), results in

$$\frac{v}{u}\,\overline{\overline{I}}\,\overline{\overline{I}}\overline{\overline{I}}\,\bar{C}_t\,\bar{D}_u\,[\frac{3v^2}{u} + v](\bar{A}_r\cdot\bar{B}_s) = 0\overline{\overline{I}} \qquad (B.30)$$

Since $\frac{v}{u} \neq 0$, $3v^2 \neq uv$ and $\bar{A}_r\cdot\bar{B}_s \neq 0$,

we have $$\bar{C}_t\,\bar{D}_u = \overline{\overline{I}} \qquad (B.31)$$

and $$\bar{A}_r \cdot \bar{B}_s = 1/(3v+u). \qquad (B.32)$$

Substituting back in (B.29), the inverse is expressed as

$$\overline{\overline{P}} = \frac{1}{u}^{*}\,[\overline{\overline{I}} - \frac{v^{*}}{3v^{*}+u^{*}}\,\overline{\overline{I}}\,\overline{\overline{I}}] \qquad (B.33)$$

Substituting from (B.33), (B.24) and (B.23) in (B.21) and carrying some lengthy but ordinary manipulations we obtain

$$\Delta\overline{\overline{\sigma}} = x\,(\overline{\overline{\varepsilon}} - L\overline{\overline{\sigma}}') + y\,(\overline{\overline{\varepsilon}}:\overline{\overline{I}})\,\overline{\overline{I}} \qquad (B.34)$$

where $$x = \frac{2G}{1+2GL} \qquad (B.35)$$

$$y = \frac{1}{[1+(2G+3\lambda)L]}\,[\frac{\lambda}{1+2GL} + \frac{(2G+3\lambda)^2 L}{3}] \qquad (B.36)$$

The limiting cases that can be derived from (B.34) are

i) Elastic Solids

where $h \to \infty$, and we recover

$$\Delta\bar{\bar{\sigma}} = [2G\,\bar{\bar{\bar{\bar{I}}}} + \lambda\,\bar{\bar{I}}\,\bar{\bar{I}}]:\bar{\bar{\varepsilon}} = \bar{\bar{\bar{\bar{K}}}}:\bar{\bar{\varepsilon}}$$

ii) Rigid Plastic Solids

where $2G \to \infty$, and we recover (B-8).

APPENDIX C

CONVENTIONAL DEEP DRAWING

I - Elastic Solution of Problem Solved By Rozsa

1. One term solution, i.e., $a_1 \neq 0$, $a_i = 0$, $i = 2,3.....$

$$\frac{t\sigma_o}{D} = \frac{C_1+C_2n^2+C_3n^4}{C_4+C_5n^2} \qquad (C.1)$$

where D is the flexural rigidity

$$C_1 = -32\,R_1^6 + \frac{128}{3}R_1^4 - \frac{64}{3}R_1^2 + \frac{32}{3}$$

$$C_2 = \frac{2}{3}R_1^6 + 20\,R_1^2 - 16\ln R_1 + \frac{2}{3R_1^2} - \frac{44}{3} - \frac{20}{3}R_1^4$$

$$C_3 = -\frac{R_1^6}{6} + R_1^4 - 3\,R_1^2 + 4\ln R_1 + \frac{1}{2R_1^2} + \frac{10}{6} \qquad (C.2)$$

$$C_4 = \frac{1}{3(1-R_1^2)}\left[2\,R_1^8 - 8\,R_1^6 + 12\,R_1^4 - 8\,R_1^2 + 2\right]$$

$$C_5 = \frac{1}{1-R_1^2}\left[\frac{-7}{24}R_1^8 + \frac{5}{3}R_1^6 - \frac{9}{2}R_1^4 + \frac{11}{3}R_1^2 - \ln R_1 + 4\,R_1^2\ln R_1 - \frac{13}{24}\right]$$

2. Two term solution, i.e. a_1 and $a_2 \neq 0$, $a_i = 0$, $i = 3,4$ ....

For the case n=0, the buckling condition can be written as

$$k = \frac{t\sigma_o}{D} = \frac{C_1a_1^2+C_2a_2^2+C_3a_1a_2}{C_4a_1^2+C_5a_2^2+C_6a_1a_2} \qquad (C.3)$$

The minimization procedure with respect to a_1 and a_2 leads

$$\begin{vmatrix} (2C_1 - 2k\,C_4) & (C_3 - k\,C_6) \\ (C_3 - k\,C_6) & (2C_2 - 2k\,C_5) \end{vmatrix} \begin{Bmatrix} a_1 \\ a_2 \end{Bmatrix} = 0 \qquad (C.4)$$

a_1 and $a_2 \neq 0$

For the non homogeneous solution, the determinant of

$$\begin{vmatrix} (2C_1 - 2k\,C_4) & (C_3 - k\,C_6) \\ (C_3 - k\,C_6) & (2C_2 - 2k\,C_5) \end{vmatrix} = 0 \qquad (C.5)$$

The solution of (C.5) gives the minimum condition for

$k = \frac{h\sigma_o}{D}$, with respect to a_1 and a_2. The quantities in (C.5) are defined as below.

$$C_1 = -2R_1^6 + \frac{8}{3}R_1^4 - \frac{4}{3}R_1^2 + \frac{2}{3}$$

$$C_2 = -\frac{33}{5}R_1^{10} + 14\,R_1^8 - 10\,R_1^6 + \frac{8}{3}R_1^4 - \frac{1}{3}R_1^2 + \frac{4}{15}$$

$$C_3 = -7\,R_1^8 + 12\,R_1^6 - \frac{20}{3}R_1^4 + \frac{4}{3}R_1^2 + \frac{1}{3} \qquad (C.6)$$

$$C_4 = \frac{1}{24(1-R_1^2)}\left[R_1^8 - 4\,R_1^6 + 6\,R_1^4 - 4\,R_1^2 + 1\right]$$

$$C_5 = \frac{1}{4(1-R_1^2)}\left[\frac{3}{20}R_1^{12} - \frac{3}{5}R_1^{10} + \frac{11}{12}R_1^8 - \frac{2}{3}R_1^6 + \frac{R_1^4}{4} - \frac{1}{15}R_1^2 + \frac{1}{60}\right]$$

$$C_6 = \frac{1}{4(1-R_1^2)}\left[\frac{3}{10}R_1^{10} - \frac{7}{6}R_1^8 + \frac{5}{3}R_1^6 - R_1^4 + \frac{1}{6}R_1^2 + \frac{1}{30}\right]$$

II - Buckling Criterion for Elastic-Plastic Solids

(Classical Approach)

$$t^{*2} = \frac{8}{3R^2}\frac{\bar{\sigma}}{E}\frac{[C_4+C_5 n^2]}{[C_1+C_2 n^2+C_3 n^4]} \qquad (C.7)$$

where $C_1 = b_1 (1-\frac{\mu}{3}) + d_1 (1+\mu)$

$C_2 = b_2 (1-\frac{\mu}{3}) + d_2 (1+\mu) + e$

$C_3 = b_3 (1-\mu/3)$

$b_1 = \frac{80}{3} R^6 - 32 R^4 + 16 R^2 - \frac{32}{3}$

$b_2 = -\frac{4}{3} R^6 + 6 R^4 - 12 R^2 + 8 \ln R + \frac{22}{3}$ (C.8)

$b_3 = \frac{R^6}{6} - R^4 + 3R^2 - 4 \ln R - \frac{1}{2R^2} - \frac{5}{3}$

$d_1 = 8(2 R^6 - 4 R^4 + 2 R^2)$

$d_2 = 8(\frac{-R^6}{2} + \frac{7}{4} R^4 - \frac{5}{2} R^2 + \ln R + \frac{5}{4})$

$e = \frac{4}{3}(\frac{3}{2} R^6 - 3R^4 - R^2 + 4 \ln R - \frac{1}{2R^2} + 3)$

$C_4 = -\frac{1}{4} R^8 + \frac{8}{9} R^6 - R^4 + \frac{2}{3} \ln R + \frac{13}{36}$

$C_5 = \frac{7}{64} R^8 - \frac{5}{9} R^6 + \frac{9}{8} R^4 - R^2 - \frac{1}{24} \ln R - \frac{1}{2} \ln^2 R + \frac{185}{576}$

III - Buckling Criterion for Rigid-Plastic Solids

1. Kulkarni's approach. (equation 3.25)

$$t^{*2} = \frac{\sigma^*}{R^2}\,\frac{(3n+2\nu-1)^2}{(n-1)}\left[\frac{C_4+C_5\,n^2}{C_1+C_2 n^2+C_3 n^4}\right] \qquad (C.9)$$

where $C_1 = \frac{32}{3}(R^6-1)$

$$C_2 = 8\left(\frac{R^6}{3} - R^4 + R^2 - \frac{1}{3}\right) \qquad (C.10)$$

$$C_3 = \frac{R^6}{6} - R^4 + 3R^2 - 4\ln R - \frac{1}{2R^2} - \frac{5}{3}$$

C_4 and C_5 are given by equations (C.8).

2. Full expression (equation 2.47)

$$t^{*2} = 3\,\frac{\sigma^*}{R^2}\left[\frac{C_4 + C_5\,n^2}{F_1 + F_2\,n^2 + F_3\,n^4}\right] \qquad (C.11)$$

where $\sigma^* = \bar{\sigma}/E$

$$F_1 = 2C_1 + \frac{32}{9}\sigma^*\left[-R^6 + 6\ln R + 1\right] \qquad (C.12)$$

$$F_2 = 2C_2 + 2\sigma^*\left[\frac{-R^6}{9} + 3R^4 - 6R^2 - \frac{1}{R^2}\right.$$

$$\left. - 9\ln^2 R - \frac{4}{3}\ln R + \frac{37}{9}\right]$$

$$F_3 = 2C_3 + 2\sigma^*\left[\frac{5}{36}R^6 - \frac{3}{4}R^4 + \frac{3}{2}R^2\right.$$

$$+ 2 \ln {}^{2}R - \frac{7}{3} \ln R - \frac{3}{4R^2} - \frac{5}{36}]$$

C_1, C_2 and C_3 are given by equations (C.10) and C_4 and C_5 are given by equations (C.8)

$$Z = \frac{3(n-1)}{(3n+2\nu-1)^2} \quad , \tag{C.13}$$

and Poissons ratio, ν, is taken as 1/3.

IV - Modified Elastic-Plastic Analysis with Stretching and Bending Included

$$E_1 = \int\{2(h-\sigma_{11}-\sigma_{22})(\epsilon_{11}^{o2} + \epsilon_{12}^{o2})$$

$$-\bar{\sigma}\left[\left(\frac{u^*,\theta}{r}\right)^2+\left(\frac{v^*,\theta}{r}\right)^2+\ln\frac{r}{R_o}\left((u^*,r)^2+(v^*,r)^2+\left(\frac{u^*,\theta}{r}\right)^2+\left(\frac{v^*,\theta}{r}\right)^2\right)\right]\}dS \tag{C.14a}$$

$$E_2 = n^2\{R^{2n}D_6+R^{-2n}D_7-2 \ln R + D_9\} \tag{C.14b}$$

$$E_3 = n^2\{R^{2n}D_1+R^{-2n}D_2 - R^2D_3-2R^2 \ln R\, D_4\} \tag{C.14c}$$

$$D_1 = \frac{1}{2(n-1)^2}\{16(n-1)^3h^*+(14n^3-60n^2+ 78n - 31)\} \tag{C.14d}$$

$$D_2 = \frac{-1}{2(n+1)^2}\{16(n+1)^3 h^*+(14n^3+60n^2+78 n + 31)\} \tag{C.14e}$$

$$D_3 = \frac{1}{(n^2-1)^2}\{(2 n^2+2) -32(n^2-1)^2(h^*+2)\} \tag{C.14f}$$

$$D_4 = \frac{16\ n^2-15}{n^2-1} \qquad (C.14g)$$

$$D_6 = \frac{n-1}{2n^2} \qquad (C.14h)$$

$$D_7 = \frac{-(n+1)}{2n^2} \qquad (C.14i)$$

$$D_9 = \frac{1}{n^2} \qquad (C.14j)$$

$$h^* = h/\bar{\sigma} \qquad (C.14k)$$

u^*,θ etc. $\equiv \partial u^*/\partial\theta$

In (C.14a) σ_{11} and σ_{22} are of opposite sign, however the sign is negative for R=1.1 - 1.6 and positive only in a small region near the inner edge for r=1.7 and 1.8. The first integral is therefore always positive definite. On the other hand ϵ_{ij}^{02} is in the order of $v_i,_j^2$ and h is always larger than $\bar{\sigma}$. Accordingly the result of (C.14a) will be positive definite.

V - Proposed Rigid-Plastic Constitutive Equations

$$D_1 = 16\left[\frac{5}{3}R^6 - 2R^4 + R^2 - \frac{2}{3}\right]$$

$$D_2 = \frac{5}{3}R^6 - 14R^2 + 16\ln R - \frac{1}{R^2} + \frac{40}{3}$$

$$D_3 = \frac{R^6}{6} - R^4 + 3R^2 - 4\ln R - \frac{1}{2R^2} - \frac{5}{3}$$

$$E_1 = -\frac{32}{9}R^6 + \frac{64}{3}\ln R + \frac{32}{9}$$

$$E_2 = -\frac{2}{9}R^6 + 6R^4 - 12R^2 - \frac{2}{R^2} - 16\ln^2 R - \frac{8}{3}\ln R + \frac{74}{9}$$

$$E_3 = \frac{5}{18}R^6 - \frac{3}{2}R^4 + 3R^2 + 4\ln^2 R - \frac{14}{3}\ln R - \frac{3}{2R^2} - \frac{5}{18}$$

$$C_4 = -\frac{R^8}{4} + \frac{8R^6}{9} - R^4 + \frac{2}{3}\ln R + \frac{13}{36}$$

$$C_5 = \frac{7}{64}R^8 - \frac{5}{9}R^6 + \frac{9}{8}R^4 - R^2 - \frac{1}{24}\ln R - \frac{1}{2}\ln^2 R + \frac{185}{576}$$

APPENDIX D

CONICAL DIE

I - Strain Rates and Change in Curvature

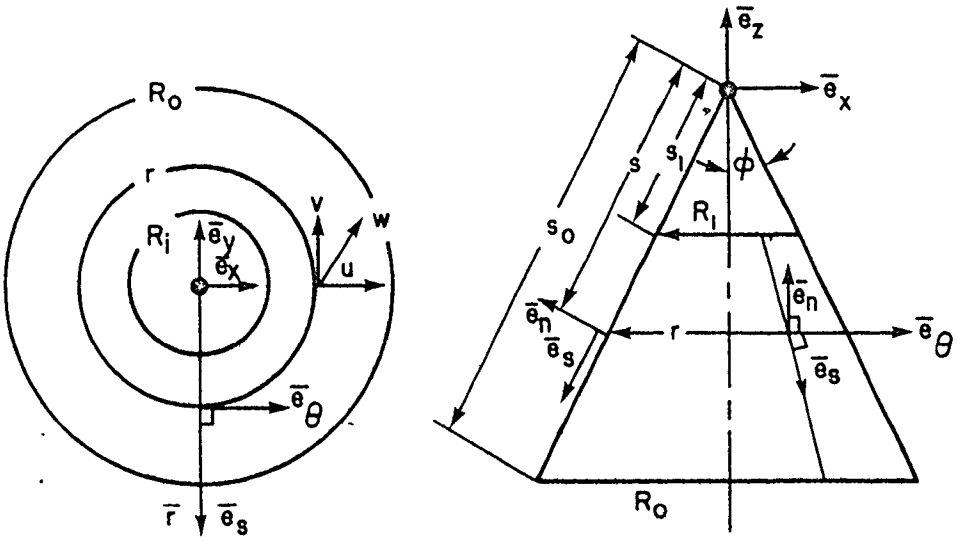

Figure D.1 - Coordinate System

$\bar{e}_x$, $\bar{e}_y$ and $\bar{e}_z$ is the unit orthogonal cartesian reference set (R.H.). $\bar{e}_s$, $\bar{e}_\phi$ and $\bar{e}_n$ form a right hand (R.H.) orthonormal set that is defined in terms of $\bar{e}_x$, $\bar{e}_y$ and $\bar{e}_z$

$$\bar{r} = r \cos\theta\, \bar{e}_x + r \sin\theta\, \bar{e}_y - s \cos\phi\, \bar{e}_z \qquad (D.1)$$

where $r = s \sin\phi$

Base Vectors

$$\bar{g}_s = \frac{\partial \bar{r}}{\partial s} = \sin\phi \cos\theta\, \bar{e}_x + \sin\phi \sin\theta\, \bar{e}_y - \cos\phi\, \bar{e}_z$$

$$g_{ss} = \sqrt{\bar{g}_s \cdot \bar{g}_s} = 1$$

Since $$\bar{e}_i = \frac{\bar{g}_i}{g_{ii}}$$

therefore $$\bar{e}_s = \bar{g}_s \qquad (D.2)$$

$$\bar{g}_\theta = \frac{\partial \bar{r}}{\partial \theta} = - s \sin \phi \sin \theta \, \bar{e}_x + s \sin \phi \cos \theta \, \bar{e}_y$$

$$g_{\theta\theta} = \sqrt{\bar{g}_\theta \cdot \bar{g}_\theta} = r = s \sin \phi$$

$$\bar{e}_\theta = \frac{\bar{g}_\theta}{g_{\theta\theta}} = - \sin \theta \, \bar{e}_x + \cos \theta \, \bar{e}_y \qquad (D.3)$$

$$\bar{e}_n = \bar{e}_s \times \bar{e}_\theta$$

$$= \cos \phi \cos \theta \, \bar{e}_x + \cos \phi \sin \theta \, \bar{e}_y + \sin \phi \, \bar{e}_z \qquad (D.4)$$

The 3 base vectors form a R.H. orthonormal set.

Along a parametric curve s_i, we have

$$d\bar{r}_i = d\alpha_i \frac{\partial \bar{r}}{\partial \alpha_i} = d\alpha_i \, \bar{g}_i$$

squaring $$d\bar{r} \cdot d\bar{r} = (d\alpha_i)^2 (\bar{g}_i \cdot \bar{g}_i)$$

or $$ds_i = d\alpha_i \, g_{ii}$$

$$\frac{\partial}{\partial s_1} = \frac{\partial}{\partial s} \tag{D.5}$$

$$\frac{\partial}{\partial s_2} = \frac{1}{r}\frac{\partial}{\partial \theta} = \frac{1}{s \sin \phi}\frac{\partial}{\partial \theta} \tag{D.6}$$

Curvatures

For parametric line s (θ = constant)

(i) Twist $K_1^{(+)} = -K_{12}$, "rotation about $\bar{e}_s$"

$$K_1^{(+)} = -\bar{e}_\phi \cdot \frac{\partial \bar{e}_n}{\partial s} = 0$$

(ii) Normal curvature $K_1^{(n)} = K_{11}$, "rotation about $\bar{e}_\theta$"

$$K_1^{(n)} = \bar{e}_1 \cdot \frac{\partial \bar{e}_n}{\partial s_1} = 0$$

(iii) Geodesic curvature $K_1^{(g)} = K_{13}$, "rotation about $\bar{e}_n$"

$$K_1^{(g)} = \bar{e}_\phi \cdot \frac{\partial \bar{e}_s}{\partial s_1} = 0$$

For parametric line θ (s = constant)

(i) Twist $K_2^{(+)}$

$$K_{21} = K_2^{(+)} = \bar{e}_s \cdot \frac{1}{r}\frac{\partial \bar{e}_n}{\partial \theta} = 0$$

(ii) Normal curvature $K_2^{(n)} = -K_{22}$

$$K_2^{(n)} = -\bar{e}_\phi \cdot \frac{\partial \bar{e}_n}{\partial s_2} = -\frac{1}{r}\cos\phi$$

(iii) Geodesic curvature $K_2^{(g)} \equiv K_{23}$

$$K_2^{(g)} = - \bar{e}_s \cdot \frac{\partial \bar{e}_\theta}{\partial s_2} = \frac{1}{r} \sin \phi$$

The components of the curvature tensor are therefore given by

$$K_{ij} = \frac{1}{r} \begin{matrix} 0 & 0 & 0 \\ 0 & \cos \phi & \sin \phi \end{matrix} \qquad (D.7)$$

Change of Curvature Tensor

$$k_{11} = - \frac{\partial \phi_{13}}{\partial s_1} + K_{12} \phi_{12} + K_{13} \phi_{23}$$

$$k_{12} = - \frac{\partial \phi_{23}}{\partial s_1} - K_{11} \phi_{12} - K_{13} \phi_{13}$$

$$k_{13} = \frac{\partial \phi_{12}}{\partial s_1} - K_{11} \phi_{23} + K_{12} \phi_{13} \qquad (D.8)$$

$$k_{21} = - \frac{\partial \phi_{13}}{\partial s_2} - K_{22} \phi_{21} + K_{23} \phi_{23}$$

$$k_{22} = - \frac{\partial \phi_{23}}{\partial s_2} + K_{21} \phi_{21} - K_{23} \phi_{13}$$

$$k_{23} = - \frac{\partial \phi_{21}}{\partial s_2} - K_{21} \phi_{23} + K_{22} \phi_{13}$$

where

$$\phi_{11} = \frac{\partial u^o}{\partial s_1} - v^o K_{13} + w K_{11}$$

$$\phi_{12} = \frac{\partial v^o}{\partial s_1} + u^o K_{13} + wK_{12}$$

$$\phi_{13} = \frac{\partial w}{\partial s_1} - u^o K_{11} - v^o K_{12} \qquad (D.9)$$

$$\phi_{21} = \frac{\partial u^o}{\partial s_2} - v^o K_{23} + wK_{21}$$

$$\phi_{22} = \frac{\partial v^o}{\partial s_2} + u^o K_{23} + wK_{22}$$

$$\phi_{23} = \frac{\partial w}{\partial s_2} - u^o K_{21} - v^o K_{22}$$

Substituting from (D.7) and (D.9) into (D.8), we have

$$k_{11} = -\frac{\partial^2 w}{\partial s^2}$$

$$k_{12} = \frac{-1}{s \sin \phi}\left[-\frac{1}{s}\frac{\partial w}{\partial \theta} + \frac{\partial^2 w}{\partial s \partial \theta} + \frac{v^o}{s}\cos\phi\right]$$

$$k_{21} = -\frac{1}{s \sin \phi}\frac{\partial^2 w}{\partial s \partial \theta} - \frac{\cos \phi}{(s \sin \phi)^2}\frac{\partial u^o}{\partial \theta} + \frac{1}{s^2 \sin \phi}\frac{\partial w}{\partial \theta}$$

$$k_{22} = -\frac{1}{(s \sin \phi)^2}\frac{\partial^2 w}{\partial \theta^2} - \frac{1}{s}\frac{\partial w}{\partial s} + \frac{\cos \phi}{(s \sin \phi)^2}\frac{\partial v^o}{\partial \theta}$$

For the special case when u^o and $v^o << w$

$$k_{11} = -\frac{\partial^2 w}{\partial s^2}$$

$$k_{12} = k_{21} = \frac{-1}{s \sin \phi}\left(\frac{\partial^2 w}{\partial s \partial \theta} - \frac{1}{s}\frac{\partial w}{\partial \theta}\right) \qquad (D.10)$$

$$k_{22} = \frac{-1}{(s \sin \phi)^2} \frac{\partial^2 w}{\partial \theta^2} - \frac{1}{s} \frac{\partial w}{\partial s}$$

Strain Rate Tensor

$$\epsilon_{11}^{o} = \frac{\partial u^o}{\partial s}$$

$$\epsilon_{22}^{o} = \frac{\partial v^o}{\partial s_2} + \frac{u^o}{s} + \frac{w}{r} \cos \phi \qquad (D.11)$$

$$\epsilon_{12}^{o} = \frac{1}{2} \left(\frac{\partial v^o}{\partial s} + \frac{1}{s \sin \phi} \frac{\partial u^o}{\partial \theta} - \frac{v^o}{s} \right)$$

for the special case when u^o and $v^o \ll w$

$$\epsilon_{11}^{o} = 0 = \epsilon_{12}^{o}$$

$$\epsilon_{22}^{o} = \frac{w}{r} \cos \phi \qquad (D.12)$$

II - Proposed Rigid-Plastic Constitutive Equations

$$E_1 = -\frac{3}{8} L^8 + \frac{4}{3} L^6 - \frac{3}{2} L^4 + \frac{13}{24} + \ln L$$

$$E_2 = \frac{7}{32} L^8 - \frac{10}{9} L^6 + \frac{9}{4} L^4 - 2L^2 - \frac{1}{12} \ln L - \ln^2 L + \frac{185}{288}$$

$$K_i = 4(h^* X_i + Y_i)$$

$$X_1 = 2\left[\frac{L^6}{6} - L^4 + 3L^2 - 4 \ln L - \frac{1}{2L^2} - \frac{5}{3}\right]$$

$$Y_1 = 4\left[\frac{5}{36} L^6 - \frac{3}{4} L^4 + \frac{3}{2} L^2 - \frac{7}{3} \ln L + 2 \ln^2 L - \frac{3}{4L^2} - \frac{5}{36}\right]$$

$$X_2 = \frac{5}{6} L^6 - 7L^2 + 8 \ln L - \frac{1}{2L^2} + \frac{20}{3}$$

$$Y_2 = - \frac{L^6}{9} + 3L^4 - 6L^2 - \frac{4}{3} \ln L - 8 \ln {}^2L - \frac{1}{L^2} + \frac{37}{9}$$

$$X_3 = 10L^6 - 12L^4 + 6L^2 - 4$$

$$Y_3 = - \frac{4}{3} L^6 + \frac{4}{3} + 8 \ln L$$

BIBLIOGRAPHY

1. J.M. Alexander, "An Appraisal of the Theory of Deep Drawing", Met. Reviews, 1960, vol. 5, pp. 349-511.

2. W.A. Bakofen, "Deformation Processing", 1972, Addison-Wesley Pub. Comp., Reading, Mass.

3. W.N. Baldwin and T.S. Howald, "Folding in the Cupping Operation", Trans. A.S.M., 1947, vol. 38, pp. 757-788.

4. S.B. Batdorf, "Theories of Plastic Buckling", J. Aero. Sci., 1949, vol. 16, pp. 405-408.

5. K.J. Bathe and E.L. Wilson, "Numerical Methods in Finite Element Analysis", 1976, Prentice-Hall.

6. Z.P. Bazant, "A Correlation Study of Formulations of Incremental Deformation and Stability of Continuous Bodies", J. Appl. Mech., 1971, pp. 919-927.

7. O. Bruhns and K. Thermann, "Note on a Paper by R.N. Dubey and S.T. Ariaratnam", Int. J. Engng. Sci., 1975, vol. 13, pp. 117-119.

8. D.O. Brush and B.O. Almroth, "Buckling of Bars, Plates and Shells", 1975, McGraw Hill, N.Y..

9. B. Budiansky, "A Reassessment of Deformation Theories of Plasticity", J. Appl. Mech., 1959, vol. 26, pp. 259-264.

10. B. Budiansky, "Remarks on Theories of Solid and Structural Mechanics", In Problems of Hydrodynamics and Continuum Mechanics, SIAM, 1969, pp. 77-83.

11. B. Budiansky, "Theory of Buckling and Postbuckling Behavior of Elastic Structures", Advances in Appl. Mech., 1974, vol. 14, pp. 2-65.

12. B. Budiansky and N.M. Wang, "On the Swift Cup Test", J. Mech. Phys. Solids, 1966, vol. 14, pp. 357-374.

13. B. Budiansky and J.W. Hutchison, "Buckling: Progress and Challenge", In Trends in Solid Mechanics, 1979, pp. 93-116.

14. J. Chakrabarty, "Bifurcation Phenomenon and the Rate-Problem in Plasticity", Int. J. Mech. Sci., 1969, vol. 11, pp. 659-666.

15. J. Chakrabarty, "On the Problem of Uniqueness under Pressure Loading", ZAMP, 1969, vol. 20, pp. 696-706.

16. J. Chakrabarty, "On Uniqueness and Stability in Rigid-Plastic Solids", Int. J. Mech. Sci., 1969, vol. 11, pp. 723-731.

17. W.H. Chen, "Necking of a Bar", Int. J. Solids Structures, 1971, vol. 7, pp. 685-717.

18. D.C. Chiang and S. Kobayashi, "The Effect of Anisotropic Characteristics on the Stresses and the Strains in Deep Drawing", Trans. ASME, J. Eng. for Ind., 1966, vol. 88, pp. 443-448.

19. C.C. Chu, "Bifurcation of Elastic-Plastic Circular Cylindrical Shells Under Internal Pressure", J. Appl. Mech., 1979, vol. 46, pp. 889-894.

20. S.Y. Chung and H.W. Swift, "Cup Drawing from a Flat Circular Blank", Proc. Inst. M. Eng., 1951, vol. 165, pp. 199-228.

21. G.R. Cowper and E.T. Onat, "The Initiation of Necking and Buckling in Plane Plastic Flow", Proc. 4th U.S. Nat. Congr. Appl. Mech., 1962, pp. 1023-1029.

22. G. Dahlquist and A. Bjorck, "Numerical Methods", 1974, Prentice Hall.

23. R.N. Dubey, "Instabilities in Thin Elastic-Plastic Tubes", Int. J. Solids Structures, 1969, vol. 5, pp. 699-711.

24. R.N. Dubey, "On Objective Stress-Rate in the Constitutive Relation for Elastic-Plastic Solids", 1972, Int. Symp. on Foundations of Plasticity, Ed. A. Sawczuk, vol. 1, pp. 382-385.

25. R.N. Dubey, "Shear Modulus During Elastic-Plastic Deformation", Mech. Res. Comm., 1975, vol. 2, pp. 205-208.

26. R.N. Dubey, "Thick-Body Bifurcations of Elastic and Elastic/Plastic Solids in Plane Strain: A Correlation Study Using Principal Axes Technique", 1975, Solid Mechanics Division, Univ. of Waterloo Press, Waterloo, Ont.

27. R.N. Dubey, "Incremental Theory of Plasticity: A New Approach", Mech. Res. Comm., 1977, vol. 4, pp. 35-39.

28. R.N. Dubey, "Incremental Theory of Plasticity: Some Observations", Ibid., 1977, vol. 4, pp. 75-77.

29. R.N. Dubey, "On Bifurcation in Elastic-Plastic Solids", Nuclear Engng. and Design, 1978, vol. 49, pp. 217-222.

30. R.N. Dubey, "Bifurcation in Elastic-Plastic Plates", Trans. CSME, to appear.

31. R.N. Dubey and S.T. Ariaratnam, "Necking Instabilities in Elastic-Plastic Plates", Int. J. Engng. Sci., 1972, vol. 10, pp. 145-154.

32. R.N. Dubey and Z. Mroz, "On the Relation Between Stress and Strain Rates for Elastic-Plastic Solids", Archieves of Mechanics, 1973, vol. 25, pp. 383-388.

33. R.N. Dubey and N.C. Lind, "Re-Assessment of the Incremental Elastic-Plastic Constitutive Relation", Mech. Res. Comm., 1976, vol. 3, pp. 411-415.

34. R.N. Dubey and M.J. Pindera, "Effect of Rotation of Principal Axes on Effective Shear Modulus in Elastic-Plastic Solids", J. Struct. Mech., 1977, vol. 5, pp. 77-85.

35. J. Duncan and W. Johnson, "Approximate Analyses of Loads in Axi-symmetric Deep Drawing", 9th Int. MTDR Conf., Pergamon Press, 1969, pp. 303-318.

36. A. Elkholy, "Bifurcation Analysis of Elastic-Plastic Solids using the Principal Axes Technique", Ph.D. Dissertation, Dept. of Mech. Eng., Univ. of Waterloo, 1978, Waterloo, Ontario.

37. M. Feigen, "Inelastic Behavior under Combined Tension and Torsion", Proc. 2nd U.S. Nat. Congr. Appl. Mech., 1954, pp. 469-476.

38. S. Fukui, H. Yuri and K. Yoshida, "Analysis of Deep Drawing of Cylindrical Shell Based on Total Strain Theory and Some Formability Tests", Aero. Res. Inst., Report No. 332, 1958, University of Tokyo, Japan.

39. G.W. Geckeler, "Plastic Folding of Walls of Hollow Cylinders and other Folding Phenomena" (In German), ZAMM, 1928, vol. 8, pp. 341-352.

40. G. Gerard, "Secant Modulus Method for Determining Plate Instability Above the Proportional Limit", J. Aero. Sci., Jan. 1946, pp. 38-44.

41. A.E. Green and W. Zerna, "Theoretical Elasticity", 1968, Oxford Univ. Press., Oxford.

42. J. Havranek, "The Effect of Mechanical Properties of Sheet Steels on the Wrinkling Behavior During Deep-Drawing of Conical Shells", Proc. of the 9th I.D.D. R.G., 1976, pp. 245-263.

43. H.D. Hibbitt, P.V. Marcal and J.C. Rice, "A Finite Element Formulation for Problems of Large Strain and Large Displacement", Int. J. Solids Structures, 1970, vol. 10, pp. 1069-1086.

44. R. Hill, "Mathematical Theory of Plasticity", 1956, Corr. Reprint, 1st Ed., Oxford Univ. Press.

45. R. Hill, "On the Problem of Uniqueness in the Theory of a Rigid-Plastic Solid - I", J. Mech. Phys. Solids, 1956, vol. 4, pp. 247-255.

46. R. Hill, "New Horizons in the Mechanics of Solids", Ibid., 1956, vol. 5, pp. 66-74.

47. R. Hill, "On the Problem of Uniqueness in the Theory of a Rigid-Plastic Solid - III", Ibid., 1957, vol. 5, pp. 153-161.

48. R. Hill, "On Uniqueness and Stability in the Theory of Finite Elastic Strain", Ibid., 1957, vol. 5, pp. 229-241.

49. R. Hill, "A General Theory of Uniqueness and Stability in Elastic-Plastic Solids", Ibid., 1958, vol. 6, pp. 236-249.

50. R. Hill, "Some Basic Principles in the Mechanics of Solids Without a Natural Time", Ibid., 1959, vol. 7, pp. 209-225.

51. R. Hill, "Uniqueness in General Boundary-Value Problems for Elastic and Inelastic Solids", Ibid., 1961, vol. 9, pp. 114-130.

52. R. Hill, "Bifurcation and Uniqueness in Non-Linear Mechanics of Continua", Muskhelishvili vol., SIAM, Philadelphia, 1961, pp. 155-164.

53. R. Hill, "Uniqueness Criteria and Extremum Principles in Self-Adjoint Problems of Continuum Mechanics", J. Mech. Phys. Solids, 1962, vol. 10, pp. 185-194.

54. R. Hill, "The Essential Structure of Constitutive Laws for Metal Composites and Polycrystals", Ibid., 1967, vol. 15, pp. 79-95.

55. R. Hill, "Eigenmodal Deformations in Elastic/Plastic Continua", Ibid., 1967, vol. 15, pp. 371-386.

56. R. Hill, "On the Classical Constitutive Relations for Elastic-Plastic Solids", In Recent Progress in Appl. Mech., The Folke Odqvist Volume, 1967, pp. 241-249.

57. R. Hill, "On Constitutive Inequalities for Simple Materials - I", J. Mech. Phys. Solids, 1968, vol. 16, pp. 229-242.

58. R. Hill, "Constitutive Inequalities for Isotropic Elastic Solids Under Finite Strain", Proc. Roy. Soc. Lond., 1970, A314, pp. 457-472.

59. R. Hill, "Aspects of Invariance in Solid Mechanics", Advances in Appl. Mech., 1978, vol. 18, pp. 1-75.

60. R. Hill and M.J. Sewell, "A General Theory of Inelastic Column Failure - I and II", J. Mech. Phys. Solids, 1960, vol. 8, pp. 105-111 and 112-118.

61. N. Hoff, "Buckling and Stability", J. Roy. Aero Soc., 1954, vol. 58, pp. 3-52.

62. J.W. Hutchison, "Elastic-Plastic Behaviour of Polycrystalline Metals and Composites", Proc. Roy. Soc. Lond., 1970, A319, 247-272.

63. J.W. Hutchison, "Finite Strain Analysis of Elastic-Plastic Solids and Structures", In Numerical Solutions of Non-linear Structural Problems, Ed. R.F. Hartung, ASME, 1973, AMD - vol. 6, pp. 17-29.

64. J.W. Hutchison, "Imperfection Sensitivity in the Plastic Range", J. Mech. Phys. Solids, 1973, vol. 21, pp. 191-204.

65. J.W. Hutchison, "Plastic Buckling", Advances in Appl. Mech., 1974, vol. 14, pp. 67-144.

66. J.W. Hutchison and K.W. Neale, "Sheet Necking - II: Time-Independent Behavior", Division of Applied Sciences, 1977, DAS M-4, Harvard Univ., Cambridge, Mass.

67. W. Johnson and B.W. Mellor, "Engineering Plasticity", 1962, Van Nostrand, Princeton, N.J.

68. M. Karima, P.C. Chakravarti and R. Sowerby, "Some Theoretical Fundamentals in Bifurcation Analysis", Manufacturing Research and Design Group, Report No. 142, 1979, McMaster University, Hamilton, Ont.

69. M. Karima and R. Sowerby, "A Bifurcation Approach to the Study of Wrinkling During Deep Drawing", Manufacturing Research and Design Group, Report No. 144, 1980, McMaster University, Hamilton, Ont.

70. N. Kawai, "Critical Conditions of Wrinkling in Deep-Drawing of Sheet Metals", Bulletin of JSME, 1961, vol. 4, pp. 169-192.

71. S. Keeler, "Huygen Tractrix Deep Drawing Dies", Machinery, Dec. 1969, pp. 141-142.

72. W.T. Koiter, "Stress-Strain Relations, Uniqueness and Variational Theorems for Elastic-Plastic Materials with a Singular Yield Surface", Quart. Appl. Math., 1953, vol. 11, pp. 350-354.

73. A.K. Kulkarni, "Sheet Wrinkling in Metal Forming Operations", Ph.D. Dissertation, Dept. of Civil Eng., University of Waterloo, 1971, Waterloo, Ont.

74. A. Kumar, "Uniqueness of Plane Strain Deformation of Rigid-Plastic Solids under Lateral Pressure", J. Appl. Mech., 1979, vol. 46, pp. 959-961.

75. H.L. Langhaar, "Energy Methods in Applied Mechanics", 1962, John Wiley and Sons.

76. E.H. Lee, "Elastic-Plastic Deformation at Finite Strains", J. Appl. Mech., 1969, vol. 36, pp. 1-6.

77. E.H. Lee, R.L. Mallett and W.H. Yang, "Stress and Deformation Analysis of the Metal Extrusion Process", Comp. Meth. Appl. Mech. Eng., 1977, vol. 10, pp. 339-353.

78. D. Leigh, "Nonlinear Continuum Mechanics", 1968, McGraw Hill Book Company, N.Y..

79. T.H. Lin, "Physical Theory of Plasticity", Advances in Appl. Mech., 1971, vol. 11, pp. 255-311.

80. L.E. Malvern, "Introduction to the Mechanics of Continuous Medium", 1969, Prentice-Hall.

81. J. Mandel, "Généralisation de la Théorie de Plasticité de W.T. Koiter", Int. J. Solids Structures, 1965, vol. 1, pp. 273-295.

82. J.B. Martin, "Plasticity: Fundamentals and General Results", 1975, The MIT Press, Cambridge, Mass..

83. E.F. Masur, "On the Definition of Stress Rate", Quart. Appl. Math., 1961, vol. 19, pp. 160-163.

84. O. May, German Patent No. 658898, 1938.

85. R.M. McMeeking and J.R. Rice, "Finite-Element Formulations for Problems of Large Elastic-Plastic Deformation", Int. J. Solids Structures, 1975, vol. 11, pp. 601-616.

86. M. Michno and W. Findley, "A Historical Perspective of Yield Surface Investigations for Metals", Int. J. Non-Linear Mech., 1976, vol. 11, pp. 59-82.

87. J.P. Miles, "Bifurcation in Plastic Flow Under Uniaxial Tension", J. Mech. Phys. Solids, 1971, vol. 19, pp. 89-102.

88. J.P. Miles, "Fluid-Pressure Eigenstates and Bifurcation in Tension Specimens Under Lateral Pressure", Ibid., 1973, vol. 21, pp. 145-162.

89. J.P. Miles, "The Initiation of Necking in Rectangular Elastic-Plastic Specimens Under Uniaxial and Biaxial Tension", Ibid., 1975, vol. 23, pp. 197-213.

90. M. Miyagawa, "Mechanism of Wrinkling in Deep Drawing of Sheet Metals",
1st Report, Theory of Flat Die Drawing, pp. 390-398
2nd Report, Experiment of Flat Die Drawing, pp. 399-407
3rd Report, Theory of Conical Die Drawing, pp. 407-411
4th Report, Experiment of Conical Die Drawing, pp. 412-415
Trans. JSME, 1957, vol. 23.

91. M. Miyagawa, "A General Consideration of Blank Holding in Deep-Drawing of Sheet Metals", Bulletin of JSME, 1958, vol. 1, pp. 95-101.

92. G.G Moore and J.F. Wallace, "Theoretical Study of Tube Sinking Through Conical Dies", J. Mech. Eng. Sci., 1961, vol. 3, pp. 225-235.

93. G.G. Moore and J.F. Wallace, "Theories and Experiments on Tube Sinking Through Conical Dies", Proc. Inst. Mech. Eng., 1968, vol. 168, pp. 1-9.

94. J.L. Morrison and W.M. Shepherd, "An Experimental Investigation of Plastic Stress-Strain Relations", Proc. Inst. Mech. Eng., 1950, vol. 163, pp. 1-17.

95. E.M. Moshinin and K.G. Kachikyan, "Stability of Blanks When Stamping", Russ. Eng. J., 1965, No. 6, pp. 53-58.

96. S. Mujumdar, "Buckling of a Thin Annular Plate under Uniform Compression", AIAA Journal, 1971, vol. 9, pp. 1701-1707.

97. P.M. Naghdi and J.C. Rowley, "An Experimental Study of Biaxial Stress-Strain Relations in Plasticity", J. Mech. Phys. Solids, 1954, vol. 3, pp. 63-80.

98. P.M. Naghdi, J.C. Rowley and C.W. Beadle, "Experiments Concerning the Yield Surface and the Assumption of Linearity in the Plastic Stress-Strain Relations", J. Appl. Mech., 1955, pp. 416-420.

99. K. Naruse and H. Takeyama, "Bifurcation Analysis of a Deep-Drawn Flange without a Blank Holder - Fundamental Analysis of Flange Wrinkling in Deep-Drawing of Circular Sheet Metals I", J. Jap. Soc. Tech. of Plasticity, 1977, vol. 18, pp. 739-746. (In Japanese)

100. K. Naruse and H. Takeyama, "Effects of Restraining Flange Wrinkling by Spring-Type Blank Holder - Fundamental Analysis of Flange Wrinkling in Deep-Drawing of Circular Sheet Metals II", Ibid., 1979, vol. 20, pp. 386-391. (In Japanese)

101. H. Naziri and R. Pearce, "The Effect of Plastic Anisotropy on Flange Wrinkling Behavior During Sheet Metal Forming", Int. J. Mech. Sci., 1968, vol. 10, pp. 681-694.

102. K.W. Neale, "A General Variational Theorem for the Rate Problem in Elasto-Plasticity", Int. J. Solids Structures, 1972, vol. 8, pp. 865-876.

103. K.W. Neale, "Bifurcation in an Elastic-Plastic Cylindrical Shell Under Torsion", J. Appl. Mech., 1973, vol. 40, pp. 826-828.

104. K.W. Neale, "A Method for the Estimation of Plastic Buckling Loads", Int. J. Solids Structures, 1974, vol. 10, pp. 217-230.

105. K.W. Neale, "Phenomenological Constitutive Laws in Finite Plasticity", Rapport Technique No. KN-14-80, 1980, Département de Génie Civil, University of Sherbrooke, Québec.

106. A. Needleman, "A Numerical Study of Necking in Circular Cylindrical Bars", J. Mech. Phys. Solids, 1972, vol. 20, pp. 111-127.

107. A. Needleman, "A Numerical Study of Uniaxial Compression in Circular Elastic-Plastic Columns", Int. J. Solids Structures, 1973, vol. 9, pp. 981-998.

108. A. Needleman and V. Tvergaard, "Necking of Biaxially-Stretched Elastic-Plastic Circular Plates", J. Mech. Phys. Solids, 1977, vol. 25, pp. 159-183.

109. S. Nemat-Nasser, "Continuum Bases for Consistent Numerical Formulations of Finite Strains in Elastic and Inelastic Structures", In Finite Elements Analysis of Transient Non-Linear Structural Behavior, Eds. T. Belytschko, J.R. Osias and P.V. Marcal, ASME, 1975, pp. 85-98.

110. S. Nemat-Nasser, "Decomposition of Strain Measures and their Rates in Finite Deformation Elastoplasticity", Int. J. Solids Structures, 1979, vol. 15, pp. 155-166.

111. V.V. Novozhilov, "Thin Shell Theory", 2nd Ed., 1964, Noordhoff Ltd.

112. G. Oehler, "Deep Drawing without a Blank-Holder by Bending around Convex-Shaped Dies", Eng. Digest, 1963, vol. 24, pp. 81-83.

113. W. Olszak, Z. Mróz and P. Perzyna, "Recent Trends in the Development of the Theory of Plasticity", 1963, The MacMillan Company, N.Y.

114. E. Onat and D. Drucker, "Inelastic Instability and Incremental Theories of Plasticity", J. Aero. Sci., 1953, vol. 20, pp. 181-186.

115. G. Oravas, "Thin Shells: Engineering Fitness and Architectural Form - I and II", Architectural Record, 1960, pp. 216-221 and 246-250.

116. C.E. Pearson, "Bifurcation Criterion and Plastic Buckling of Plates and Shells", J. Aero. Sci., July 1950, pp. 417-424.

117. R. Peters, N. Dow and S.B. Batdorf, "Preliminary Experiments for Testing Basic Assumptions of Plasticity Theories", Proc. Soc. Stress Analysis, 1949, vol. 7, pp. 127-140.

118. A. Phillips, "Pointed Vertices in Plasticity", In Plasticity, Proc. 2nd Symp. on Naval Struct. Mech., Eds. E.H. Lee and P. Symonds, Pergamon Press, 1960, pp. 202-214.

119. W. Prager, "An Elementary Discussion of Definitions of Stress Rate", Quart. Appl. Math., 1961, vol. 18, pp. 403-407.

120. M. Rozsa, "Stability of Thin Annular Plates Compressed Along the Outer or the Inner Edge by Uniformly Distributed Radial Forces", Acta Technica Academiae Sc. Hungaricae, 1966, vol. 53, pp. 359-377.

121. G. Sacks and W.H. Baldwin, "Folding in Tube Sinking", Trans. ASME, 1946, vol. 68, pp. 647-654.

122. G. Sacks and W.H. Baldwin, "Stress Analysis in Tube Sinking", Ibid., 1946, vol. 68, pp. 655-662.

123. J.L. Sanders, "Plastic Stress-Strain Relations Based on Linear Loading Functions", Proc. 2nd U.S. Nat. Congr. Appl. Mech., 1954, pp. 455-460.

124. B.W. Senior, "Flange Wrinkling in Deep-Drawing Operations", J. Mech. Phys. Solids, 1956, vol. 4, pp. 235-246.

125. M.J. Sewell, "A General Theory of Elastic and Inelastic Plate Failure: Part I", J. Mech. Phys. Solids, 1963, vol. 11, pp. 377-393.

126. M.J. Sewell, "Inverse Rigid/Plastic Constitutive Equations", Int. J. Engng. Sci., 1964, vol. 2, pp. 317-325.

127. M.J. Sewell, "The Static Perturbation Technique in Buckling Problems", J. Mech. Phys. Solids, 1965, vol. 13, pp. 247-265.

128. M.J. Sewell, "A Survey of Plastic Buckling", In Stability, Ed. H. Leipholz, 1972, Chapter 5, pp. 85-197, Univ. of Waterloo Press, Waterloo, Ont.

129. M.J. Sewell, "A Yield Corner Lowers the Buckling Stress of an Elastic-Plastic Plate Under Compression", J. Mech. Phys. Solids, 1973, vol. 21, pp. 19-45.

130. M.J. Sewell, "A Plastic Flow Rule at a Yield Vertex", Ibid., 1974, vol. 22, pp. 469-490.

131. F.R. Shanley, "The Column Paradox", J. Aero. Sci., 1946, vol. 13, pp. 678.

132. F.R. Shanley, "Inelastic Column Theory", Ibid., 1947, vol. 14, pp. 261-268.

133. G. Shawki, "Spannungen und Krafte beim Niederhalterlosen Tiefziehen mit Konischen Ringen", Zeit Metallk., 1961, vol. 8, pp. 532-537.

134. G. Shawki, "Die Grenzen beim Niederhalterlosen Tiefziehen von Feinblech", Ibid., 1961, vol. 10, pp. 704-710.

135. G. Shawki, "Wanddickenverlauf beim Tiefziehen ohne Niederhalter", Ibid., 1961, vol. 11, pp. 763-767.

136. I.S. Sokolnikoff, "Mathematical Theory of Elasticity", 1956, McGraw Hill, N.Y.

137. B. Storåkers, "Bifurcation and Instability Modes in Thick-walled Rigid-Plastic Cylinders Under Pressure", J. Mech. Phys. Solids, 1971, vol. 19, pp. 239-351.

138. B. Storåkers, "On Uniqueness and Stability of Elastic-Plastic Deformation", Archieves of Mechanics, 1975, vol. 27, pp. 821-839.

139. S. Stören and J.R. Rice, "Localized Necking in Thin Sheets", J. Mech. Phys. Solids, 1975, vol. 23, pp. 421-441.

140. S.W. Swift, "Stresses and Strains in Tube Drawing", Phil. Mag. Ser., 1949, vol. 7, pp. 883.

141. S. Timoshenko and J.M. Gere, "Theory of Elastic Stability", 1961, 2nd Ed., McGraw Hill, N.Y.

142. S. Timoshenko and Woinowsky-Krieger, "Theory of Plates and Shells", 1959, 2nd Ed., McGraw Hill, N.Y.

143. N. Triantafyllidis and A. Needleman, "An Analysis of Wrinkling in the Swift Cup Test", 1979, Brown University report no. NSF-ENG76-16421/5, Providence, R.I.

144. K. Washizu, "Variational Methods in Elasticity and Plasticity", 1968, Pergamon Press.

145. A.S. Wifi, "An Incremental Complete Solution of the Stretch-Forming and Deep-Drawing of a Circular Blank Using a Hemispherical Punch", Int. J. Mech. Sci., 1976, vol. 18, pp. 23-31.

146. D.M. Woo, "Analysis of Cup Drawing Process", J. Mech. Eng. Sci., 1964, vol. 6, pp. 116-131.

147. D.M. Woo, "On the Complete Solution of Deep Drawing Problem", Int. J. Mech. Sci., 1968, vol. 10, pp. 83-94.

148. D.M. Woo, "Analysis of Deep-Drawing Over a Tractrix-Die", J. Eng. Metals and Tech., 1976, pp. 337-341.

149. N.J. Young, "Bifurcation Phenomena in the Plane Compression Test", J. Mech. Phys. Solids, 1976, vol. 24, pp. 77-91.

150. H. Zeigler, "On the Concepts of Elastic Stability", Advances in Appl. Mech., 1956, vol. 4, pp. 351-403.